NASA/TM—2009-215292

Experimental Investigations of Space Shuttle BX–265 Foam

B.A. Lerch and R.M. Sullivan
Glenn Research Center, Cleveland, Ohio

April 2009

NASA STI Program . . . in Profile

Since its founding, NASA has been dedicated to the advancement of aeronautics and space science. The NASA Scientific and Technical Information (STI) program plays a key part in helping NASA maintain this important role.

The NASA STI Program operates under the auspices of the Agency Chief Information Officer. It collects, organizes, provides for archiving, and disseminates NASA's STI. The NASA STI program provides access to the NASA Aeronautics and Space Database and its public interface, the NASA Technical Reports Server, thus providing one of the largest collections of aeronautical and space science STI in the world. Results are published in both non-NASA channels and by NASA in the NASA STI Report Series, which includes the following report types:

- TECHNICAL PUBLICATION. Reports of completed research or a major significant phase of research that present the results of NASA programs and include extensive data or theoretical analysis. Includes compilations of significant scientific and technical data and information deemed to be of continuing reference value. NASA counterpart of peer-reviewed formal professional papers but has less stringent limitations on manuscript length and extent of graphic presentations.

- TECHNICAL MEMORANDUM. Scientific and technical findings that are preliminary or of specialized interest, e.g., quick release reports, working papers, and bibliographies that contain minimal annotation. Does not contain extensive analysis.

- CONTRACTOR REPORT. Scientific and technical findings by NASA-sponsored contractors and grantees.

- CONFERENCE PUBLICATION. Collected papers from scientific and technical conferences, symposia, seminars, or other meetings sponsored or cosponsored by NASA.

- SPECIAL PUBLICATION. Scientific, technical, or historical information from NASA programs, projects, and missions, often concerned with subjects having substantial public interest.

- TECHNICAL TRANSLATION. English-language translations of foreign scientific and technical material pertinent to NASA's mission.

Specialized services also include creating custom thesauri, building customized databases, organizing and publishing research results.

For more information about the NASA STI program, see the following:

- Access the NASA STI program home page at *http://www.sti.nasa.gov*

- E-mail your question via the Internet to *help@sti.nasa.gov*

- Fax your question to the NASA STI Help Desk at 301–621–0134

- Telephone the NASA STI Help Desk at 301–621–0390

- Write to:
  NASA Center for AeroSpace Information (CASI)
  7115 Standard Drive
  Hanover, MD 21076–1320

NASA/TM—2009-215292

Experimental Investigations of Space Shuttle BX–265 Foam

B.A. Lerch and R.M. Sullivan
Glenn Research Center, Cleveland, Ohio

National Aeronautics and
Space Administration

Glenn Research Center
Cleveland, Ohio 44135

April 2009

Acknowledgments

The authors appreciate the generous support of the ET Project at NASA Marshall Space Flight Center. We gratefully acknowledge the following people for providing BX–265 foam: J. Scotty Sparks and Mike Prince (Marshall), Bob Speece (NASA Kennedy Space Center), and Eloy Martinez (Lockheed Martin at Marshall). Much thanks goes to Chris Burke (ASRC Aerospace Corporation at NASA Glenn Research Center) for his efforts on the optical dilatometer; Dan Scheiman (ASRC at Glenn) for conducting the thermomechanical analysis, thermogravimetric analysis, and glass transition temperature tests; and William Brown (Sierra Lobo at Glenn Research Center) for performing the drying experiments. The hard work of several summer students in characterizing foam is also appreciated: Elizabeth Freund, Dana Fedor, Jessica Fedor, and Charlene Dvoracek.

Level of Review: This material has been technically reviewed by technical management.

Available from

NASA Center for Aerospace Information
7115 Standard Drive
Hanover, MD 21076–1320

National Technical Information Service
5285 Port Royal Road
Springfield, VA 22161

Available electronically at http://gltrs.grc.nasa.gov

Experimental Investigations of Space Shuttle BX–265 Foam

B.A. Lerch and R.M. Sullivan
National Aeronautics and Space Administration
Glenn Research Center
Cleveland, Ohio 44135

Summary

This report presents a variety of experimental studies on the polyurethane foam, BX–265. This foam is used as a close-out foam insulation on the space shuttle external tank. The purpose of this work is to provide a better understanding of the foam's behavior and to support advanced modeling efforts. The following experiments were performed: Thermal expansion was measured for various heating rates. The in situ expansion of foam cells was documented by heating the foam in a scanning electron microscope. Expansion mechanisms are described. Thermogravimetric analysis was performed at various heating rates and for various environments. The glass transition temperature was also measured. The effects of moisture on the foam were studied. Time-dependent effects were measured to give preliminary data on viscoelastoplastic properties.

Introduction

The primary purpose of the foam on the space shuttle external tank (ET) is to provide thermal insulation. While the foam has been successful in its function, it has not been without troubles. Since the beginning of the shuttle program, foam shedding has been observed during ascent. Early in the program this was deemed only as a minimal problem. However, since the destruction of the orbiter *Columbia* by a piece of foam debris, the interest in foam shedding has greatly increased. Since the destruction of *Columbia* the foam suddenly became viewed as more of a structural material, and much effort has been put into the characterization of structural properties, the analyses of foam stresses, and the prediction of cracking. As part of this effort, the Mechanics and Lifing Branch at NASA Glenn Research Center has been requested by the ET Project at NASA Marshall Space Flight Center to help improve the thermostructural models for the foam. This report is one of several (refs. 1 to 5) detailing the work. This report deals with an experimental portion of the Glenn effort and focuses entirely on the behavior of the BX–265 foam. Most of the information is new; however, some of the experiments have been performed before and are repeated for completeness and to support and verify existing data previously generated by the ET Project.

In order to develop and characterize structural models for the polymeric foam, a number of input parameters are required. To obtain some of these, a series of coupon-level tests that document properties characterizing the foam was performed. Some of these properties already exist within the project, and others are still being generated. Still others are more specialized and need to be determined as the level of model sophistication increases. Note that for this study, because the foam experiences a large range of temperatures on the ET, thermal expansion was studied in detail. This test can simulate the thermal loads on the ET foam during the ascent of the shuttle, can be performed readily in a laboratory setting, and represents one of the more complicated events in the life of this foam as will be described throughout this report. For other input parameters, knowledge of the foam constituents was obtained. The foam can actually be thought of as a structure itself, which consists of a polymeric cellular skeleton with the cell interior containing a mixture of gases. There are certain modeling approaches that can take advantage of these two constituents and build a "composite" structural model. Since the in situ foam properties are a product of the foaming process, it is difficult—if not impossible—to get accurate properties of the polymeric skeleton. Manufacturing a "poreless" polymer as one would do with a composite (i.e., a neat or fiberless composite) is not possible. Therefore properties for the polymeric skeleton are usually assumed

from a variety of monolithic polymeric materials, or backed out using a model along with foam test data. As an added dimension, there is a whole range of ancillary effects that can affect the foam properties, which expand the total range of tests but give more insight into defining both the behavior of the polymeric skeleton and the response of the foam. Some of these are temperature, loading rates, environment, foam conditioning, and humidity.

A major goal of this study is to investigate the thermal expansion of the BX–265 foam. This will provide coefficient of thermal expansion (CTE) data for use in stress analyses of the foam on the ET. A detailed understanding of the mechanisms of thermal expansion will also be provided. This will help guide the development and improvement of the structural models. The ET Project is already aware that high loads can be established in the foam due only to the significant thermal gradients that the foam experiences along with the differences in thermal expansion between the metallic tank and various foams used on the tank. This highlights the importance of thoroughly understanding the thermal expansion behavior of the foam. During service the foam experiences temperatures from –250 up to 340 °C (–418 to 644 °F): a 600 °C (1112 °F) range. This report focuses on the high-temperature behavior of the foam, because this is the more complicated regime to test in and the models require more detail in this regime to capture the expansion behavior. As a result, foam constituent properties are elucidated, allowing the models to be improved. At cryogenic temperatures any time dependency of strains in the polymer skeleton and significant pressure increases due to cell gas expansion should be negligible. Some data are taken at temperatures as low as –196 °C (–320 °F, liquid nitrogen); this was done to better compare the thermal expansion data generated in this report with existing data.

As mentioned above, a major portion of this report deals with the thermal expansion behavior of BX–265 foam. Thermal expansion is evaluated as a function of spray lot, orientation with respect to the knit lines, foam density, and heating rates. The mechanisms of thermal expansion are described and related, where possible, to the other variables affecting the foam. Data are also given for the thermal expansion of the polymer skeleton. Thermogravimetric analysis is performed on the foam and the volatile species are identified using infrared spectroscopy. The composition of the gases in the foam cells has also been analyzed. Moisture contents of the foam have been studied by conditioning the foam in either humidity chambers or drying ovens. The weight gains and losses have been measured. The thermal expansion of conditioned foam was also tested. This is of practical as well as scientific interest since the foam can experience a range of moisture conditions depending on the local humidity and weather experienced during the life of an ET. Finally, the creep behavior of the foam was investigated mainly to give time-dependent properties for the development of some of the models. While at first glance creep of the foam may be thought of as a non-issue, particularly since the ascent of the ET only lasts 7 min, it should be pointed out that the foam gets hot, reaching temperatures much higher than the polymeric glass transition temperature. Any structural loads acting on the foam during this short exposure to high temperatures can cause time-dependent deformation of the foam.

While the goal of this work is to advance the state of the thermostructural models for ET foams, the modeling work will not be presented in this report. That is the topic of other reports. However, some general mention will be made of the models herein, especially how the observations can affect the model development.

Foam Sources

The polyurethane foam, BX–265, was the only foam studied in detail and presented in this report. Various sources of foam representing different spray lots and spray locations were used. In total 12 different blocks of foam were studied and are shown in table I. Blocks 1 to 3 were 203- by 152- by 38-mm (8- by 6- by 1.5-in.) blocks sent on March 22, 2005, specifically for this project courtesy of J.S. Sparks (Marshall). Blocks 1C, 2F, and 8E were 203- by 152- by 38-mm blocks sent on December 7, 2005, specifically for this project courtesy of M. Prince (Marshall). The ballistic cylinders were sent on September 23, 2003, by P. Kopfinger (Lockheed Martin at Michoud Assembly Facility) for ballistic testing for Return to Flight efforts. These specimens (labeled T–1s) were cylinders 31.75 mm (1.25 in.) in

TABLE I.—FOAM SOURCES OF BX–265
USED IN THIS REPORT

Foam	Supplier
Blocks 1 to 3	J.S. Sparks,[a] 3/22/05
Blocks 1C, 2F, 8E	M. Prince,[a] 12/7/05
Ballistic cylinders (2T)	P. Kopfinger,[b] 9/23/03
KSC–1 to KSC–4	B. Speece,[c] 3/17/06
LOX	E. Martinez,[b] 3/14/06

[a]From NASA Marshall Space Flight Center.
[b]From Lockheed Martin at NASA Michoud Assembly Facility.
[c]From NASA Kennedy Space Center.

TABLE II.—CHARACTERIZATION OF BX–265 FOAMS

Block	Average cell size,[a] μm						Knit lines per centimeter	Density, g/cm^3
	Height	*n*	Standard deviation	Width	*n*	Standard deviation		
1	171	18	57	107	36	27	1.4	0.035
2	173	18	55	117	36	34	1.3	.034
3	158	16	43	126	36	35	1.5	.034
1C	215	12	64	142	36	26	1.9	0.037
2F	216	22	80	142	46	47	1.0	.034
8E	197	15	58	131	39	29	2.1	.040
KSC–1	223	50	88	165	150	54	0.4	0.031
KSC–2	213	50	68	136	150	39	0.6	.028
KSC–3	227	50	95	138	150	50	0.5	.032
KSC–4	201	50	131	126	150	53	0.6	.031
LOX	193	100	61	136	100	33	1.5	0.036

[a]*n* is number of measured cells.

diameter by 76.2 mm (3.0 in.) long intended for ballistic projectiles. This batch was used seldom in the current study. Blocks labeled KSC–1 to KSC–4 of approximate size 203 by 152 by 25 mm (8 by 6 by 1 in.) were graciously provided by B. Speece at NASA Kennedy Space Center. These blocks were intended to supply specimens that had their major axis parallel to the knit lines. The foam block marked LOX was supplied by E. Martinez (Lockheed Martin at Michoud Assembly Facility) in a 610- by 610- by 51-mm (24- by 24- by 2-in.) plate for the Ice Mitigation Team. Except for blocks KSC–1 to KSC–4, all foams were sprayed at Lockheed Martin Michoud Assembly Facility. All foams were reportedly sprayed according to post-*Columbia* specifications. Most came with pedigree sheets. Each foam block was recharacterized at Glenn upon receipt. The density, average knit line separation, and cell size of the blocks are documented in table II. The foam from the Ballistic Cylinders was not characterized. Note that all other foams appear within normal ranges.

Thermal Expansion

Thermal expansion was measured by two different methods. A few specimens were tested in a commercially available thermomechanical analyzer (TMA) rig, which can be found in most polymers labs. This rig was used for verification and also for measuring thermal expansion down to liquid nitrogen temperatures. The second rig was developed in-house, specifically for use at elevated temperatures. This rig was based on a noncontacting, optical measurement of the specimen length to avoid exerting any force on the sample. Figure 1 shows the test setup. A foam sample of dimensions 51 by 12.7 by 12.7 mm (2 by 0.5 by 0.5 in.) was cut from a larger foam block and sanded slightly on all faces. Whereas the bulk

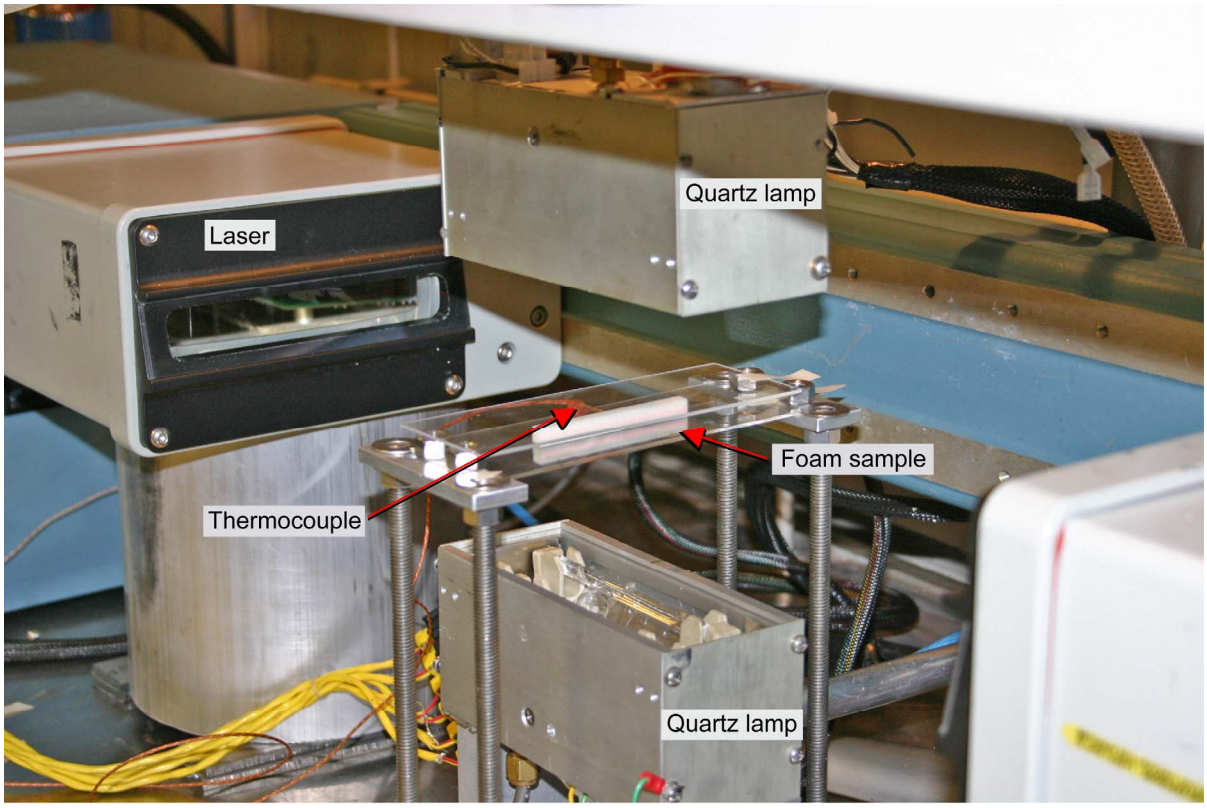

Figure 1.—Optical thermal expansion rig without black body radiators.

of this work was performed on samples 51 by 12.7 by 12.7 mm in size, other sample geometries were evaluated. A 6.4-mm (0.25-in.) square cross section was tested, but was deemed too small to yield accurate results. Specimen lengths of 25 and 76 mm (1 and 3 in.) were also examined. The 25-mm length did not give sufficient resolution of the length change. The 76-mm sample had too large of a temperature gradient along the length. The 51-mm length was chosen as a compromise between these two lengths. Each sample was measured and weighed,[1] and density was calculated both before and after the thermal expansion tests. The sample rests on two alumina rods (not shown in fig. 1) in the test rig to promote free expansion. The sample is radiantly heated indirectly by a pair of quartz lamps above and below the sample. Since the foam is translucent to light, black body radiators (absent in fig. 1) were placed between the lamps and the sample. The length of the foam specimen at the midthickness was measured using a laser micrometer having a resolution of 0.0051 mm (0.0002 in.). Temperature, time, and specimen length were captured digitally using a computer. Temperature was controlled by a single type K thermocouple embedded halfway into the center of the sample. Before conducting a new series of tests, a calibration foam sample was embedded with thermocouples to measure the temperature gradient both along the length and through the thickness of the sample. Typical gradients were 10 °C (50 °F) or less along the length and 5 °C (41 °F) or less through the thickness. Note that a large amount of time was spent trying to improve this gradient with limited success. However multiple tests and comparison to results gathered on the TMA rig assured us that this gradient was adequate. The major advantage of the optical rig over other types of dilatometers is that there is no force acting on the sample during heating, which can affect specimen displacement—especially for highly compliant materials like foams. Additionally, the quartz lamps allow a large range of heating rates to be applied. Assuming that the maximum foam temperature

[1]Note that certain handling processes (e.g., sanding) create static charges on the foam. These charges will affect its weight, especially for the small samples used in this study. All samples should have the static charges removed before weighing.

observed on the ET during ascent is 300 °C (572 °F) and that this temperature is reached in 2 min (the time at which the solid rocket boosters are jettisoned), this would equate to a heating rate of 150 °C/min (270 °F/min). Most dilatometers employ a resistance furnace that has a large thermal mass and is incapable of heating and cooling at such high rates. The optical rig can accommodate these rates. The bulk of the thermal expansion work was performed at a heating rate of 5 °C/min (9 °F/min), which is the standard rate. The results from other heating rates will be presented later in this report.

Standard Heating Rate

A number of specimens were cut from block 3, and both heating and cooling curves were established starting at temperatures of 20 °C (68 °F). The samples were heated to some maximum temperature not exceeding 230 °C (446 °F) and then cooled at the same rate to 20 °C. The maximum temperature was varied to examine the cooling portion of the curve from various upper temperatures. The data for thermal expansion are shown in figure 2. These data are all for measurements taken along the 51-mm length of the sample, which is perpendicular to the rise direction. The foam starts with a slow rate of expansion as the temperature is raised above 20 °C. An approximate value for CTE over the temperature range 20 to 90 °C (68 to 194 °F) is 2×10^{-4}/°C (1.1×10^{-4}/°F). At temperatures approaching 100 °C (212 °F) there begins a rapid expansion of the sample resulting in a tangent CTE of approximately 5×10^{-3}/°C (2.8×10^{-3}/°F). This increase reaches a maximum in the vicinity of about 150 °C (302 °F). At still higher temperatures the foam begins to shrink. Presumably the shrinkage would continue until the specimen length was shorter than before the test, but this would not happen until much higher temperatures (~300 to 350 °C, or 572 to 662 °F) than were conducted in this study.

As the sample is cooled from an elevated temperature, it contracts. This contraction is slight and an instantaneous CTE for this cooling is approximately 1×10^{-4}/°C (5.6×10^{-5}/°F). Note that the cooling response is the same regardless of the temperature from which the foam is cooled, and this represents the reversible part of the thermal expansion. Most of the thermal expansion is irreversible. After cooling down to 20 °C, each specimen has a permanent length change compared with the original, pretest length. Figure 2 indicates that the posttest length is dependent upon where the heating was stopped and cooling began. If the test was cooled closer to the peak strain, the permanent length change is very large. If the

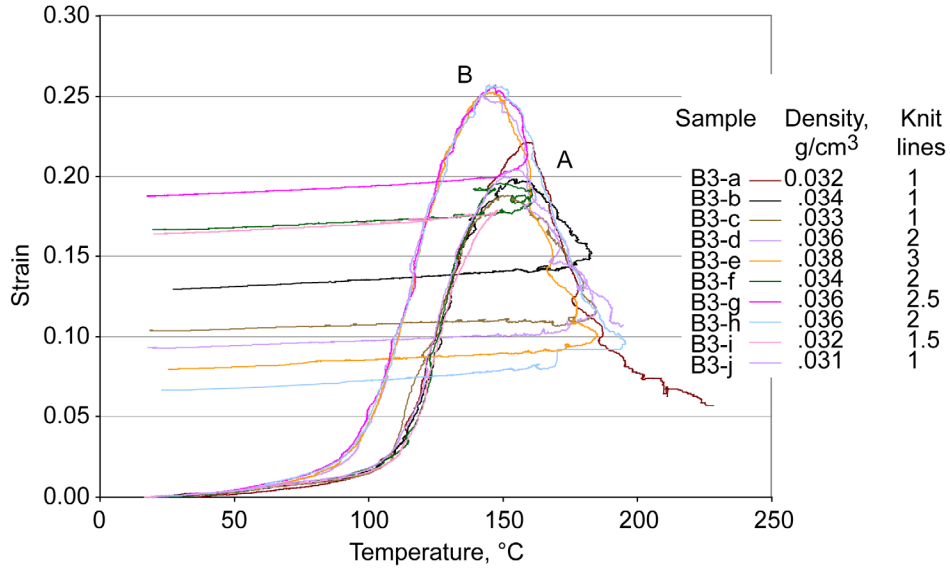

Figure 2.—Thermal expansion perpendicular to rise for BX–265 foam, block 3.

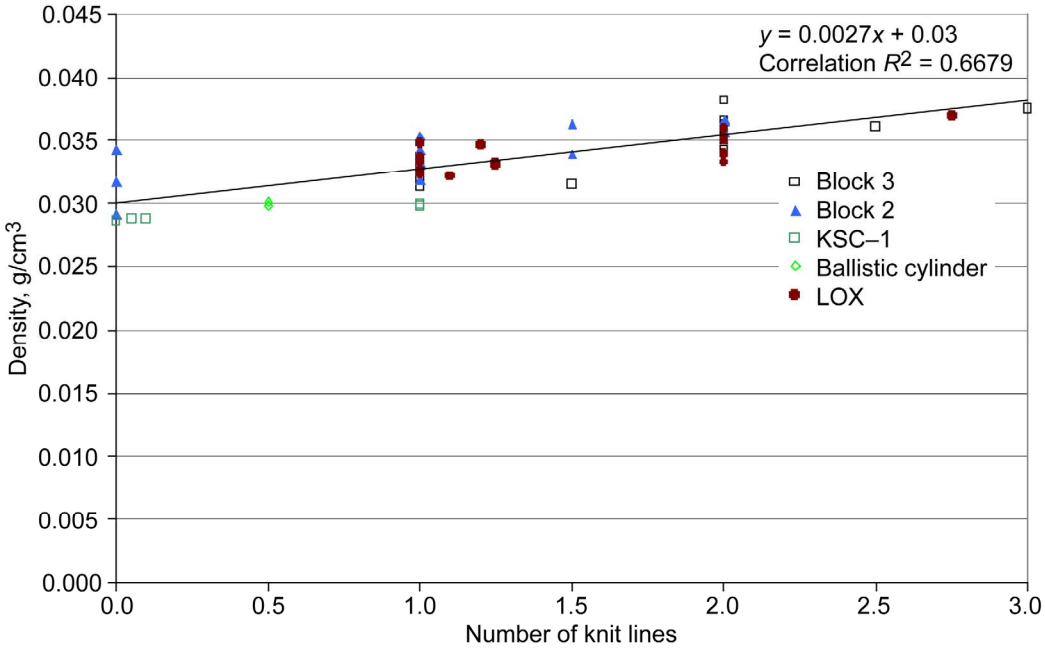

Figure 3.—Relationship between number of knit lines and density for BX–265 foam samples.

foam was just slightly heated above room temperature or heated to very large temperatures (~300 °C), it is conceivable that the foam could return to its same, or even shorter than its original length.

The peak expansion strain in figure 2 is very large and lies between 18 and 26 percent. There are two groupings of data shown in figure 2 with one group increasing to a peak strain at slightly lower temperatures, attaining slightly larger peak strains. This group, henceforth denoted as group B, possesses foam densities greater than 0.035 g/cm^3 (2.19 lb/ft^3). The group with peak expansion strains occurring at higher temperatures, but with lower peak strains, is denoted as group A and possesses foam densities less than 0.035 g/cm^3. Within the density range of the BX–265, minor variations in density are explained at least partially by the number of knit lines in the sample. Figure 3 shows the relationship between the number of knit lines and sample density for samples taken from several foam blocks. Increasing the number for knit lines increases the density and 67 percent of the variation in density (based on the coefficient of determination) can be explained by the number of knit lines. Figure 3 gives data from the majority of the thermal expansion samples run in this study, including those from other foam blocks in addition to block 3. Since the density is primarily related to the number of knit lines, the groupings of thermal expansion data in figure 2 can also be related to the number of knit lines. Group A (higher temperatures) has fewer than two knit lines in a sample, whereas group B has two or more knit lines. Samples with zero knit lines will be shown later to also fall into group A.

Thermal expansion tests were also performed on foam taken from other spray runs. The data for block 2F can be observed in figure 4. The same general trends of thermal expansion can be observed in this block as were observed in block 3 (fig. 2). The same two groupings are also observed in figure 4, although there is more scatter in the data than what was observed in figure 2. There is currently no explanation for the increased scatter, although it should be noted that block 3 had smaller cells than block 2F (table 2). There are three samples tested from block 2F that had no knit lines (2F-e, 2F-f, and 2F-g) and these fall into the high-temperature group A. It was easier to get samples with no knit lines cut out of block 2F since the knit lines were further apart than in block 3 (see table 2 for knit line density). It should also be recognized that the peak strains are slightly (20 percent) lower for block 2F, and the temperatures at which these peaks occur are also slightly lower for block 2F as compared with block 3. Therefore, while exhibiting the same general trends, there is some lot-to-lot variation in the expansion data.

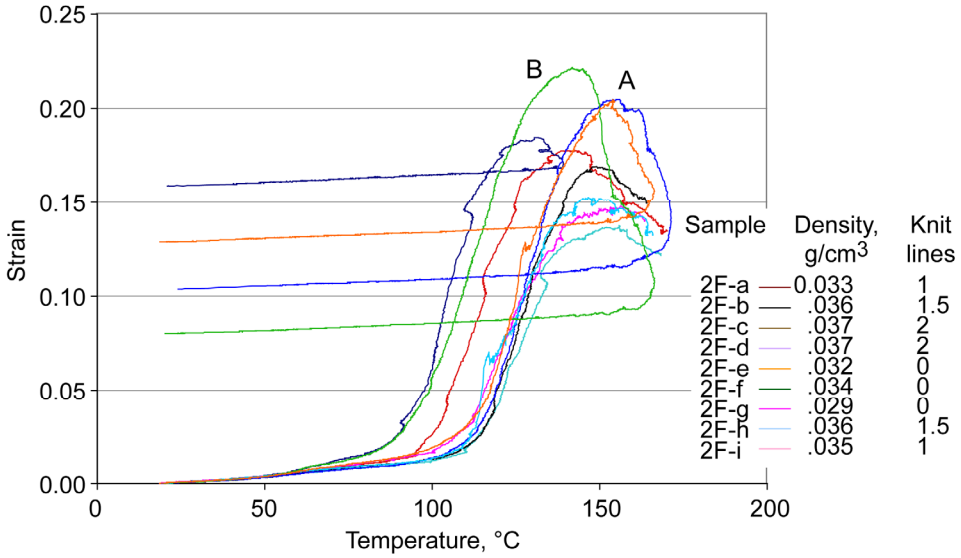

Figure 4.—Thermal expansion perpendicular to rise for BX–265 foam, block 2F.

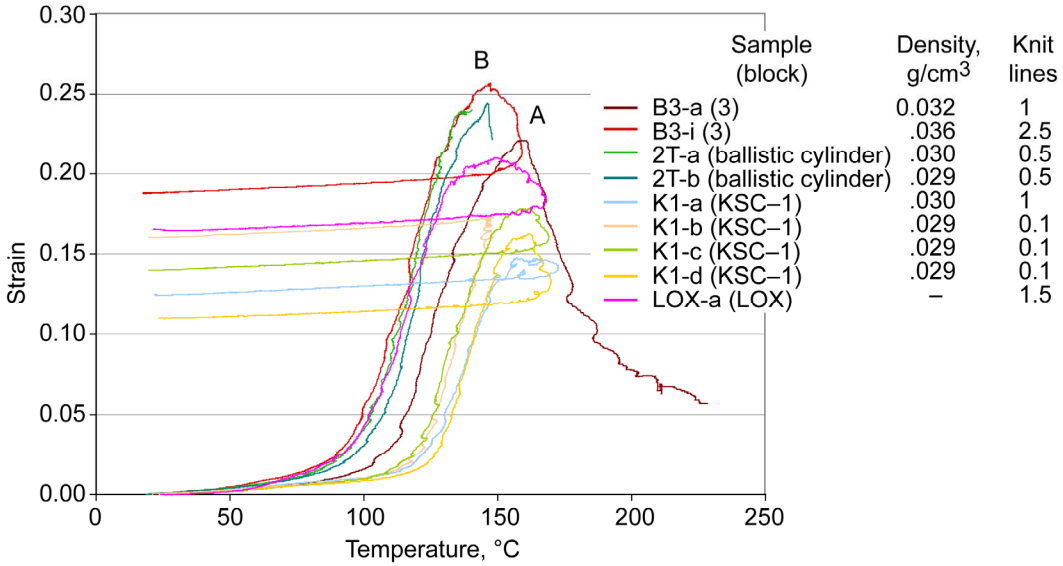

Figure 5.—Thermal expansion perpendicular to rise for BX–265 foam samples.

Variation in thermal expansion from various spray lots is shown in its entirety in figure 5. Here various thermal expansion data from four blocks of foam are depicted. Block 2F, because of its large scatter, was left out for clarity. All of the data fall into the same two groups. Specimen LOX-a from the LOX spray was unfortunately not weighed before testing and the sample density is unknown. However, the overall density of this block as shown in table 2 is 0.036 g/cm^3 (2.25 lb/ft^3) and is the highest of any of the foam blocks used in this study. For a knit line number of 1.5, the density of this particular specimen should easily place it in group B as is indeed observed in figure 5. Most of the data behave as expected, except for the two samples from the ballistic cylinders. Although both of these samples have a low density of 0.030 g/cm^3 (1.87 lb/ft^3) and 1 knit line or less, they still fall in group B. The reason for this is unclear, but might suggest that the spray conditions on this earlier batch of foam could have been different than those for the newer batches.

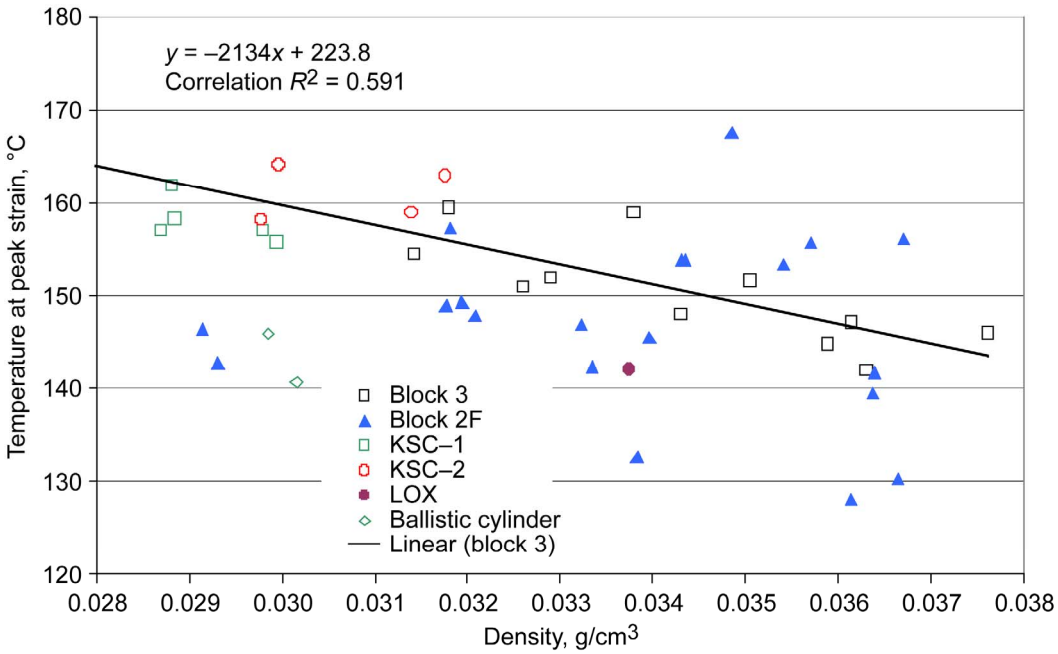

Figure 6.—Effect of density on temperature at peak thermal expansion strain for BX–265 foam samples, perpendicular-to-rise direction.

Since the thermal expansion behavior appears to be dependent upon density, the characteristic expansion values were analyzed based on both density and knit lines. Figure 6 plots the temperature of the peak strain as a function of density for all of the foam lots. There is a loose relationship shown between the density and the temperature. The best correlation is for block 3, and a trendline is fitted to these data. Even for block 3, only 60 percent of the variation in peak strain temperature can be explained by a change in density. As the data for the other blocks are added, the scatter becomes much worse and the correlation disappears. It is verified in this figure, the next two, and figure 4 that foam block 2F has a much greater amount of variation than the other blocks.

The level of the peak expansion strain is plotted versus the foam density in figure 7. There is a reasonable correlation between these two variables for block 3 and KSC–1. The foam from the ballistic cylinders falls significantly above the line, and the data from block 2F show their typical, substantial scatter. Again about half of the variation of peak strain can be explained based on density variations from the data on block 3 only. Incorporation of all of the data results in nonrelated variables.

Finally, the temperature of the peak strain is plotted in figure 8 as a function of the number of knit lines in the sample. There is again a weak correlation between the two variables when only block 3 is considered. However, the addition of all of the data reduces the correlation coefficient to near 0.

Since the optical rig was an in-house design, we wanted to check the data against those from other, more established sources. Two samples from block 3 were tested at Glenn in a standard TMA rig. The samples were 13 by 5 by 5 mm in size. After installing them in the TMA rig, the samples were prechilled to –150 °C (–238 °F) with liquid nitrogen. Using the same heating rate of 5 °C/min, the samples were then heated to various elevated temperatures. The data from both samples fall within the group A data measured in the optical rig (fig. 9). Neither of these samples contained a knit line and is therefore expected to be in group A. Data from two additional samples are also plotted in figure 9. These two samples (SRI-a and SRI-b) were run at Southern Research Institute (SRI) and supplied to us by Kristin Morgan (Marshall). These samples were tested from –250 °C up to 50 °C (–418 to 122 °F). The SRI data agree well with the TMA data, at least down to –150 °C. The upper range of the SRI data also agrees well with the data from the optical rig. In fact, CTE was calculated between the range of 0 and 50 °C (32 and 122 °F) for all three methods. The CTE values are given in table III and are in reasonable agreement.

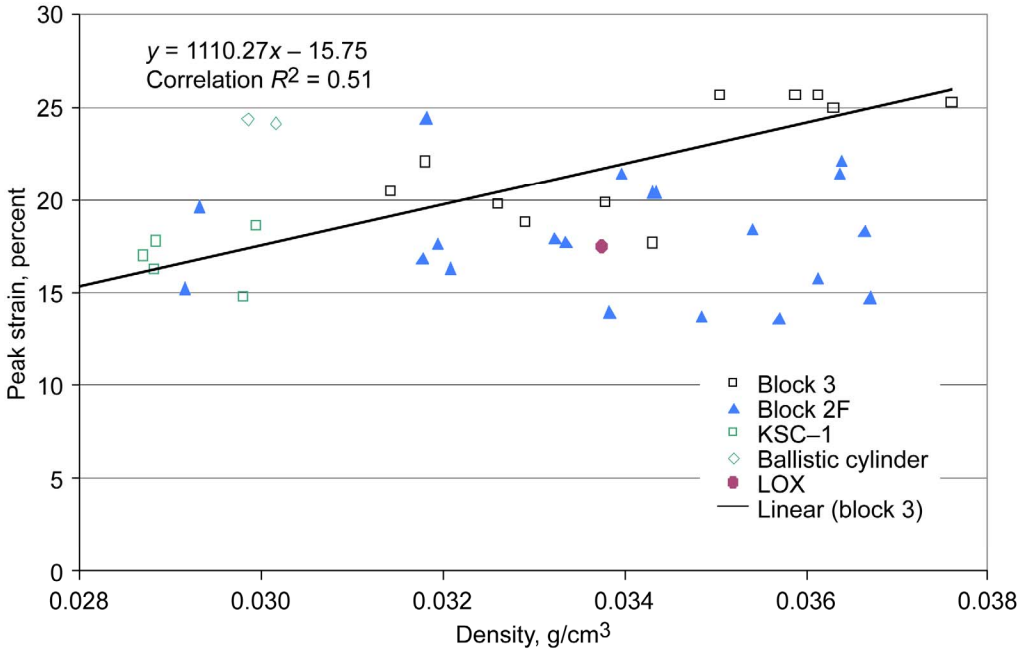

Figure 7.—Influence of density on peak expansion strain for BX–265 foam samples, perpendicular-to-rise direction.

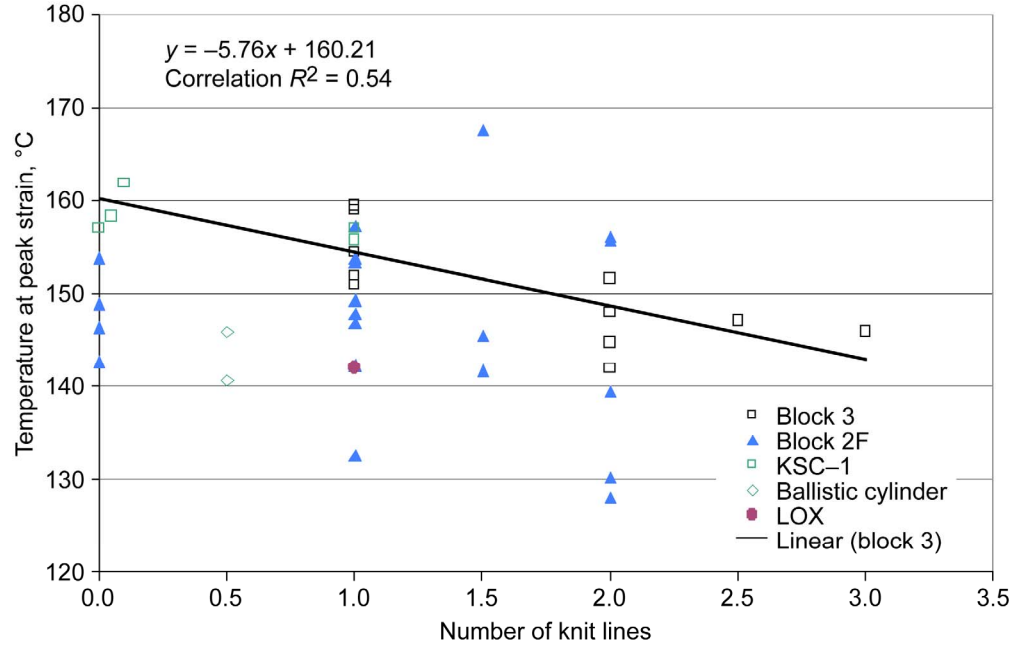

Figure 8.—Influence of knit lines on temperature of peak expansion strain for BX–265 foam samples, perpendicular-to-rise direction.

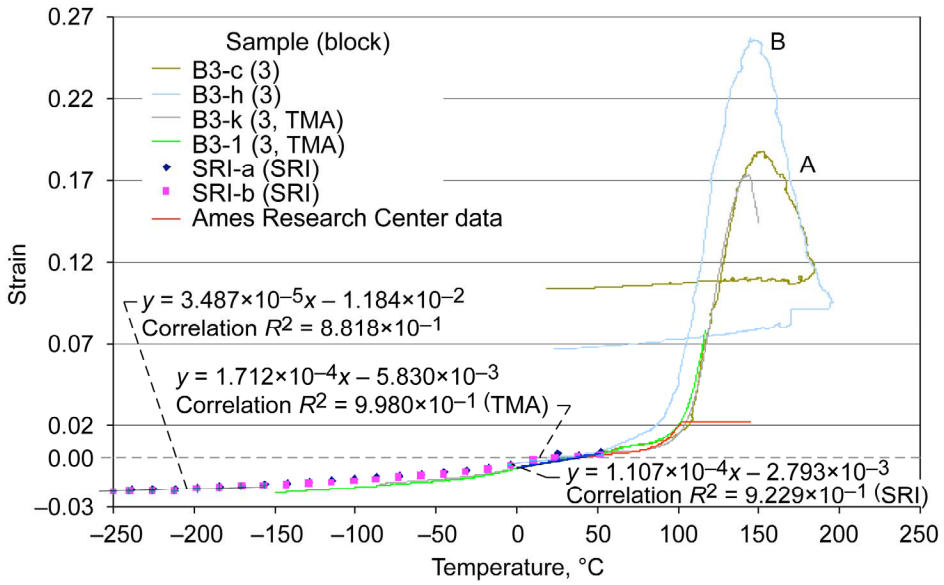

Figure 9.—Thermal expansion of BX–265 foam samples, perpendicular-to-rise direction. TMA refers to those samples analyzed in thermomechanical analyzer (TMA) rig.

TABLE III.—COEFFICIENT OF THERMAL EXPANSION (CTE) BETWEEN 0 AND 50 °C FOR BX–265 FOAMS

Measurement	CTE, $°C^{-1}$
Optical	2.0×10^{-4}
Thermomechanical analyzer	1.7×10^{-4}
Southern Research Institute	1.1×10^{-4}

These values are certainly within lot-to-lot scatter, and thus we have confidence in the data taken from the optical test rig. Some typical values for thermal expansion of polyurethane foam from the literature are 6.0×10^{-5}/°C (ref. 6), 1.2×10^{-4}/°C (ref. 7), and 5.0×10^{-5}/°C (ref. 8) (3.3×10^{-5}, 6.7×10^{-5}, and 2.8×10^{-5}/°F, respectively).

At temperatures of liquid hydrogen (–250 °C), the CTE of the BX–265 foam is 3.5×10^{-5}/°C (1.9×10^{-5}/°F), about an order of magnitude lower than at 20 °C and significantly lower than above 100 °C. Thus the foam undergoes a large change in thermal expansion as it is heated from cryogenic temperatures. The entire range of expansion strains is shown in figure 9 over the full 450 °C (810 °F) temperature excursion. Xian et al. (ref. 9) point out that the thermal expansion of polyurethane foam between liquid nitrogen and liquid hydrogen temperatures contributes only 7.6 percent of the total expansion between –253 and 20 °C (–423 and 68 °F), and therefore the CTE at liquid nitrogen is a good estimate for use at lower temperatures.

There is one final set of expansion data shown in figure 9 and that is from a test conducted at NASA Ames Research Center on BX–265 foam (Tina Panontin, NASA Ames Research Center, Return to Flight External Tank TPS Verification Microstructural Characterization and Fracture Process Assessment, March 30, 2005). Although the data fit well within the other plotted data from 0 to 100 °C (32 to 212 °F), at approximately 100 °C there is a plateau. This is obviously artificial and must be an experimental issue, possibly from the collapse of the specimen due to the force of the measuring probe.

The results to this point have addressed only thermal expansion of foam in the perpendicular-to-rise direction. Now we will introduce data for foam in the rise direction. Figure 10 compares the thermal expansion curves for foam in both directions. It can be observed that there is a major difference between the rise and perpendicular-to-rise directions. There is much less expansion in the rise direction. The peak

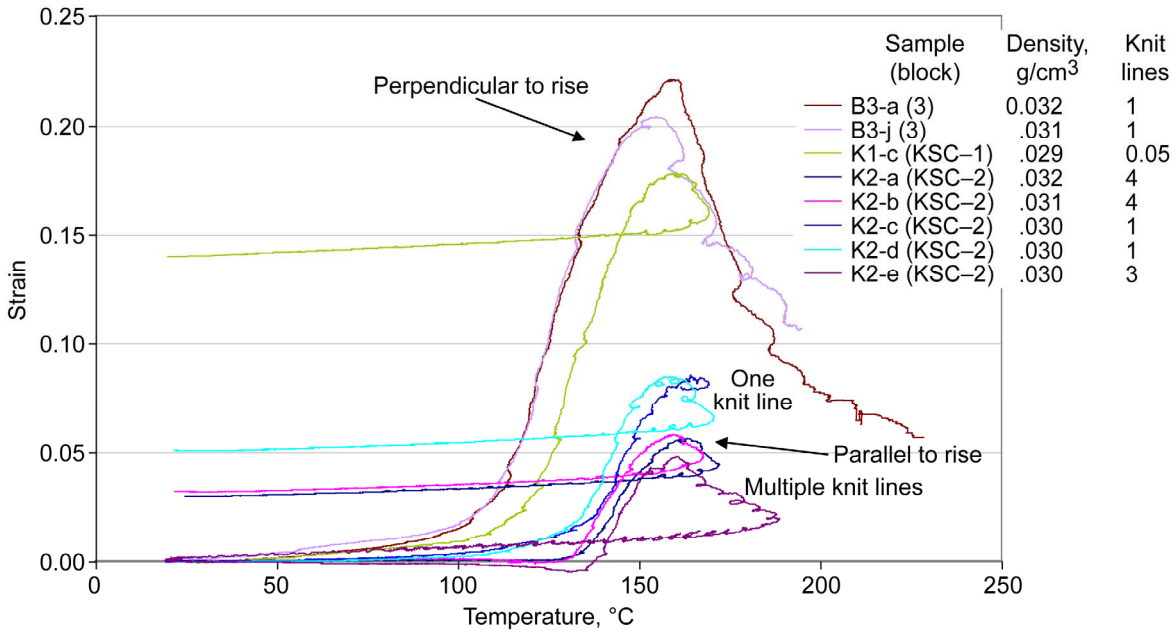

Figure 10.—Effect of orientation on thermal expansion for BX–265 foam samples.

expansion strains are about 7 percent rather than the 20 percent observed in the perpendicular-to-rise direction. This anisotropy in expansion has previously been documented for polyurethane foams (ref. 9) and polyethylene foams (ref. 10). The temperature at peak strain is approximately the same, 160 °C (320 °F). Note also that the rapid expansion to the peak does not begin until much higher temperatures, approximately 130 °C (266 °F), which is about 30 °C (86 °F) higher than that observed in the perpendicular-to-rise samples. There is once again a knit line effect on the thermal expansion. For samples that only contain one knit line, the samples expand sooner and to a greater extent than those samples containing multiple (3 and 4) knit lines. This is the reverse behavior of what was observed for the samples taken in the perpendicular-to-rise direction (fig. 2). Upon cooling, the same behavior is observed in that the contraction is rather flat, having a slope (CTE) of about 2×10^{-4}/°C. Also, there remains a permanent deformation in the foam upon cooling to room temperature as there was in a perpendicular-to-rise direction.

Figure 11 is an enlargement of figure 10 and focuses on the initial part of thermal expansion. The rise-direction samples expand very little in the first 100 °C of temperature increase compared with the perpendicular-to-rise samples. The average CTE in this range is approximately zero, compared with 2×10^{-4}/°C (1.1×10^{-4}/°F) for the perpendicular-to-rise samples. The average CTE in the rapid expansion region is 3×10^{-3}/°C (1.7×10^{-3}/°F) and is similar to the foam expansion in the perpendicular-to-rise direction. In the first 100 °C of expansion, the rise-direction samples show either an increasing expansion, zero expansion, or an increasing and then decreasing expansion. In fact, some specimens actually exhibit shrinkage compared with the original state, see for example specimen K2-e in figure 11. This appears only to happen with samples containing multiple knit lines. Those samples with only one knit line expand continuously above room temperature. Note that Ames data also shows contraction to negative strains for this orientation (fig. 11, Ames data) and also to the same magnitude of –0.4 percent.

Mechanisms

In this section the physical mechanisms of thermal expansion are examined. To do this, a small piece of foam was placed inside of a scanning electron microscope (SEM) and heated in situ using a hot stage[2] (fig. 12). The foam specimen (block 3) was approximately a 1-mm (0.04 in.) cube, and temperature was

[2]A hot stage is a device that holds the sample within the beam of the SEM and can be independently heated. The heat is transferred to the sample to allow viewing of the material at elevated temperature.

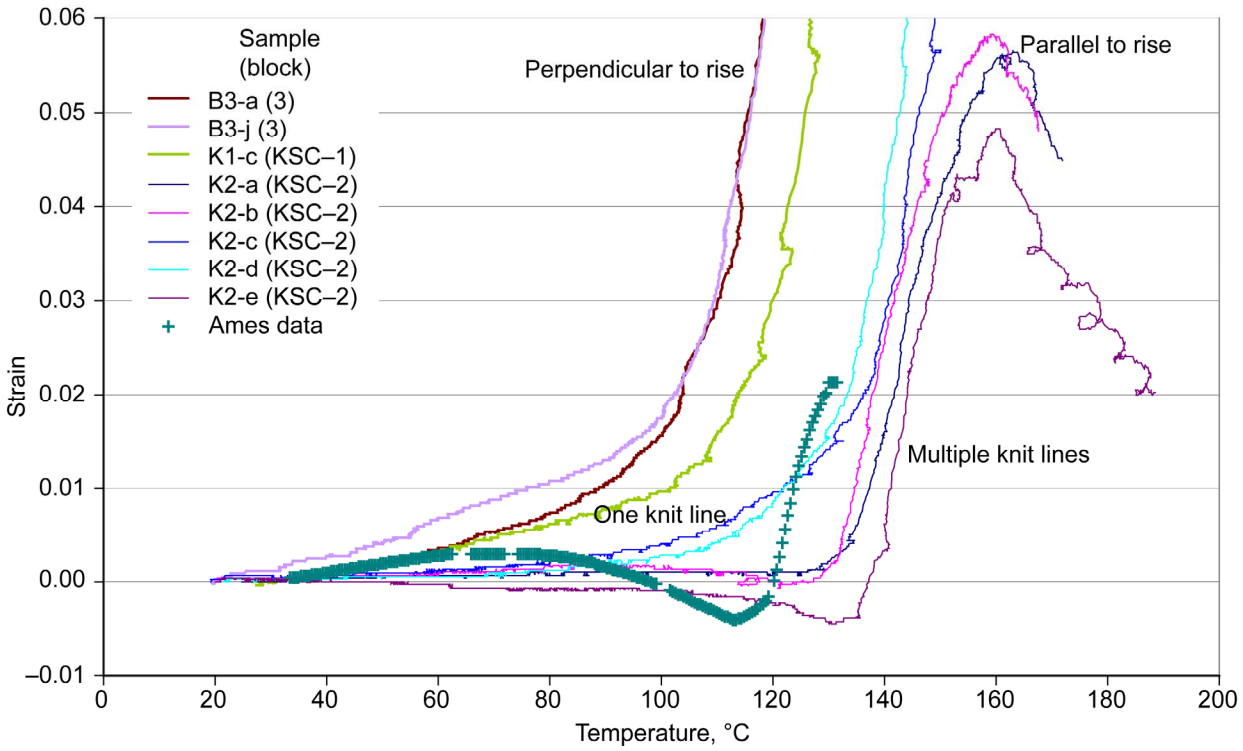

Figure 11.—Enlargement of portion of figure 10: Effect of orientation on thermal expansion for BX–265 foam samples.

measured using a type K thermocouple placed on the upper surface (the surface being imaged) of the foam. The sample was heated from underneath using a resistance heater. The temperature was increased in small intervals from 20 °C (68 °F) to no more than 220 °C (428 °F). Several areas were imaged, and the same areas were tracked at each temperature. The size of the cells was measured in directions both parallel and perpendicular to the rise direction. Any change in cellular dimension could then be measured and the thermal strains calculated. Note that the view is the surface "half-cell" and the top half of the cell underneath. While the top half-cell is open and does not contain the cell gas, it acts more of an indicator for what is happening in the cells below the surface.

Figure 13 shows an image of a larger cell at the peak expansion strain temperature of 150 °C (302 °F). The outline of the cell at this temperature is given by the white elliptical-shaped cell in the middle of the photograph. The dotted yellow line indicates the cell outline at 20 °C before the test. This outline was transcribed from another image onto this figure. The dotted red line outlines the cell after cooling back down to 20 °C from the maximum temperature of 220 °C. A number of observations can be made in this figure. First, the cell clearly grows with temperature to the peak strain temperature. Note that the cell expands more perpendicular to the long dimension of the cell (i.e., perpendicular-to-rise direction) than in the rise direction. Second, upon returning to 20 °C after heating, the cell is smaller in the width direction than it is at 150 °C, but larger than it was originally before the test. These observations are all consistent with the thermal expansion data for blocks of foam shown previously.

Measurements of the principal cell dimensions were taken and converted to strains and are given in the table associated with figure 13 for the extreme temperatures. Note that the maximum strain in the perpendicular-to-rise direction for this cell is 28.8 percent. This is similar to the strains measured during a standard CTE test in which the maximum thermal strains measured in the perpendicular-to-rise direction were between 18 and 26 percent. This is shown in the column marked "bulk," meaning that this column represents expansion strains measured in the block of foam. Peak strains between 5 and 8 percent were

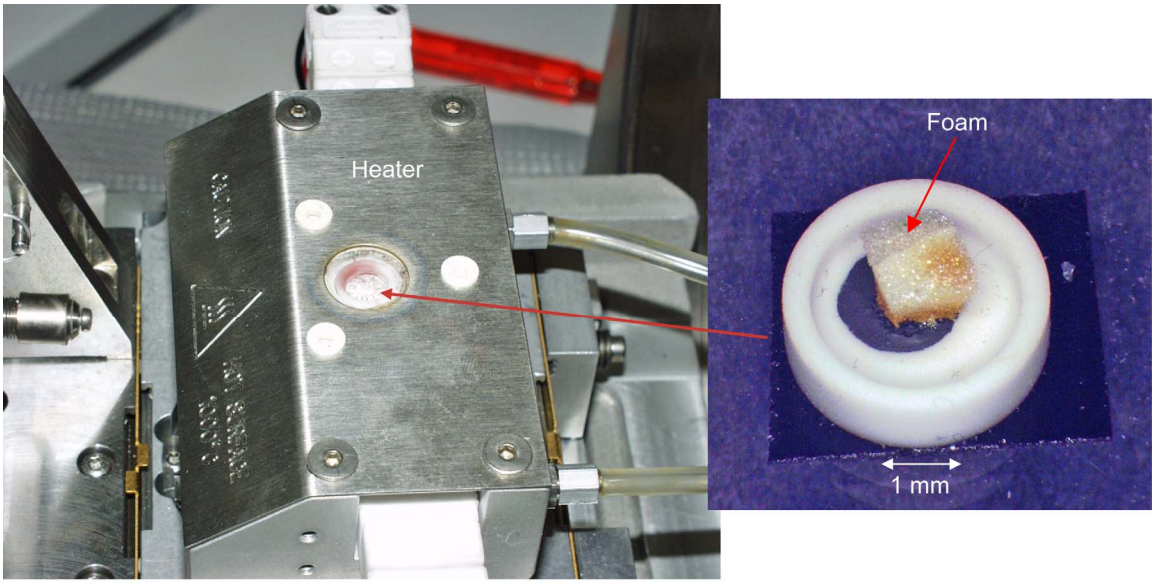

Figure 12.—Hot stage setup for heating BX–265 foam in scanning electron microscope (SEM).

Temperature, °C	Strain (with respect to initial state), percent			
	Perpendicular to rise		Parallel to rise	
	Bulk	Cell	Bulk	Cell
20	0	0	0	0
150	18 to 26	28.8	5 to 8	6.6
20	4	13.6	–2	–4.6

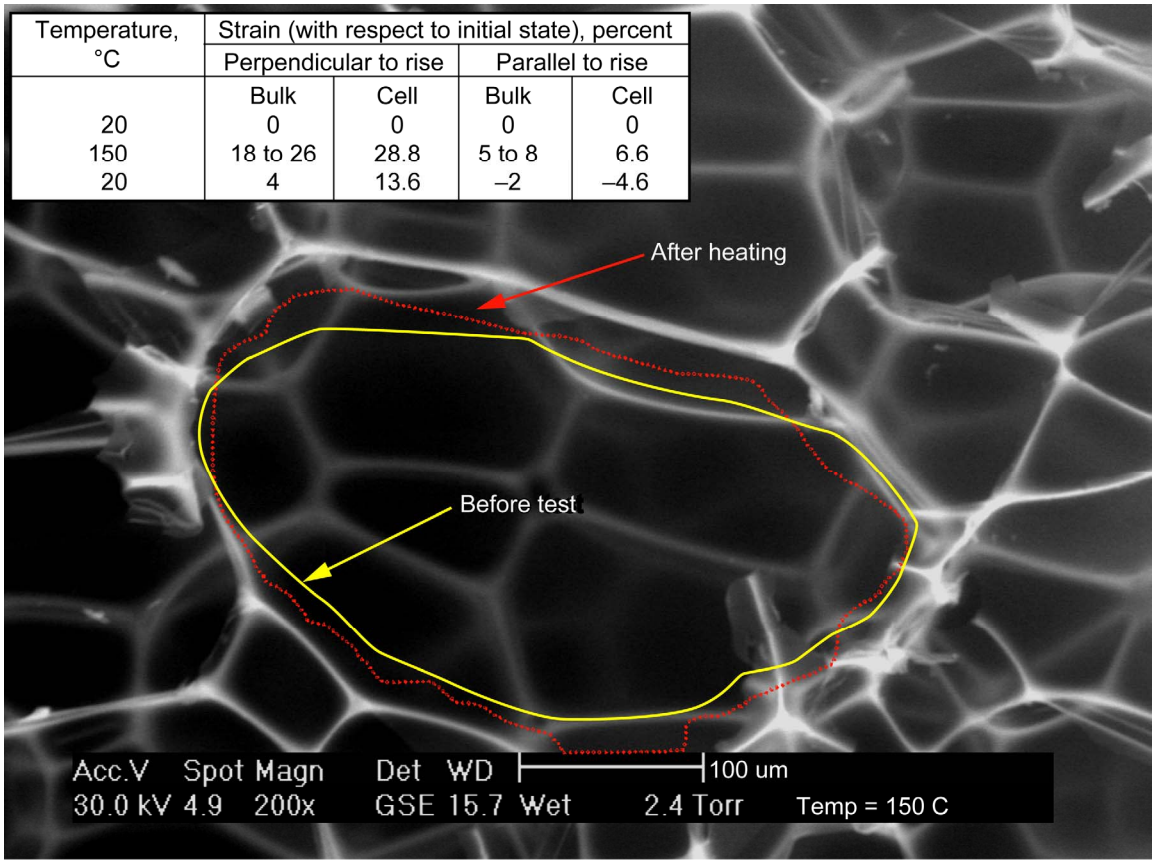

Figure 13.—BX–265 foam cell wall movement upon heating from 20 to 220 °C, then cooling back to 20 °C. Figure shows cell wall at peak strain at 150 °C and outlines initial and final positions.

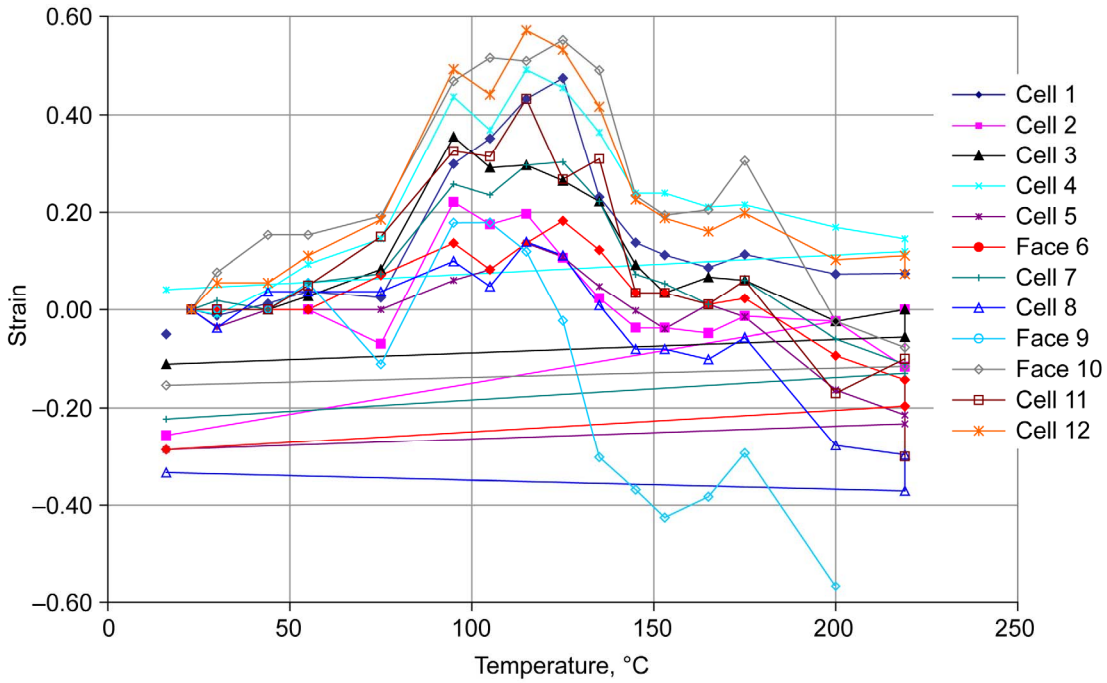

Figure 14.—Thermal expansion of individual cells for BX–265 foam, perpendicular-to-rise direction.

observed in the bulk foam measurements shown in figure 10 for an expansion in the rise direction and are in agreement with the single-cell measurement of 6.6 percent along the cell height as shown in figure 13. Thus there is definitive evidence that the individual cells expand upon heating. Likewise, they shrink upon cooling back to 20 °C as is shown in the last row of the table in figure 13.

Although this discussion involved only the single cell shown in figure 13, a number of cells were actually measured from SEM photomicrographs, and a compilation of these measurements is shown in the plots in figures 14 and 15. Expansion measurements in the perpendicular-to-rise direction for 12 cells are shown in figure 14. The same general trend in strain is observed as a function of temperature for each cell as was observed in the measurements on the bulk foam. The peak strains occurring at approximately 150 °C range from 16 to 60 percent with an average over the 12 cells of 31.4 percent. This is a bit higher than the peak strains observed in the bulk foam, where there are many more cells included in the foam response. The knit lines have also been shown to affect expansion in the bulk foam, and this could also explain the difference in average expansion. The cells on the free surface may also experience more expansion and account for this difference. It can also be observed in figure 14 that the strain upon cooling back to 20 °C is negative for some cells. This is not unexpected since the maximum temperature observed in these tests was 220 °C. Further discussion of this shrinkage will be provided at the end of this section.

Expansion measurements taken in the rise direction for the same 12 cells is shown in figure 15. A similar trend is observed for expansion strain as a function of temperature as observed in the measurements on the bulk foam. The peak strains for the 12 cells range from 3.5 to 21 percent with an average of 12 percent. This average is again slightly higher than the 7 percent seen in the expansion measurements on bulk foam (fig. 10), but is significantly less than that measured in the perpendicular-to-rise direction. The strains in the rise direction are again negative for all 12 cells upon cooling back to 20 °C. The slope of the cooling curve is approximately 3×10^{-4}/°C (1.7×10^{-4}/°F) when averaged over all cells (in both directions), which is in agreement with the values of 1 to 2×10^{-4}/°C (5.6×10^{-5} to 1.1×10^{-4}/°F) calculated from the bulk CTE curves (figs. 2 and 10).

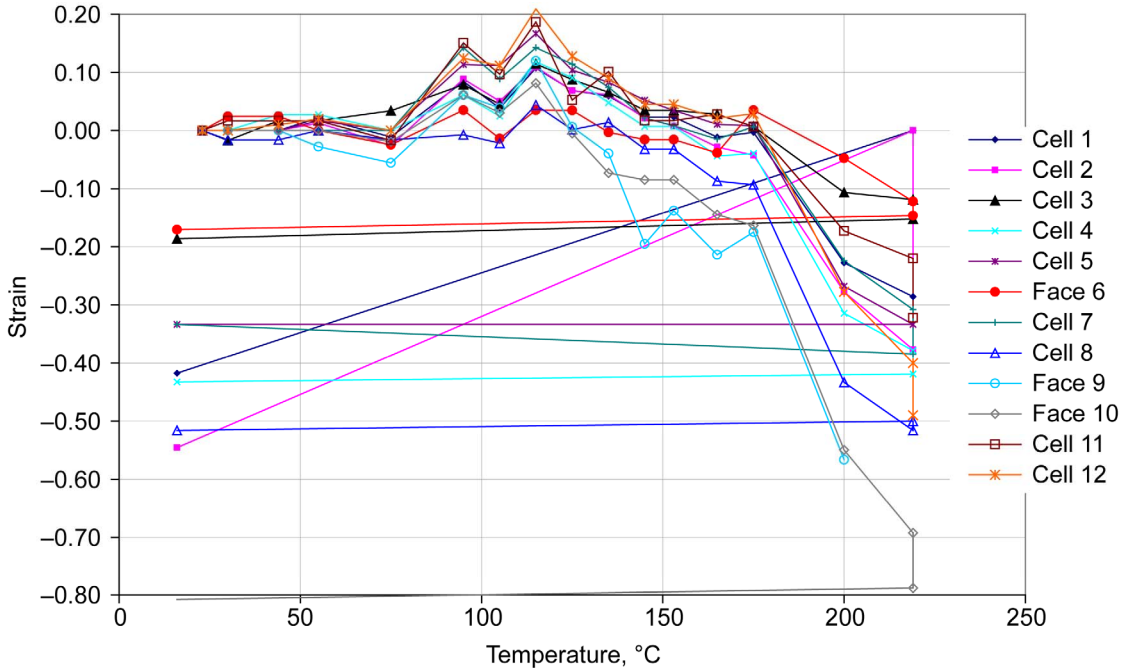

Figure 15.—Thermal expansion of individual cells for BX–265 foam, rise direction.

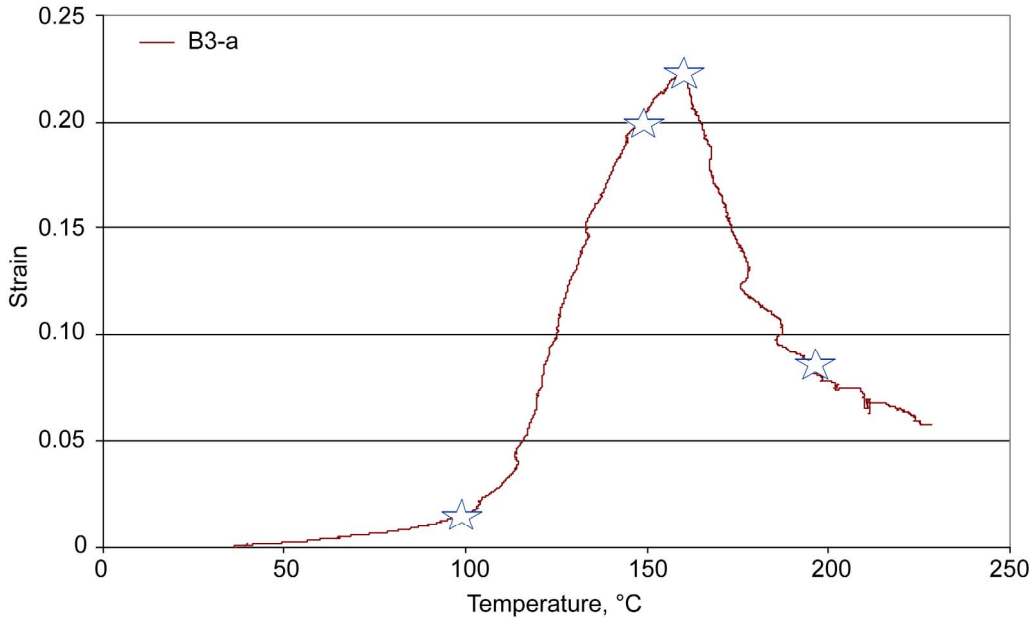

Figure 16.—Thermal expansion tests of BX–265 block 3 sample interrupted at indicated temperatures, perpendicular-to-rise direction.

Further studies of the mechanisms occurring during thermal expansion were done by interrupting heating experiments at various temperatures, cooling the samples down to room temperature, slicing the sample, and examining foam cells in the SEM. Samples were taken at the points along the expansion curve shown in figure 16. The temperatures chosen were 100, 148, 160, and 196 °C (212, 298, 320, and 385 °F). These represent the points along the CTE curve at the beginning of rapid expansion, near-peak expansion, peak expansion, and contraction, respectively. No discernable damage could be observed for

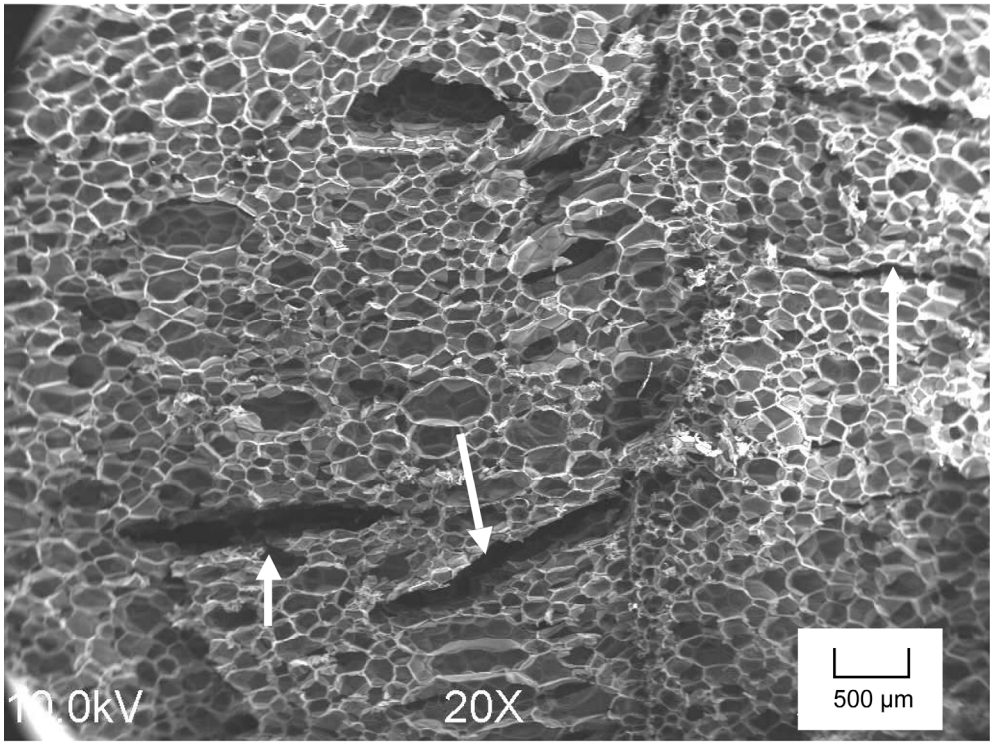

Figure 17.—Large cracks (arrows) in BX–265 block 3 foam after heating to 160 °C.

the samples heated to 100 and 148 °C, as compared with the initial state. Note that there is always some surface damage present due to sectioning of the samples. We discounted this and tried to focus on the cells immediately below the surface for evidence of cracking. We believe that some small cracks and wrinkling of the cell faces occur over this temperature range, but this would require substantially more work to verify. At 160 °C, which is at the peak strain, the foam samples contain several very large cracks (fig. 17) of approximately 1 mm (0.04 in.) in length. These cracks run parallel to the rise direction—along the long dimension of the cells—and they extend over a number of cells. Although it might appear that these cracks are somehow related to the knit line as shown in figure 17, we did not find any evidence of this. It is simply a coincidence that there is a knit line nearby in this photo. After heating to 196 °C, the cracks were even larger (fig. 18) being on the order of 2 to 2.5 mm (0.08 to 0.10 in.). It was also observed that a large number of cell faces were perforated (see fig. 19).

Cracks in the foam typically start as tears in the faces of cells (fig. 20) and terminate when reaching the cell edges (fig. 21). This indicates that the weak part of the cell is the cell face. As the local stress continues to increase, the cell edge will eventually break. The edges, because of their added thickness, are stronger.

One type of modeling we are pursuing is a micromechanics approach. For an accurate model to be developed, accurate properties are needed for the polymer solid. To this end, we attempted to determine the thermal expansion properties of the polymer skeleton by conducting further experiments in the hot stage by monitoring various polymer segments that were parts of cut or broken cells. This eliminated any effects of the pore pressure on the expansion, such that the polymer skeleton could vary on its own as the temperature changed. Examples of this are shown in figure 22, in which several polymer fragments can be observed. The arrow indicates one of these fragments. The figure shows the changes in the size of the polymer fragments at the initial temperature, the maximum temperature, and again after it was cooled down to 20 °C. By measuring the length of the edges, the expansion strain of the polymer could be calculated. Figure 22 shows that the polymer has contracted at the maximum temperature and has contracted even more after cooling back down to room temperature. A plot of expansion strain versus temperature for various edges is shown in figure 23. All nine of the measurements were averaged, and a

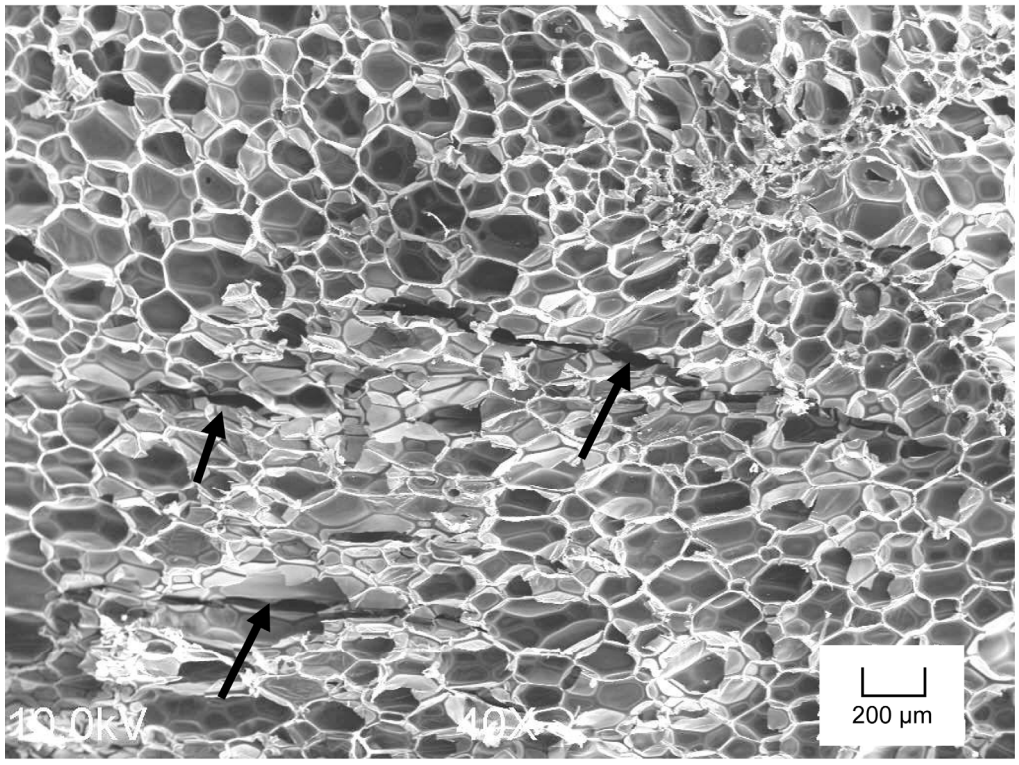

Figure 18.—Larger cracks (arrows) in BX–265 block 3 foam after heating to 196 °C.

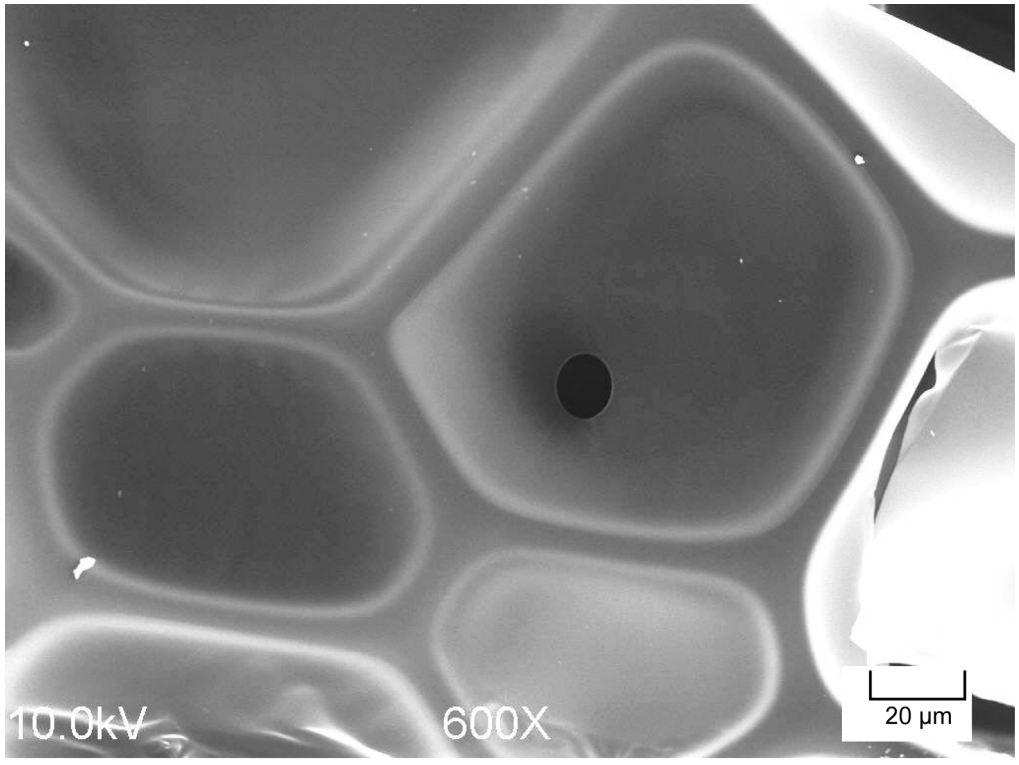

Figure 19.—Perforation in cell face of BX–265 block 3 foam after heating to 196 °C.

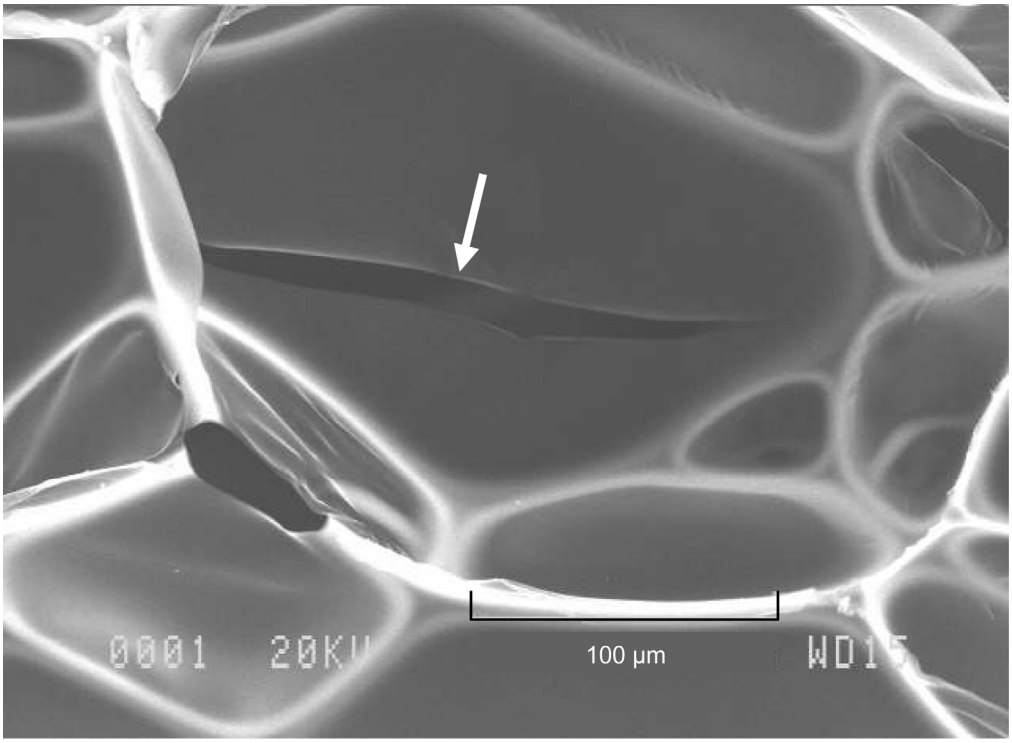

Figure 20.—Tear (arrow) in cell face of BX–265 block 3 foam after heating to 160 °C.

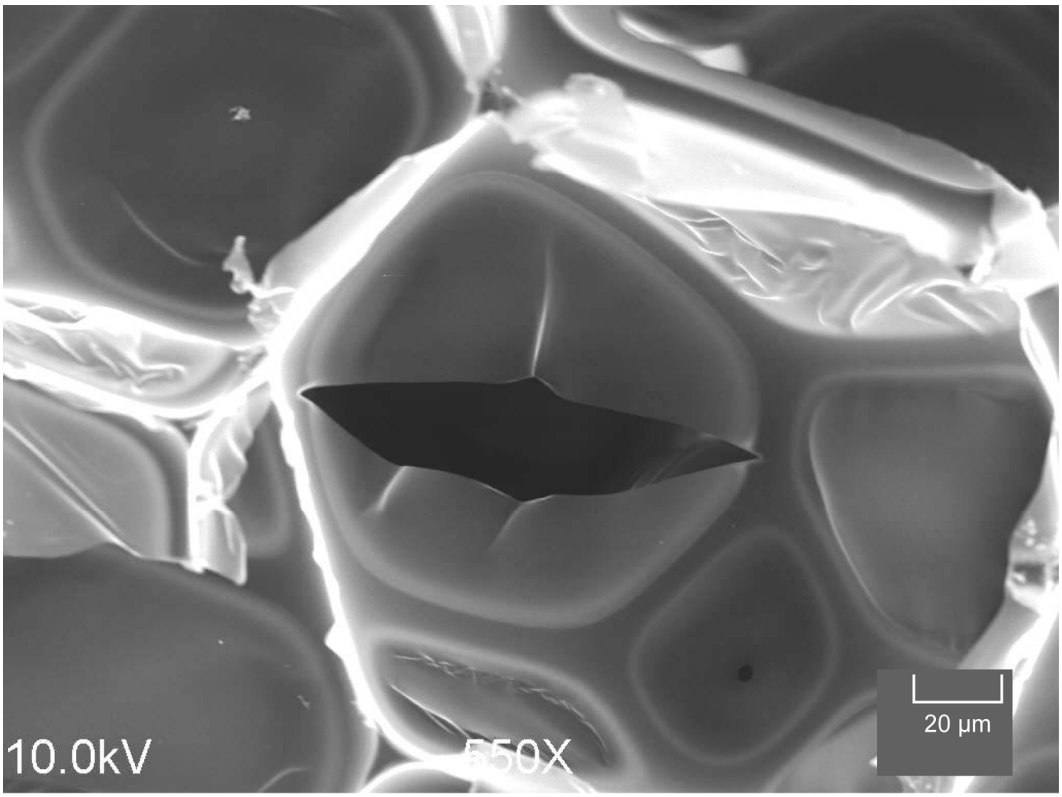

Figure 21.—Crack contained by cell face in BX–265 block 3 foam after heating to 196 °C.

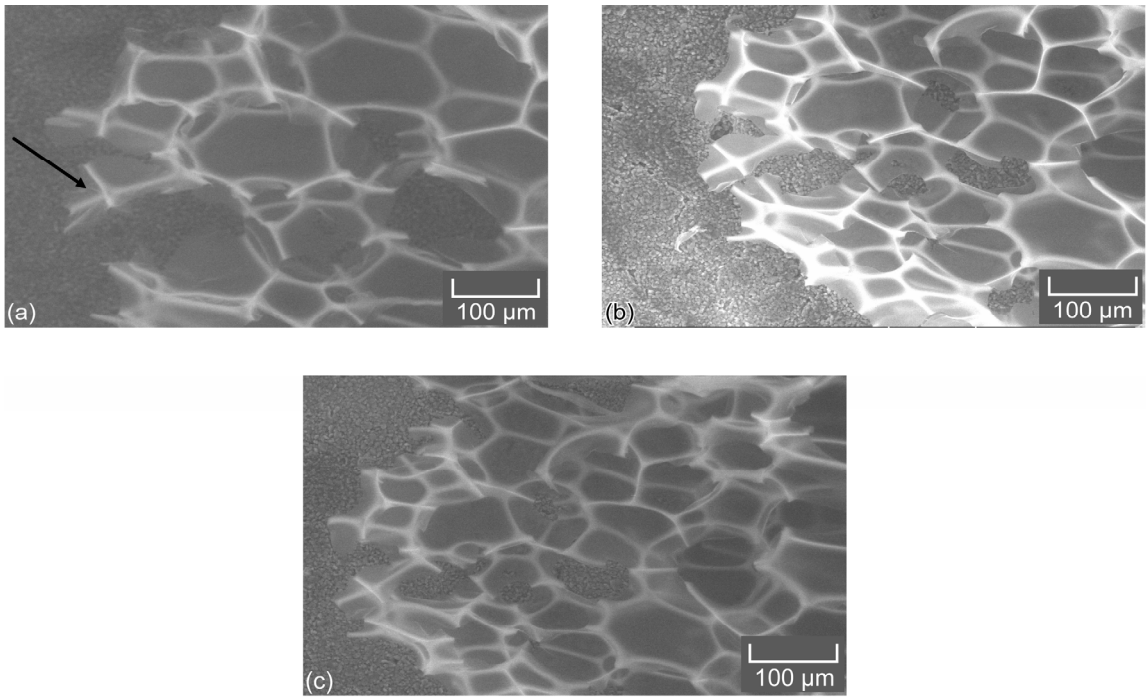

Figure 22.—BX–265 foam polymer fragments in SEM hot stage upon heating then cooling. Arrow indicates fragment. (a) Initial state, 20 °C. (b) Heated state, 175 °C. (c) Cooled state, 20 °C.

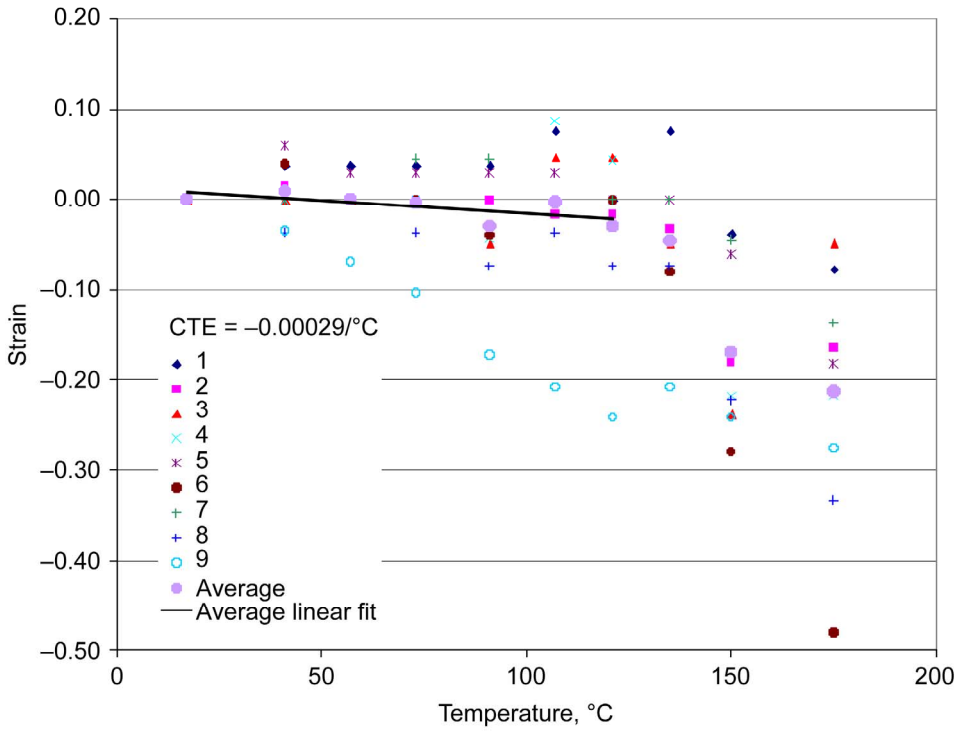

Figure 23.—Thermal expansion of BX–265 LOX block polymer skeleton. Average linear fit to 120 °C is the coefficient of thermal expansion (CTE), equal to –0.00029/°C.

slope (CTE) was fit to temperatures between 20 and 120 °C (68 and 248 °F) assuming a simple linear fit. The slope was -2.9×10^{-4}/°C (-1.6×10^{-4}/°F) and indicates that the polymer tends to contract as temperature is raised above room temperature. Above 120 °C, the polymer contracts at an even larger rate, and the CTE is on the order of -3×10^{-3}/°C (-1.7×10^{-3}/°F).

Thermogravimetric Analysis

Thermogravimetric analysis (TGA) was performed on the BX–265 foams in a commercially available unit. We wished to know the amount of polymer decomposition that occurred during heating, which could produce additional gases inside the foam cells. Various heating rates were used from 1 to 133 °C/min (2 to 239 °F/min). The analyses were performed in air, nitrogen, and a partial vacuum of 5.5 kPa (0.8 psia). The partial vacuum was chosen to simulate the atmosphere at 82 s after liftoff into the shuttle launch, the point at which *Columbia* was impacted by a piece of foam debris. TGA was conducted on specimens taken from blocks 1 to 3 and the LOX block in both block and ball-milled powder form. The powder results are mostly presented in this report (the results of the block forms were similar). Effluents were analyzed using infrared spectroscopy. TGA was also performed on moisture-conditioned and dried foams.

Samples of powder taken from BX–265 foam blocks 1 to 3 were tested for weight loss as a function of temperature. Figure 24 shows the results from each of the three blocks of foam at a heating rate of 1 °C/min in air. Note that there is excellent reproducibility among the tests.

Figure 24 shows that the foam loses weight immediately upon increasing the temperature above 20 °C (68 °F). In the first 200 °C (392 °F) the foam loses approximately 4 percent in weight. At 200 °C (392 °F) there begins a rapid loss in weight. There is an intermediate rate change that occurs between approximately 300 and 400 °C (572 and 752 °F) during which the weight loss occurs at a slower rate. At

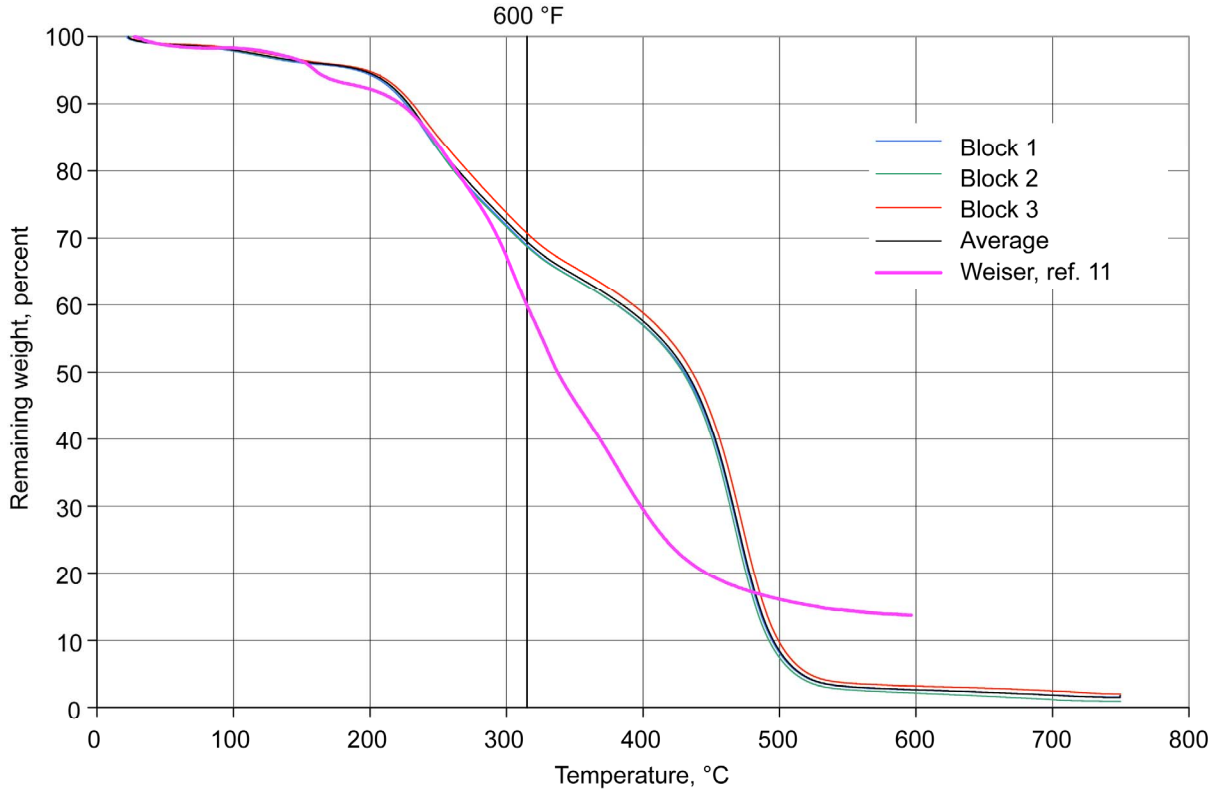

Figure 24.—Weight loss versus temperature for BX–265 powder, blocks 1 to 3, heated 1 °C/min in air. Data from Weiser (ref. 11) shown also.

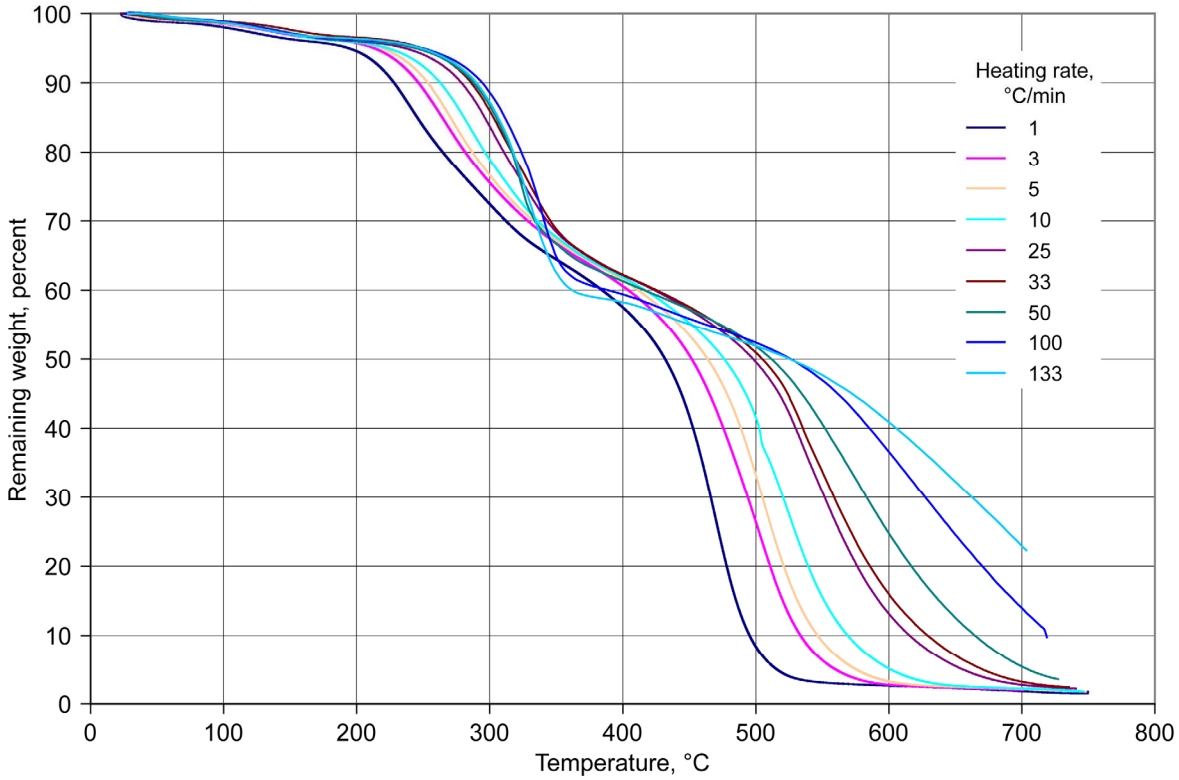

Figure 25.—Weight loss in air versus temperature at different heating rates for BX–265 powder, blocks 1 to 3.

still higher temperatures, the foam continues its rapid weight loss until the sample is almost completely consumed above 500 °C (932 °F), having a remaining weight of only 3 percent. Data from Weiser et al. (ref. 11) is also reproduced in figure 24; their foam is from the same supplier. The TGA behavior for this batch of BX–265 is slightly different, and they observed no plateau at intermediate temperatures as was observed in the current study. This may suggest some change in the polymer formulation by the supplier between the two timeframes.

The effect of heating rate on the weight loss of the foam is shown in figure 25 for tests conducted in air. The general trend is that the higher heating rates shift the weight loss curves to the right. The higher the heating rate, the more the curve is shifted. Hence at faster rates, the foam has lost less weight at any given temperature, which is a classic display of weight loss behavior associated with a kinetic process. At the two fastest heating rates, 100 and 133 °C/min (180 and 239 °F/min) there is an intermediate temperature regime over which more weight is lost at the faster rates than at the slower heating rates. One possible explanation is that a different rate reaction occurs at the faster heating rates. Another possibility is that there may be a thermal inertia effect associated with the experimental setup, in which the thermocouple reading is lagging behind the temperature of the specimen for the fast rates.

It should be kept in mind that the rate of heating of the foam during ascent was assumed to be 150 °C/min (270 °F/min). Therefore any calculations of weight loss made with slower heating rates will have to be adjusted using Arrhenius rate equations. For modeling purposes, we are only interested in foam decomposition up to 315 °C (600 °F), which is the estimated highest temperature that foams experience during ascent of the shuttle due to foam erosion on the outer surface. An enlargement of the temperature regime of interest is shown in figure 26. For any given heating rate, the weight loss curve can be approximated as bilinear. The portion at lower temperatures represents foam losing weight at a rate of

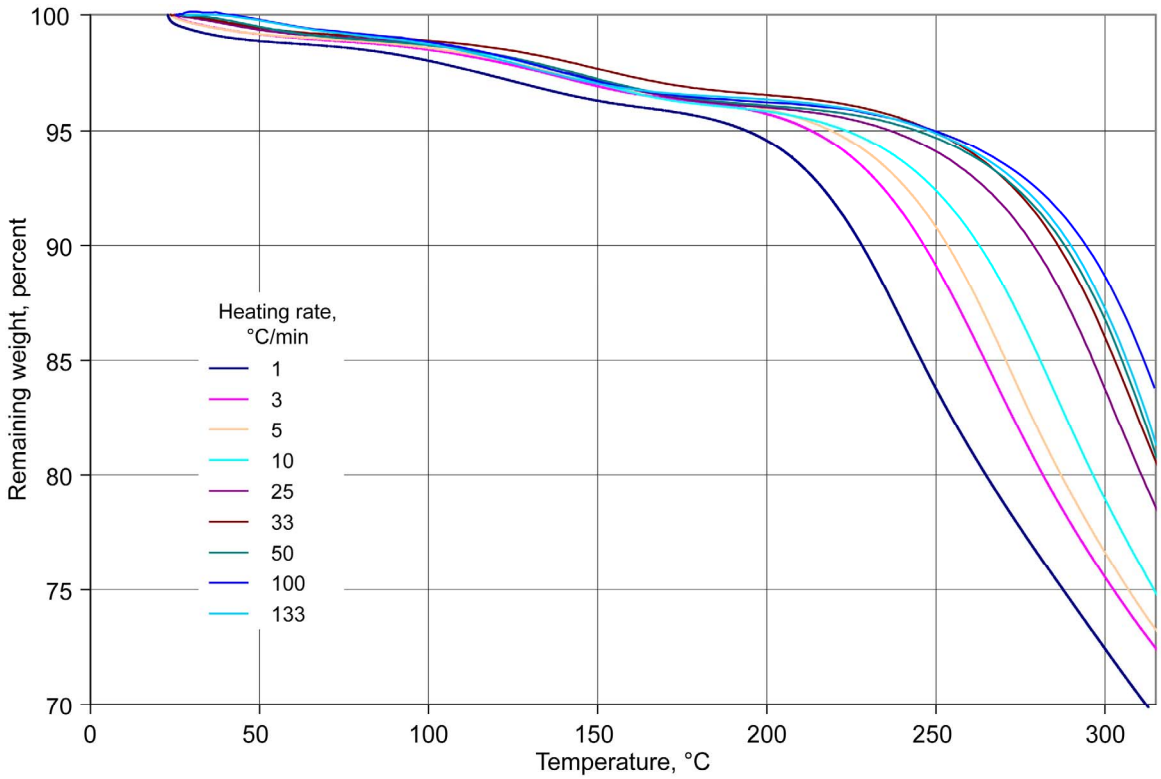

Figure 26.—Enlargement of portion of figure 25: Weight loss in air versus temperature at different heating rates for BX–265 powder, blocks 1 to 3.

0.025 percent/°C (0.014 percent/°F), and the portion at higher temperatures at a rate of 0.25 percent/°C (0.14 percent/°F). Note that at the lower temperatures, the weight loss curve could be considered as heat rate independent. This is not true at higher temperatures where gases are released from the polymer. Infrared spectroscopy of the effluents identified the species to be water at lower temperatures, chlorofluorocarbons at temperatures of 150 °C (302 °F), and carbon dioxide starting at 200 °C.

TGA was also conducted in nitrogen to see if there is an effect of oxidation on foam decomposition. The average curves are given in figure 27 for different heating rates. An expanded version of this graph is given in figure 28, showing the regime of importance for the shuttle. The results are similar to those shown for the tests conducted in air (fig. 26). A comparison is given in figure 29 for two heating rates (1 and 10 °C/min, or 2 and 18 °F/min). There is a slight difference between the air- and nitrogen-tested samples with the nitrogen-tested samples decomposing slower than the air-tested. At temperatures above 300 °C the difference widens. Figure 30 is an expanded view of this graph. Note that the data in figure 29 are all from block 1 and we expect any specimen-to-specimen scatter to be negligible, based on the results of figure 24.

The specimens tested in a vacuum of 5.5 kPa (0.8 psia) are also shown in figures 29 and 30, which indicate that they decompose at a faster rate than both their air- and nitrogen-tested counterparts at temperatures less than 315 °C (599 °F). At higher temperatures, this trend is reversed, and the air samples decompose faster than the samples tested in either vacuum or nitrogen. At the highest temperatures, the specimen tested in vacuum at a heating rate of 10 °C/min loses the least amount of weight of all of the conditions tested. This study shows that both the environment and the heating rate influence the rate of weight loss.

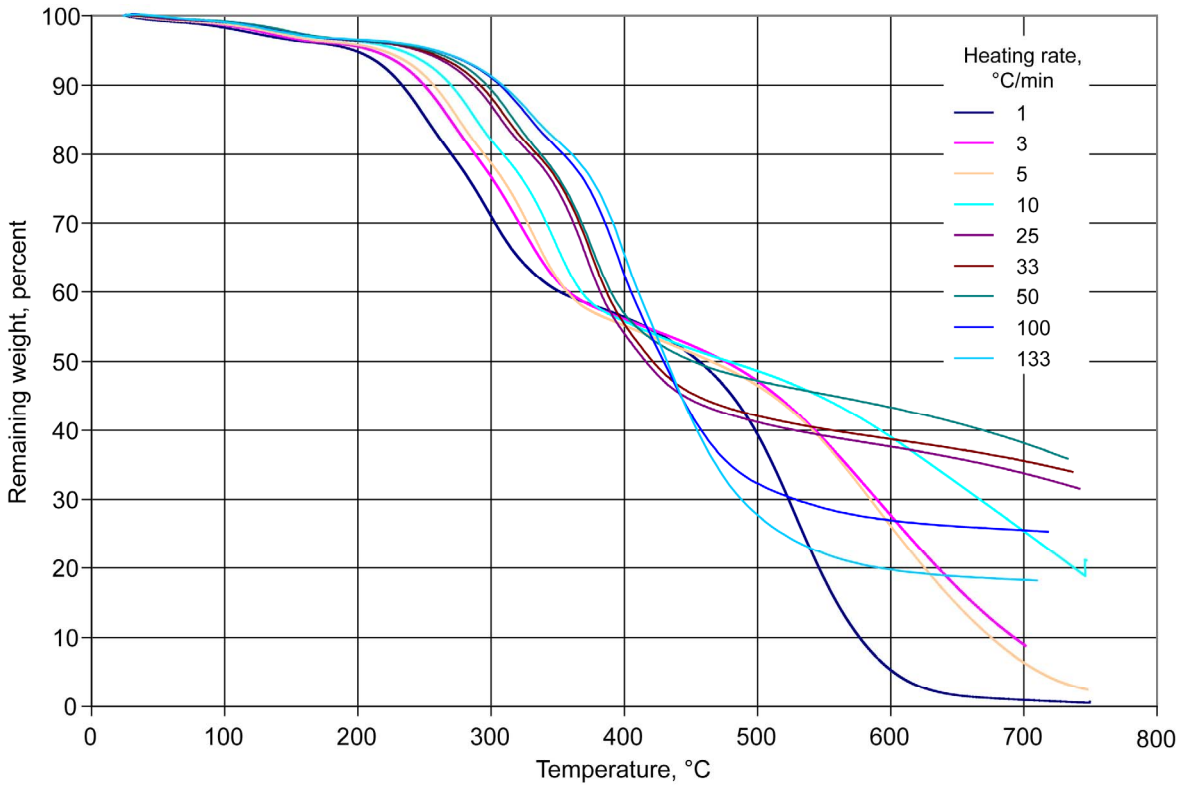

Figure 27.—Weight loss in nitrogen versus temperature at different heating rates for BX–265 powder, blocks 1 to 3.

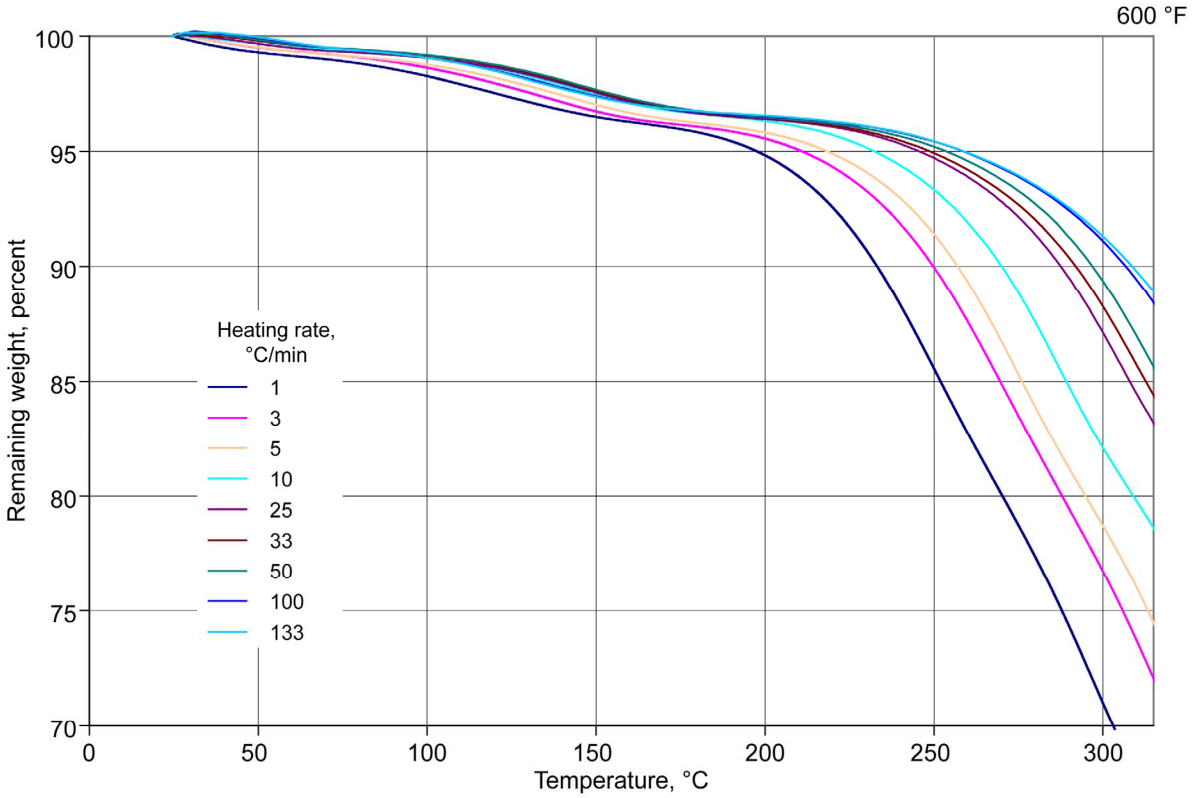

Figure 28.—Enlargement of portion of figure 27: Weight loss in nitrogen versus temperature at different heating rates for BX–265 powder, blocks 1 to 3.

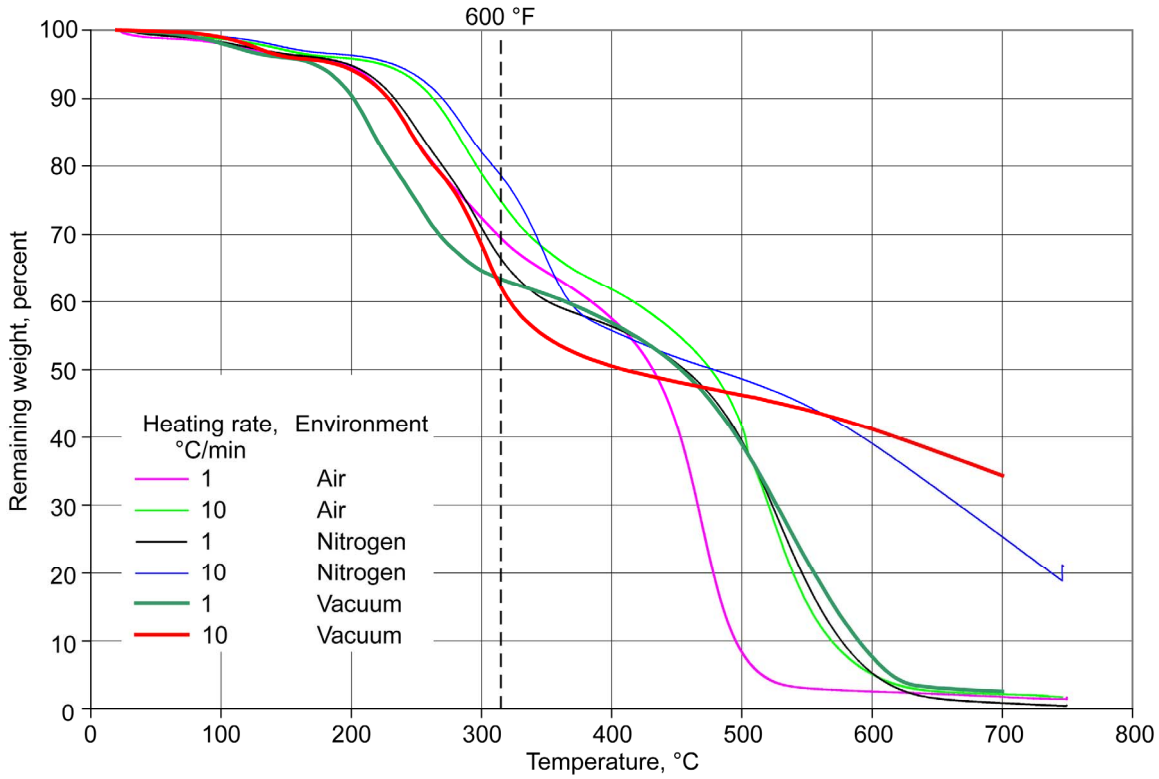

Figure 29.—Weight loss versus temperature for BX–265, block 1 powder in various environments at different heating rates, where “vacuum” is 5.5 kPa.

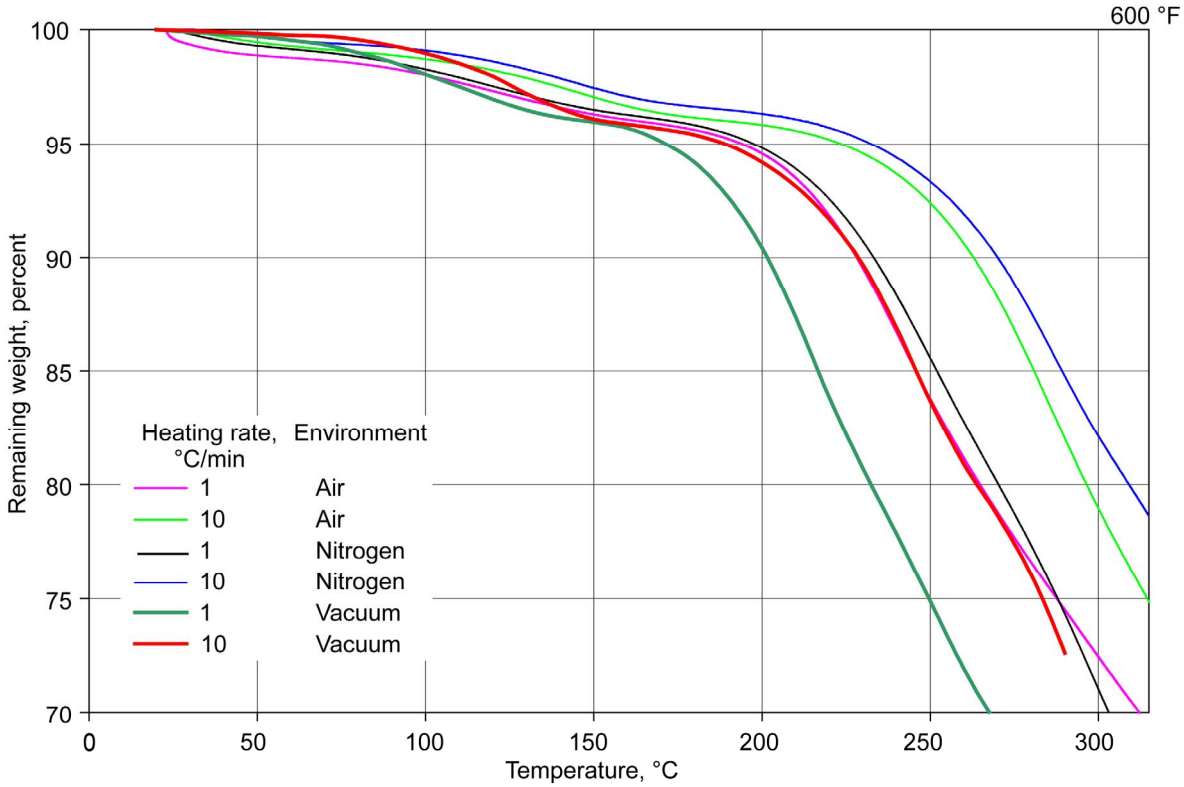

Figure 30.—Enlargement of portion of figure 29: Weight loss versus temperature for BX–265 powder, block 1, in various environments at different heating rates, where “vacuum” is 5.5 kPa.

Foam Conditioning

This section deals with the amount of moisture in the foam and its effect on thermal expansion. There are a few reasons why we wished to pursue this. First, the large peak in the thermal expansion curve (fig. 2) was hypothesized to be partially a result of the decomposition of the foam and a subsequent increase in the pore pressure. Water vapor could be one contributor to the increased pore pressure. Second, we were concerned about the ability of the foam to absorb or lose moisture based on the ambient humidity, causing a change in properties of the foam. We pursued this by conditioning foam samples cut from larger blocks in either a humidity chamber or a drying oven. The surfaces of the foam were not sealed, but left in the as-cut condition. The drying oven consisted of a roughing pump hooked to a small sample oven. The temperatures chosen for drying were 20 and 40 °C (68 and 104 °F). The 40 °C temperature was chosen based on a compromise between having a sufficiently high temperature to drive out free water, but not too high to significantly change the polymer based on both the thermal expansion behavior and the TGA curves. Also, 40 °C is a temperature not too unrealistic for a hot day in the southern United States where the ET spends its time on Earth. Moisturizing was accomplished by placing the samples in humidity ovens set to 40 °C at 95 percent relative humidity (RH). Various sample sizes were used to see if percent changes in weight varied as a function of sample size. The CTE samples (typically 13 by 13 by 51 mm, or 0.5 by 0.5 by 2 in.) were also conditioned and subsequently heated to determine the effects of conditioning on thermal expansion of the foam.

Drying

The results of drying the foam at either 20 or 40 °C can be viewed in figure 31. The percent weight loss is plotted versus cumulative time in the drying oven. The specimens were periodically removed from the oven and weighed promptly after removal. Various samples sizes (see table IV) were used, to provide various volumes and surface areas. The samples dried at room temperature show a rapid decrease in

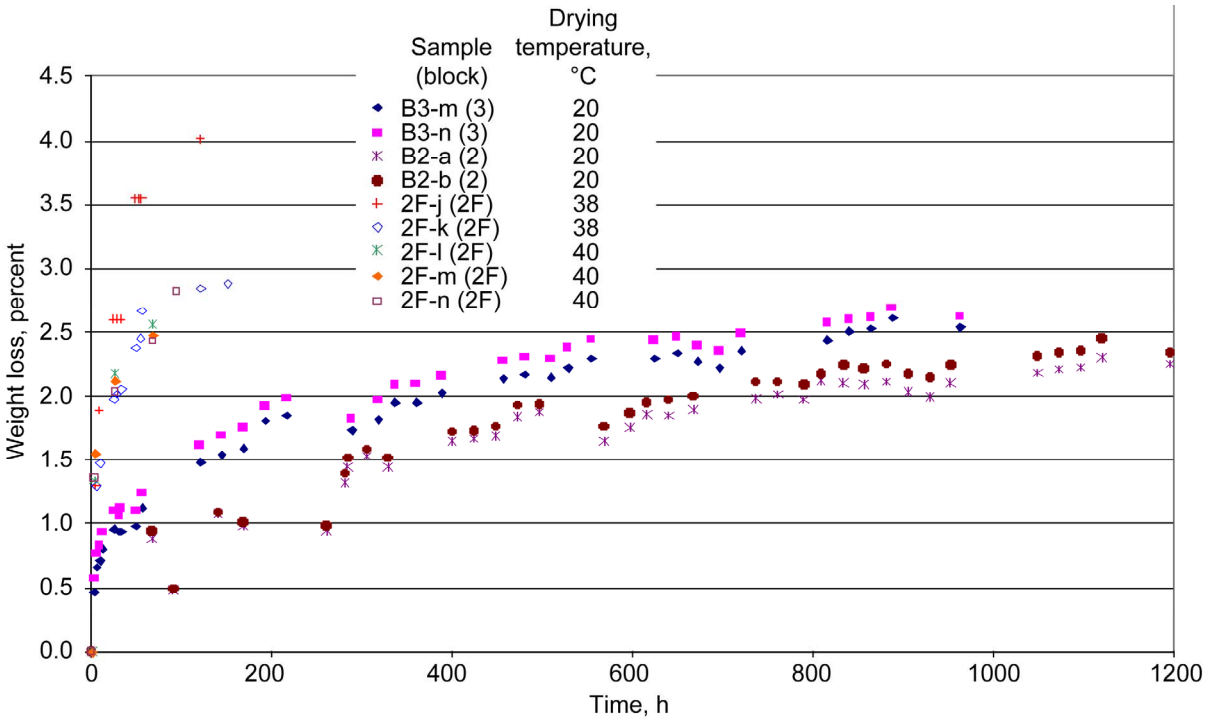

Figure 31.—Weight loss of BX–265 foam samples upon drying in vacuum oven.

TABLE IV.—SAMPLE DESCRIPTION FOR DRIED BX–265 FOAMS

Foam block	Sample number	CTE sample[a]	Conditioning temperature, °C	Dimensions, mm	Knit lines	Density, g/cm^3	Volume, mm^3	Surface area, mm^2	1/thickness, 1/cm
3	B3-m	---	20	38×25×51	?	0.033	29 500	8394	0.39
3	B3-n	---	20	51×25×51	?	.030	51 100	8606	.39
2	B2-a	---	20	33×41×23	?	0.035	32 800	6290	0.43
2	B2-b	---	20	33×25×31	?	.035	24 700	5140	.39
2F	2F-j	√	38	51×6.4×6.4	1.0	0.035	2 100	1370	1.6
2F	2F-k	---	38	51×13×13	1.0	.032	8 200	2900	0.79
2F	2F-l	√	40	51×13×13	1.0	.032	8 200	2900	.79
2F	2F-m	√	40	51×13×13	2.0	.033	8 200	2900	.79
2F	2F-n	√	40	51×13×13	2.0	.033	8 200	2900	.79

[a]Sample also used for thermal expansion tests.

TABLE V.—DESCRIPTIONS OF BX–265 LOX FOAM SAMPLES USED FOR DRYING EXPERIMENTS

Sample number	Sample dimensions, mm			Volume, mm^3	Surface area, mm^2	1/thickness, 1/cm	Density, g/cm^3	Knit lines
	Thickness	Length	Height					
LOX-b	5.51	102.8	8.89	5 100	3 060	1.81	0.0352	1.1
LOX-c	5.56	203.3	8.76	9 800	5 920	1.80	0.0367	0.9
LOX-d	6.88	50.44	6.68	2 300	1 460	1.45	0.0340	1.0
LOX-e	6.93	50.95	6.96	2 500	1 510	1.44	0.0333	0.5
LOX-f	13.2	50.62	14.2	9 500	3 150	0.76	0.0323	1.0
LOX-g	14.5	51.13	13.2	9 700	3 200	0.69	0.0335	1.6
LOX-h	14.4	96.80	13.8	19 300	5 870	0.69	0.0366	2.0
LOX-i	51.46	51.84	51.51	137 000	16 000	0.19	0.0340	6.6
LOX-j	23.3	25.40	25.63	15 000	3 680	0.43	0.0338	3.8
LOX-k	23.2	24.7	24.8	14 000	3 520	0.43	0.0346	3.0
LOX-l	24.4	51.74	23.4	29 000	6 080	0.41	0.0348	3.0
LOX-m	12.5	51.38	13.2	8 500	2 970	0.80	0.0357	2.0
LOX-n	13.5	50.98	12.4	8 500	2 970	0.74	0.0401	2.8
LOX-o	11.3	102.9	14.1	16 000	5 540	0.89	0.0349	1.3
LOX-p	13.5	76.17	13.5	14 000	4 480	0.74	0.0327	1.0
LOX-q	7.49	75.95	7.42	4 300	2 370	1.33	0.0332	1.0

weight over the first 200 h. Thereafter the rate of weight loss decreased until it saturated at 2.5 percent where presumably the equilibrium moisture content was attained. The samples from foam block 3 lost slightly more weight (0.3 percent) than the samples from block 2. Note that both of these blocks were delivered in the same shipment, and it is unknown if they were both cut from the same larger block or if they each represent a different spray run. Nonetheless, this gives some idea of scatter in drying. It can also be observed from these data and table IV that volume of the sample has no effect on weight loss. Surface area may be a factor.

When drying is conducted at a temperature of 40 °C, the amount of weight loss proceeds at a faster rate and the samples lose more weight. After 120 h, sample 2F-j has already lost 4.0 percent in weight and shows no signs of saturation. Since all of these samples were taken from the same foam block (2F), size effects become easier to sort out. Unfortunately only two sizes were employed. These limited amounts of data suggest that size can be a factor, but it could not be concluded what variable of size (e.g., surface area or volume) is important.

To further investigate the size effect, samples of widely varying sizes (fig. 32) were cut from the LOX foam. Their dimensions are given in table V, along with their density and number of knit lines. These samples were dried in a vacuum (1 inHg, or 2.5 cmHg) oven at 40 °C. The weight loss is shown in figure 33 as a function of time. The weight loss trend is similar to that shown in figure 31. However, the

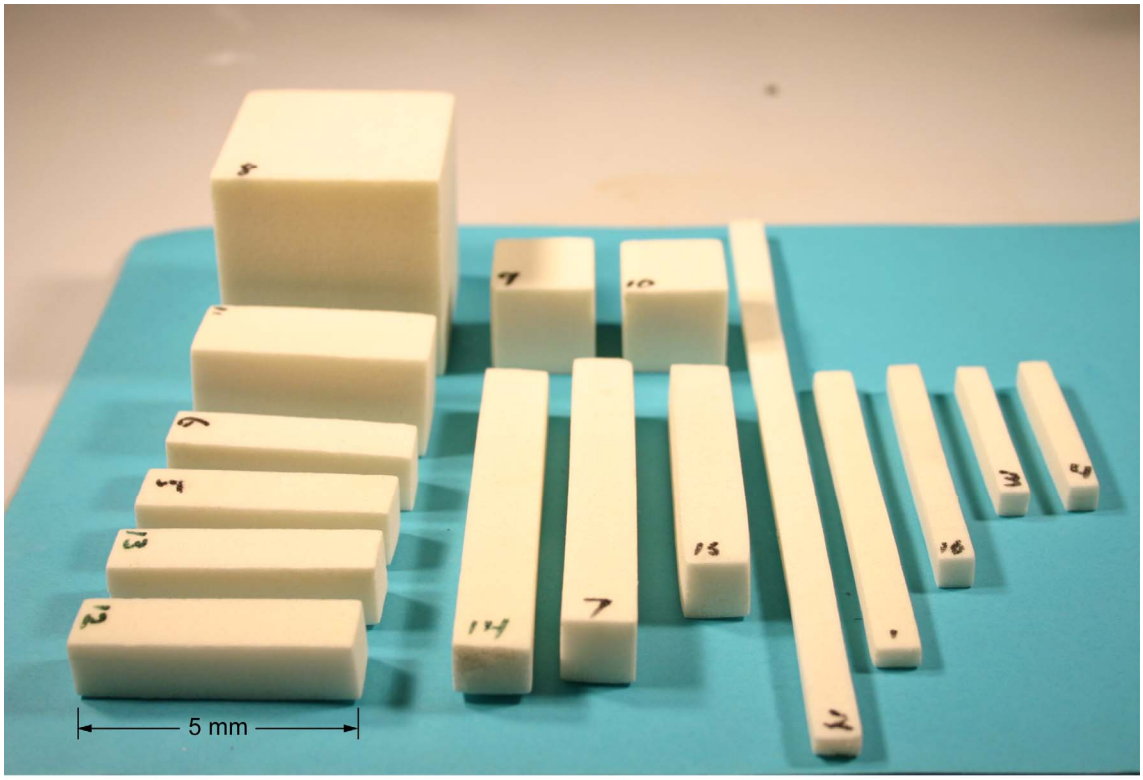

Figure 32.—Samples taken from BX–265 LOX block foam for drying experiment.

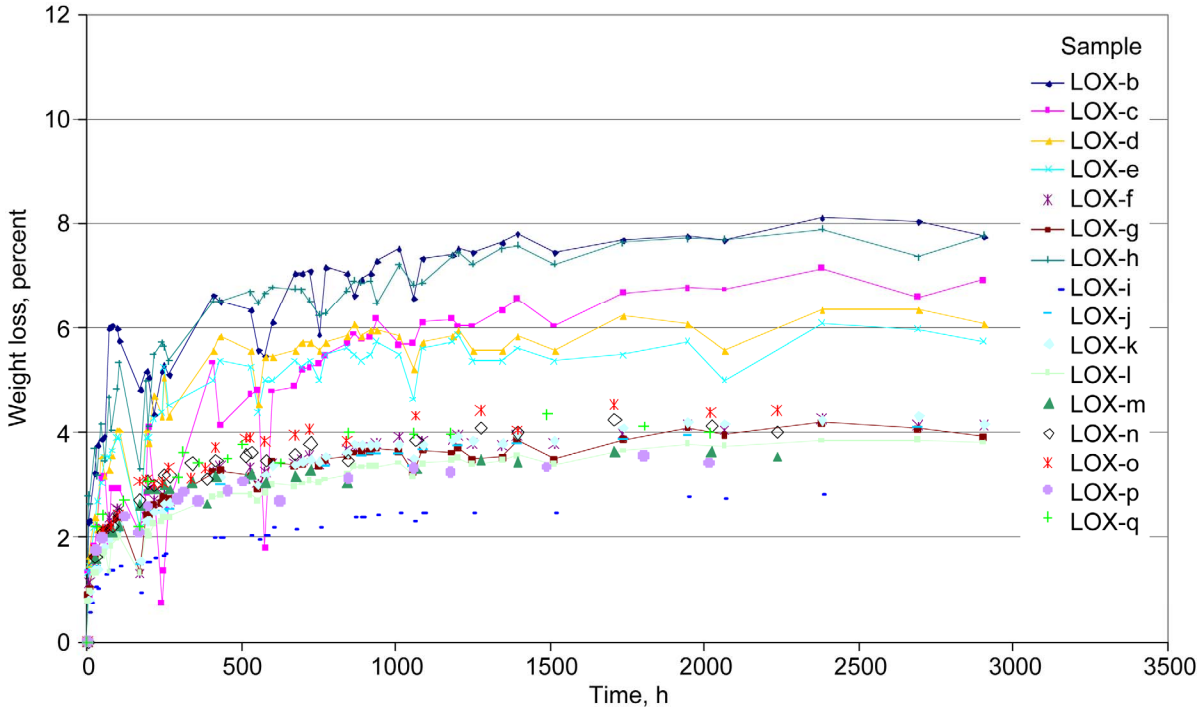

Figure 33.—Weight loss versus time for BX–265 LOX block samples (from fig. 32) in drying oven.

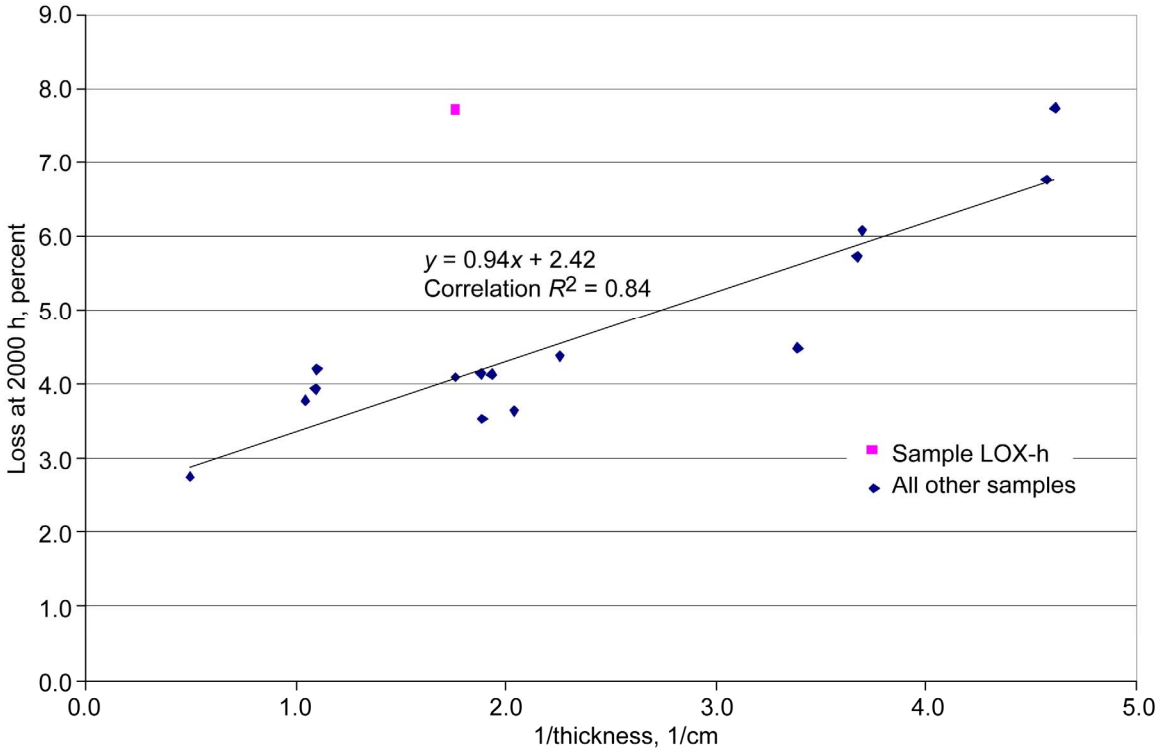

Figure 34.—Effect of thickness on weight loss for dried BX–265 LOX block samples (from fig. 32).

samples in figure 33 were run until the equilibrium moisture content was attained, somewhere between 2000 and 3000 h. Since some of the samples were added later and only accumulated 2200 h, the time to reach the equilibrium moisture content was taken to be 2000 h. It was discovered that weight loss was independent of the density, the number of knit lines, specimen volume, and surface area. However, this experiment did show a strong dependence of weight loss on sample thickness. Thinner samples lost a greater percentage of weight. The weight loss at 2000 h is plotted versus 1/thickness of the sample in figure 34, allowing a straight line to be fitted through the data. Good correlation is achieved except for one specimen: Sample LOX-h had a very high weight loss, yet represents a relatively thick sample. It is unknown why this sample is an outlier.

Four samples from block 2F (table IV) had subsequent thermal expansion tests conducted on them in the perpendicular-to-rise direction. Although a large amount of the moisture has been driven out of the samples, they have not yet reached their equilibrium moisture content during the drying process (see fig. 31). The expansion data are shown in figure 35 along with some selected curves for as-received foam (i.e., not dried). First note that the loops and squiggles in the curves for the dried samples are not a measurement of a true physical event, but are related to temperature oscillations due to poor temperature control. The curves for dried foam show limited expansion at lower temperatures followed by a rapid increase in expansion near 100 °C (212 °F). The peak strain for samples 2F-l and 2F-m occur at a temperature of 130 °C (266 °F), and this is slightly lower than the as-received samples for this same block. Additionally, the peak strains for these two curves are some of the lowest values for peak strains observed for block 2F. However, given the general scatter in the data, a strong conclusion is difficult to make regarding the effect of drying on the value of the peak strain. The cooling curves from the dried samples have the same slope as the cooling curves from nondried samples.

The two additional samples that have been dried show a peak strain at much higher temperatures (~165 °C, or 329 °F). The reason for this is not clear. This difference does not appear to be related to the number of knit lines or the number of drying hours. There is one obvious difference between these two samples and the other two dried samples. These two samples exhibited the highest weight loss during

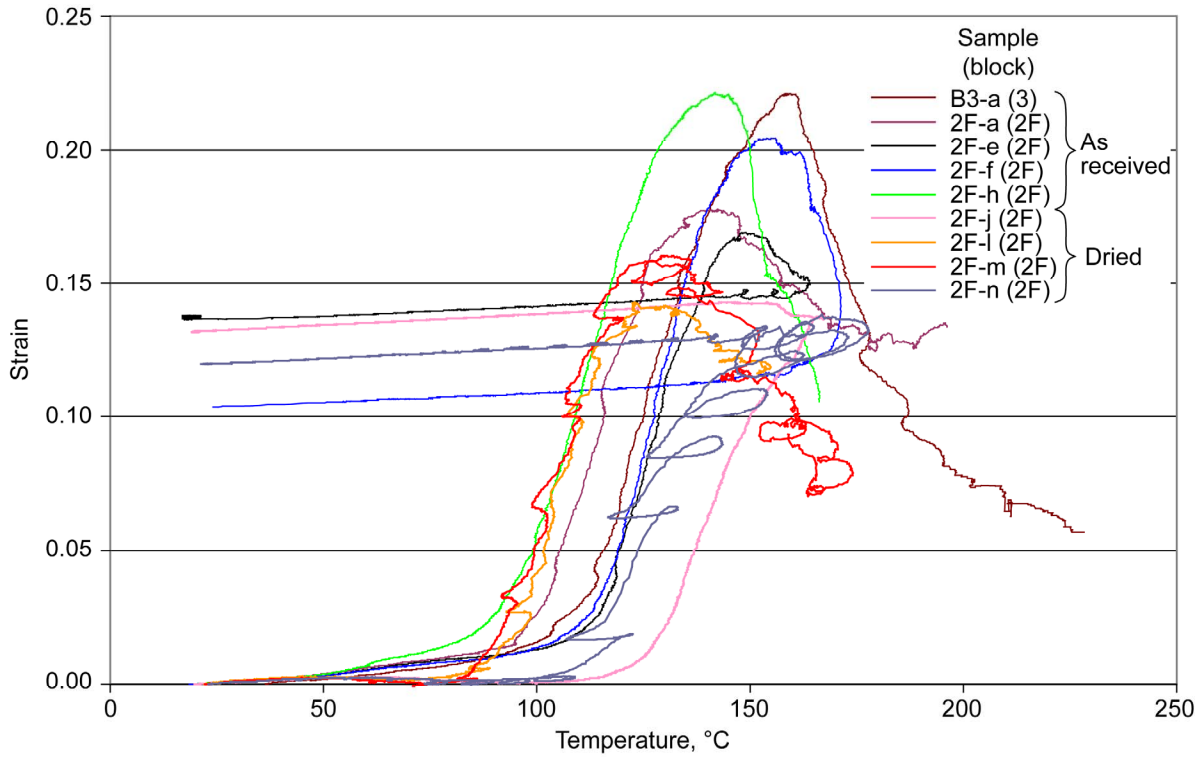

Figure 35.—Thermal expansion in perpendicular-to-rise direction of BX–265 foam samples dried at 40 °C for 72 h with as-received samples included for comparison.

drying. Sample 2F-j had a 4.0 percent weight loss and sample 2F-n had a 2.8 percent weight loss. The other two samples had weight losses of 2.5 and 2.6 percent. Thus it appears as if at higher weight loss, the higher the temperature at which the peak expansion strain occurs. These values of weight loss are shown in figure 36, which is an enlargement of the lower temperature section of figure 35. This figure also shows a change in the low-temperature, minimal expansion rates of dried foams. The dried foams increase similarly to the as-received foams up to a temperature of approximately 45 °C (113 °F), at which point the specimen begins to contract. This contraction continues until the rapid thermal expansion begins at temperatures nearing 100 °C. The exact temperature at which point the rapid increase begins varies between 80 and 110 °C (176 and 230 °F). However as indicated earlier, the higher the weight loss during drying, the higher this temperature becomes.

This weight loss due to drying is at least partially reversible. Table VI presents results for four of the foam samples that were dried from table IV and figure 31. After drying, they were removed from the dryer, left in ambient air (21 °C (70 °F) at 25 percent RH) and periodically weighed. Figure 37 shows that the foam regains as much as 1 percent weight over a 72-h period just from sitting in a room. This represents 40 percent of the weight loss due to drying. After 72 h there is minimal change in weight. This weight gain does not seem to be dependent on the size of the sample, although the data are too sparse to draw much of a conclusion.

A longer term and more detailed study on weight gain was performed as an extension of the drying test shown in figure 33. At the end of the drying test, the same 16 samples were removed from the oven, stored in the laboratory (19 °C (66 °F) at 60 percent RH), and periodically weighed up to 2480 h (103 days). The weight gain (fig. 38) from sitting in ambient humidity for 2480 h varied from 2.7 to 3.9 percent. Depending on the specific sample, the amount of weight gain was between one half to the full amount of weight loss observed from the previous drying test. It appears that the amount of weight gain is inversely proportional to sample thickness; thicker samples gain less percentage weight.

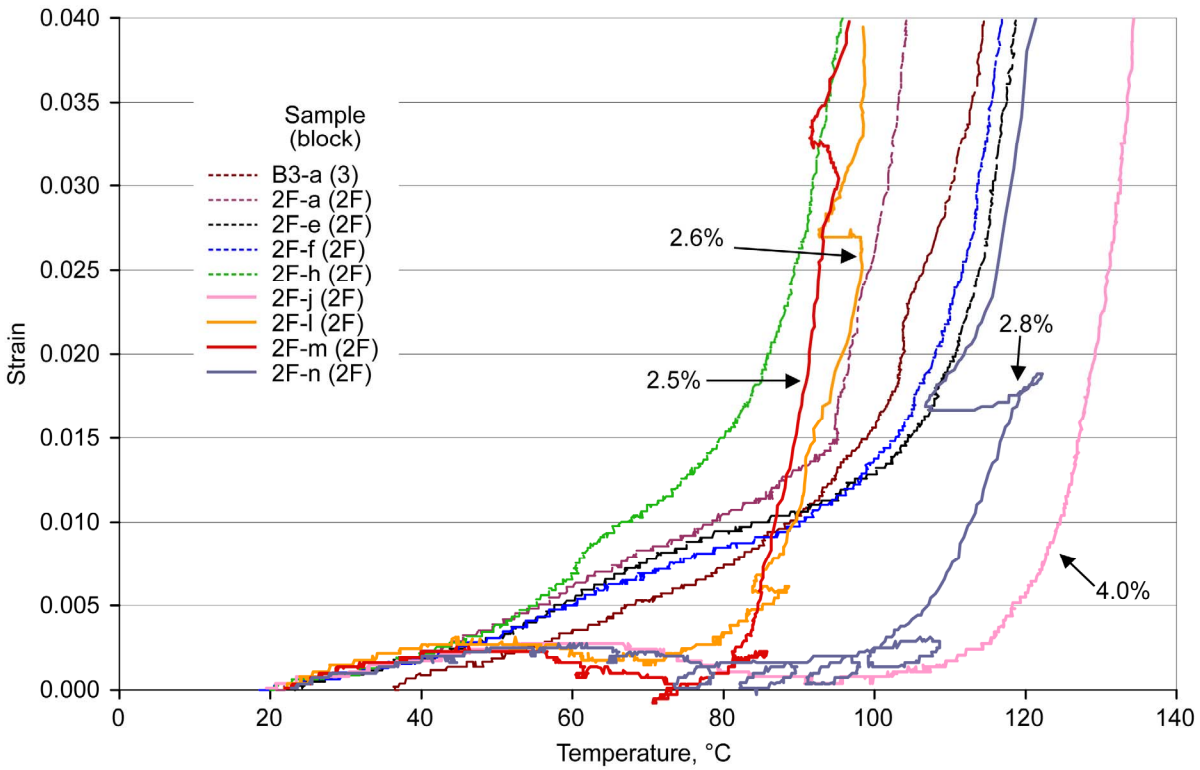

Figure 36.—Enlargement of portion of figure 35: Thermal expansion in perpendicular-to-rise direction of BX–265 foam samples dried at 40 °C for 72 h with as-received samples included for comparison.

TABLE VI.—WEIGHT GAIN OF DRIED BX–265 SAMPLES SUBSEQUENTLY STORED AT AMBIENT CONDITIONS

Time, h	Weight gain, percent			
	Block 2 sample		Block 3 sample	
	B2-a	B2-b	B3-m	B3-n
0	0.00	0.00	0.00	0.00
3	0.32	0.31	0.34	0.36
24	0.46	0.45	0.46	0.55
48	0.68	0.71	0.72	---
72	0.97	0.96	1.01	---
96	0.92	0.91	0.96	---

Moisturizing

Also, weight gain was examined by placing as-sprayed foam samples in a humidity chamber. Samples of various sizes (table VII) were exposed to 40 °C (104 °F) at 95 percent RH and periodically removed and weighed. Figure 39 shows the data for up to a 100-h exposure. The foam rapidly gains weight (approximately 1 percent) within the first 5 h. There is a slight further increase in weight gain until the weight saturates at approximately a 1-day exposure time. The maximum weight gain falls between 0.8 and 1.5 percent with thinner samples gaining less percentage weight (compare table VII with fig. 39). The weight gain is partially reversible, as removing the samples from the chamber and allowing them to sit in ambient room conditions (22 °C (72 °F) at 55 percent RH) shows a subsequent weight loss (fig. 40). Most of the weight loss occurs in the first day. This brings up the question whether the weight gain or loss is strictly a surface effect and if water is simply condensing and evaporating from the surface. This is not unreasonable since the interior of the humidity chamber is under fog conditions. To investigate this, four

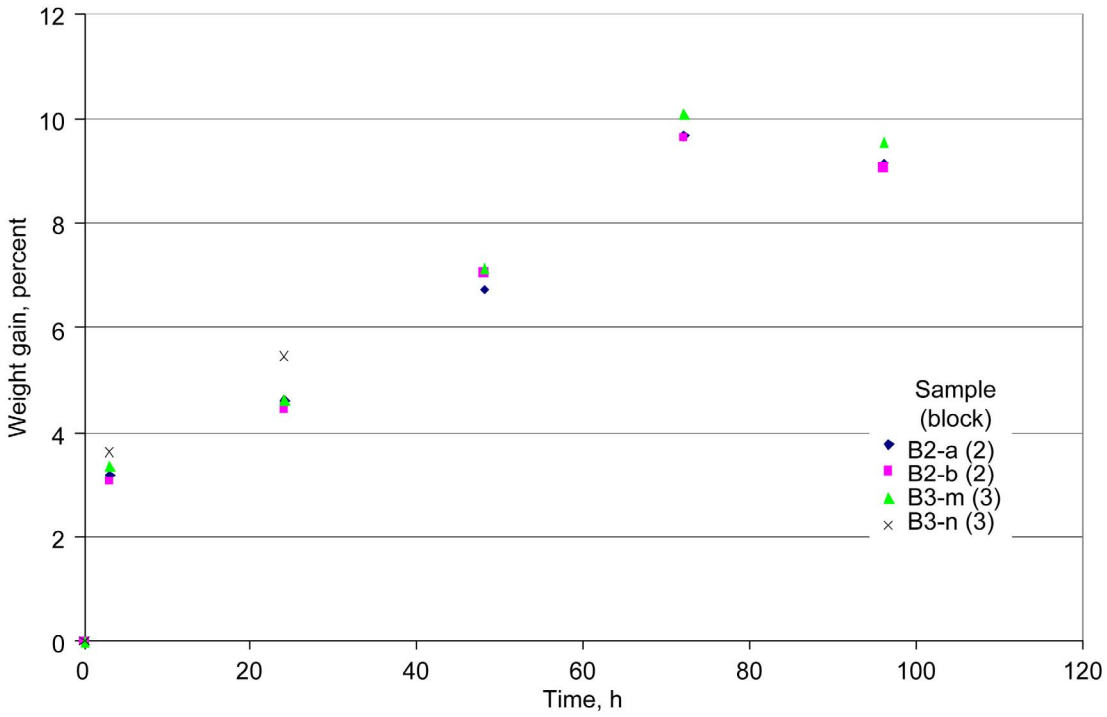

Figure 37.—Weight gain from sitting at ambient conditions for BX–265 foam samples previously dried at 20 °C (from fig. 31).

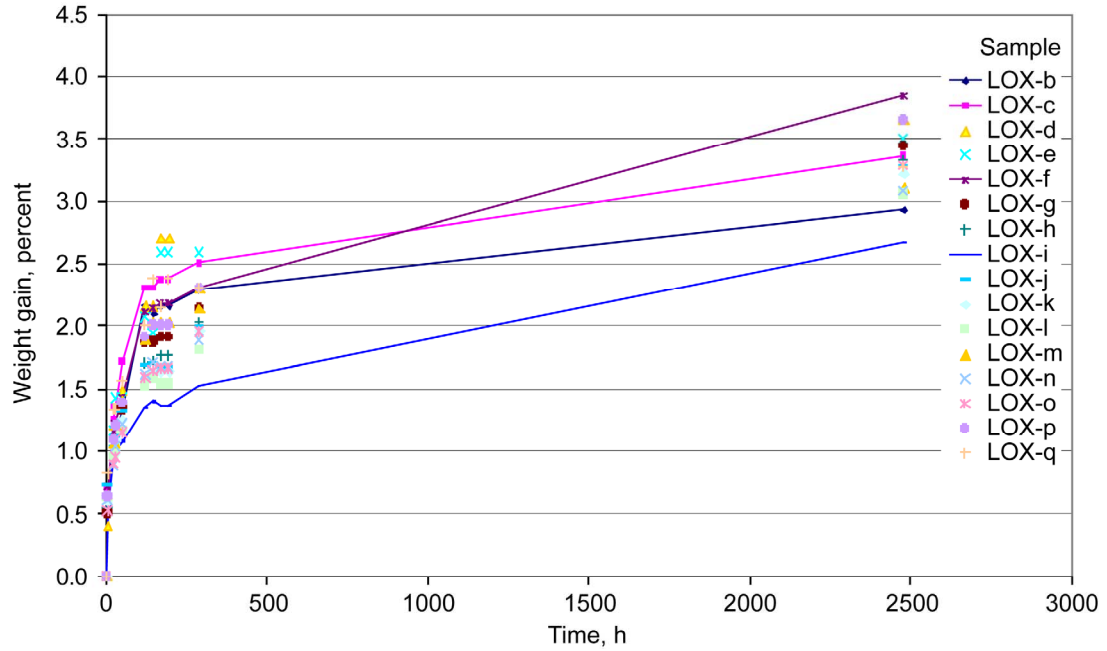

Figure 38.—Weight gain from sitting in ambient conditions for BX–265 LOX foam samples previously dried at 40 °C (from fig. 33).

TABLE VII.—LOX FOAM SAMPLES FOR MOISTURIZING EXPERIMENTS

Sample	Specimen dimensions, mm			Volume, mm^3	Surface area, mm^2	1/thickness, 1/cm	Density, g/cm^3	Knit lines
	Thickness	Length	Height					
LOX-r	12.7	25.4	13	4 100	1630	0.787	0.0.336	1.0
LOX-s	11.4	25.4	12	3 600	1480	0.874	0.0406	2.0
LOX-t	12.7	76.5	13	13 000	4350	0.787	0.0351	1.9
LOX-u	12.7	76.7	13	12 000	4230	0.787	0.0340	1.3
LOX-v	25.7	50.5	25.9	3 400	6529	0.390	0.0346	3.4
LOX-w	24.9	49.5	25.7	31 500	5620	0.402	0.0337	3.0
LOX-x	25.9	26.9	26.2	18 000	4120	0.386	0.0352	4.0
LOX-y	26.2	26.7	26.2	18 400	4170	0.382	0.0331	3.0
LOX-z	12.2	48.8	13	7 900	2810	0.819	0.0350	2.0
LOX-aa	12.4	50.3	13	7 900	2680	0.787	0.0361	1.6
LOX-bb	11.9	47.2	12	6 900	2550	0.839	0.0339	?

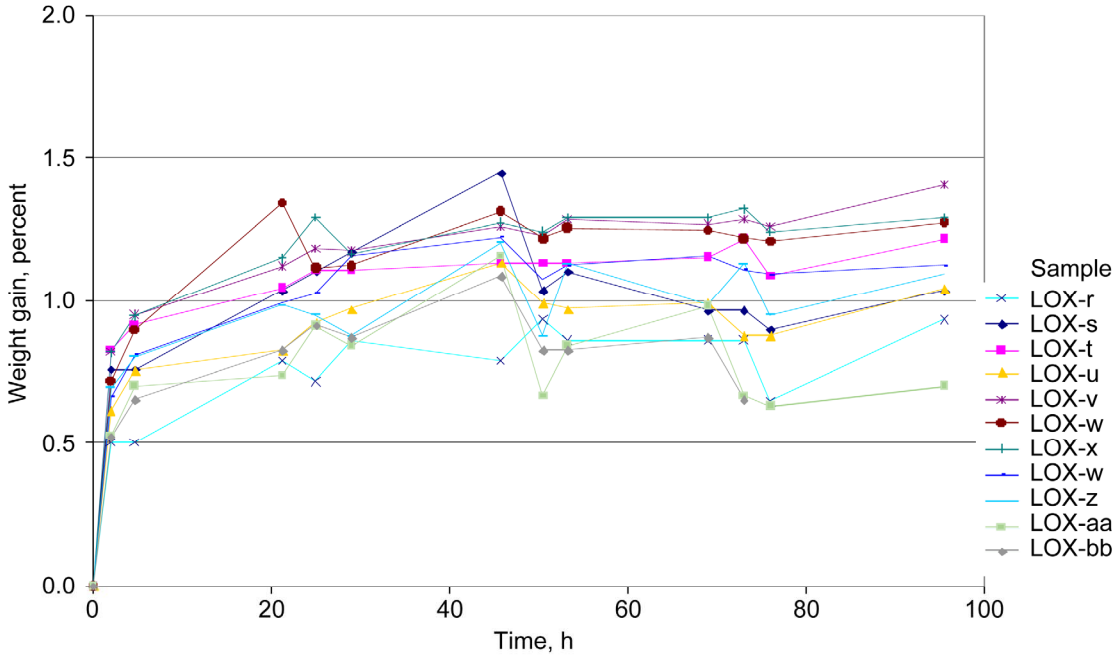

Figure 39.—Weight gain of BX–265 LOX block foam samples due to humidification at 40 °C and 95 percent relative humidity.

samples were moisturized, removed from the chamber and weighed, blotted on a tissue and re-weighed. The results are given in table VIII. The difference after blotting is negligible, suggesting that the moisture uptake is internal to the foam.

Another experiment was run to first dry the foams at 20 °C (68 °F) in the vacuum oven for 5 days. The samples were removed and placed in a humidity chamber set at 40 °C in 95 percent RH and periodically weighed. The results in figure 41 indicate a large weight gain (2.1 percent) occurring during the first 7 h. The weight gain saturates at 2.6 percent at approximately 150 h. There was no significant difference in weight gain between the two thicknesses. Note that the weight gain observed here is almost twice what the as-received foam displayed after it was moisturized (compare figs. 39 and 41). Conditioning foam from the LOX block at 40 °C in 95 percent RH for 5 days followed by thermal expansion tests is shown in figures 42 and 43. The thermal expansion tests in these figures were conducted in the TMA rig over a temperature range from –150 to 150 °C (–238 to 302 °F). The figures show that there is not much difference between the moisturized and the as-sprayed expansion curves. The

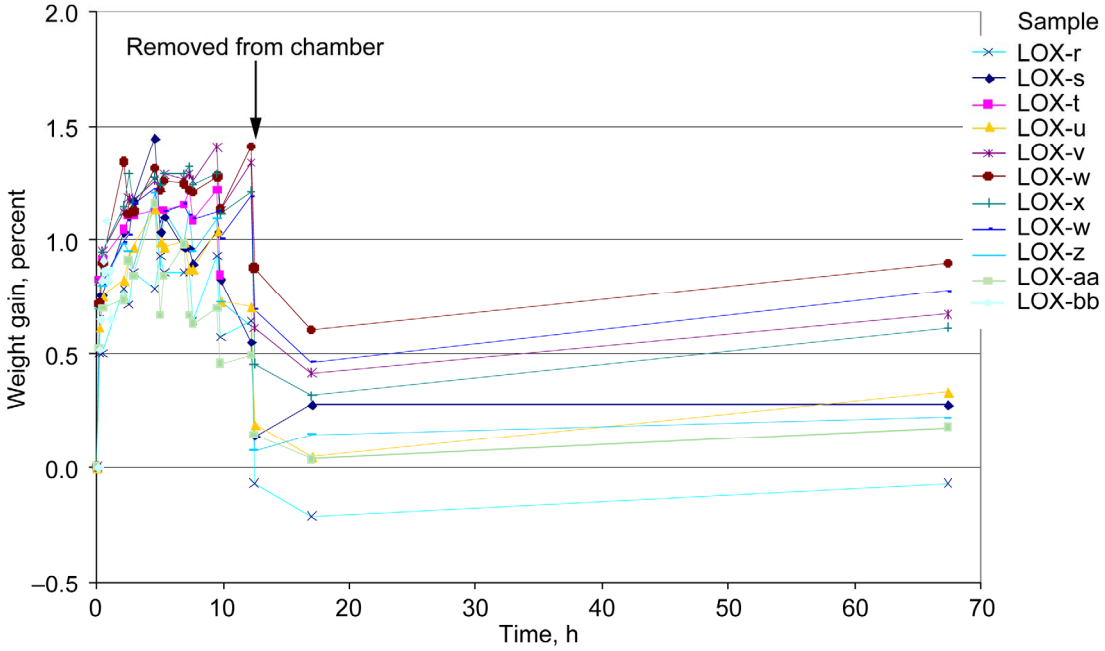

Figure 40.—Weight loss from sitting in ambient conditions for BX–265 LOX block foam samples after previous moisturizing at 40 °C and 95 percent relative humidity (fig. 39).

TABLE VIII.—BC–265 FOAM WEIGHT LOSS FROM BLOTTING[a]

Initial weight, g	Weight after blotting, g	Difference, g	Weight loss, percent
0.1402	0.1402	0.0000	0.00
0.2455	0.2455	0.0000	0.00
0.2309	0.2308	0.0001	0.04
0.2308	0.2305	0.0003	0.13

[a]LOX block samples were moisturized at 40 °C and 95 percent relative humidity, then blotted on tissue.

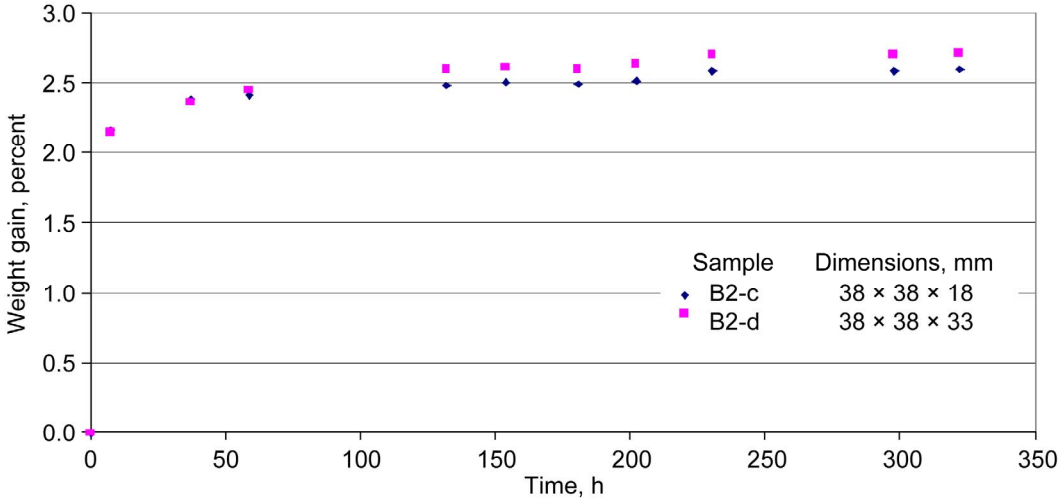

Figure 41.—Weight gain from moisturizing BX–265 block 2 foam samples at 40 °C and 95 percent relative humidity after previous drying at 20 °C in vacuum oven.

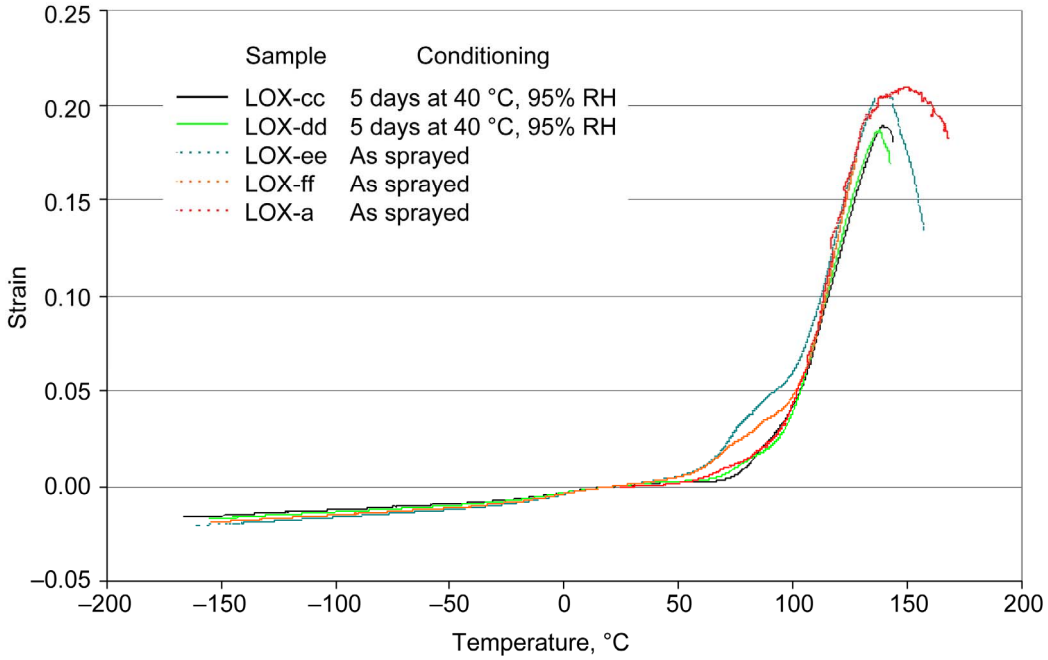

Figure 42.—Thermal expansion of BX–265 LOX block foam samples, in perpendicular-to-rise direction, as sprayed and as moisturized at 40 °C and 95 percent relative humidity (RH).

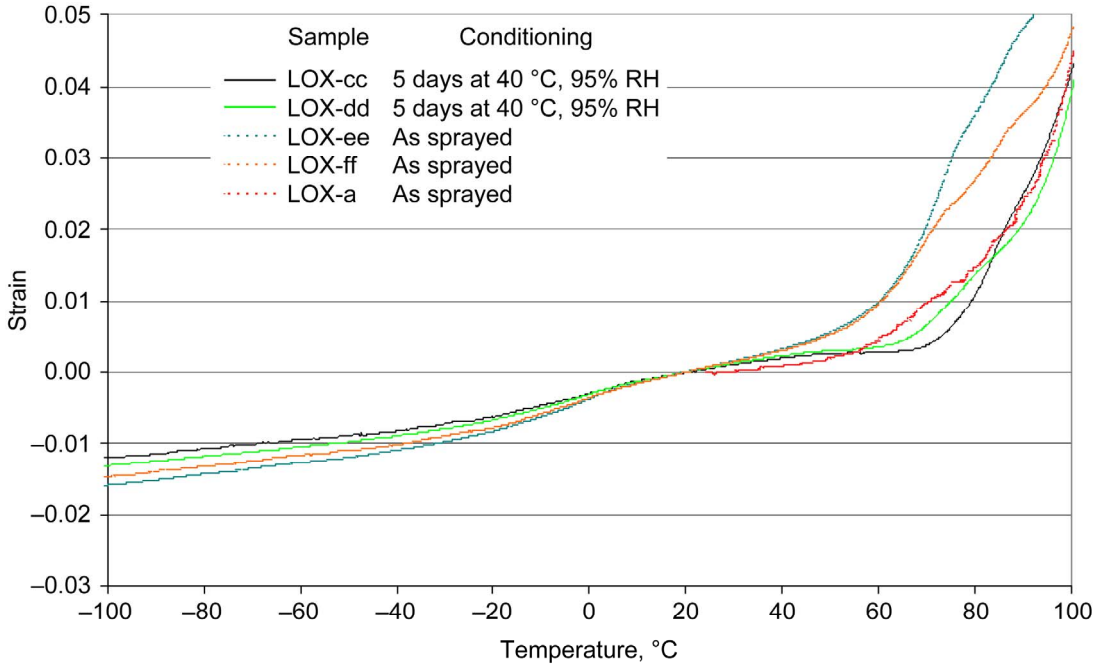

Figure 43.—Enlargement of portion of figure 42: Thermal expansion of BX–265 LOX block foam samples, in perpendicular-to-rise direction, as sprayed and as moisturized at 40 °C and 95 percent relative humidity (RH).

conditioning tended to flatten the thermal expansion behavior up until the area of rapid expansion. The moistened foam behaves more like the dried foam having a plateau region between 20 and 60 °C (68 and 140 °F). There is no apparent difference in the peak strains after moisture uptake compared to the as-sprayed foam. At subzero temperatures, the expansion curves for the moisturized foams are shallower, but the difference between these and the as-sprayed foam is small.

Figures 44 and 45 show the expansion behavior in the rise direction of moisturized foam. It appears as if the moisturizing results in a lower temperature (70 °C, or 158 °F) at which the rapid expansion begins compared with the as-sprayed foam. The peak expansion strain is the same for both moisturized and as-sprayed foam. The temperature at which the peak occurs is lower by 2 to 16 °C (4 to 29 °F) than for the as-sprayed foam.

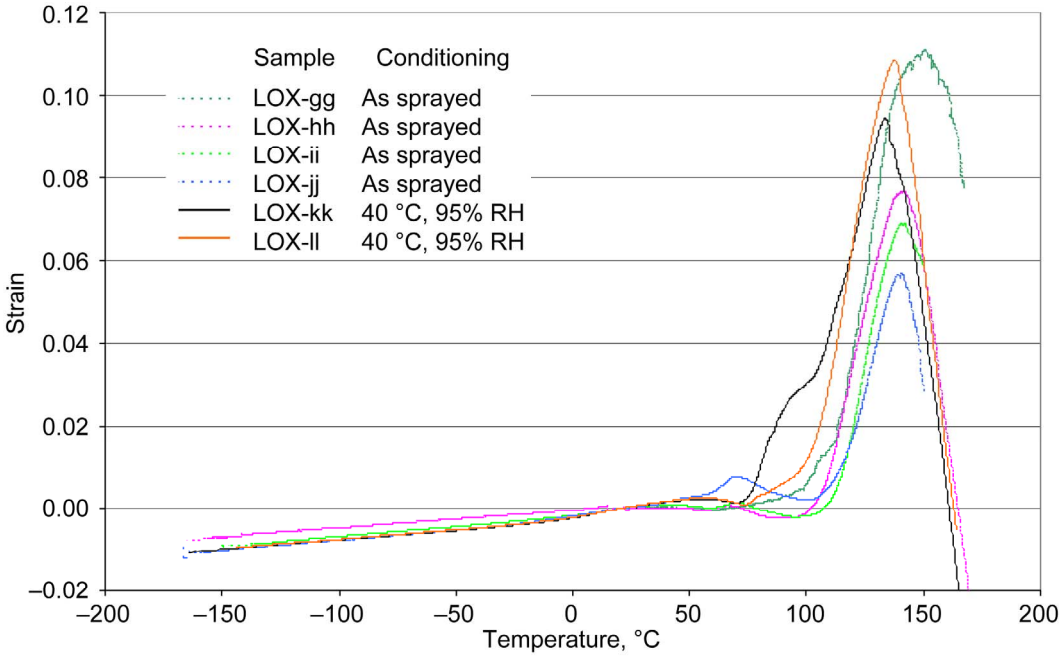

Figure 44.—Thermal expansion of BX–265 LOX block foam samples, in rise direction, as sprayed and as moisturized at 40 °C and 95 percent relative humidity (RH).

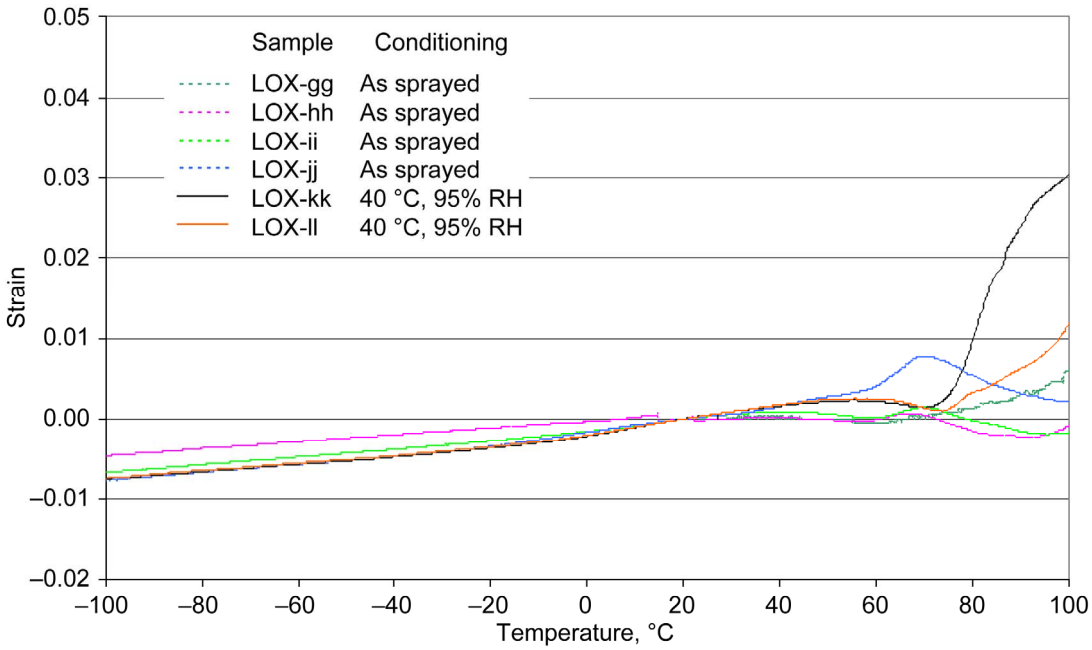

Figure 45.—Enlargement of portion of figure 44: Thermal expansion of BX–265 LOX block foam samples, in rise direction, as sprayed and as moisturized at 40 °C and 95 percent relative humidity (RH).

Heating Rate Effects

All of the heating rates up to now for the thermal expansion tests have been at 5 °C/min (9 °F/min). However, the foam heating rate during the shuttle ascent is much higher and was estimated to be 150 °C/min (270 °F/min). From the TGA tests we know that heating rate affects foam weight loss. The question now is whether heating rate has an effect on the thermal expansion. Also, because the liberation of gases, the expansion of the gases with temperature, and the diffusion of the gases through the polymer during increasing temperature are all time-related events, it is expected that heating rate will have a significant effect on thermal expansion. In this section various heating rates are examined during the thermal expansion tests.

Heating rates of 0.5, 1, 5, 30, 35, 65, and 73 °C/min (0.9, 2, 9, 54, 63, 117, and 131 °F/min) were employed for thermal expansion samples tested in the perpendicular-to-rise direction. The results are shown in figure 46. For heating rates of 5 °C/min and less, no effect of heating rate is observed. Keep in mind that the standard effects of knit lines and density apply in this region as previously discussed. As the heating rate is increased, the area of rapid expansion occurs at increasingly lower temperatures. At the highest heating rates the region of rapid expansion occurs almost immediately at 25 °C (77 °F). It can be observed in figure 46 that the slope of the rapid expansion curve (i.e., the instantaneous CTE) is the same regardless of heating rate. In other words, this portion of the curves is parallel to one another. It should also be pointed out that the maximum strains are also similar, reaching values of approximately 20 percent. However, at the faster heating rates the peak strain is maintained over a large temperature range (~70 °C, or 126 °F) before the foam begins to shrink with increasing temperature. Identical behavior can be observed for expansion measurements taken in the rise direction (fig. 47). Above a heating rate of 5 °C/min, the region of rapid rise occurs at much lower temperatures, and the peak strain is maintained over a larger temperature range.

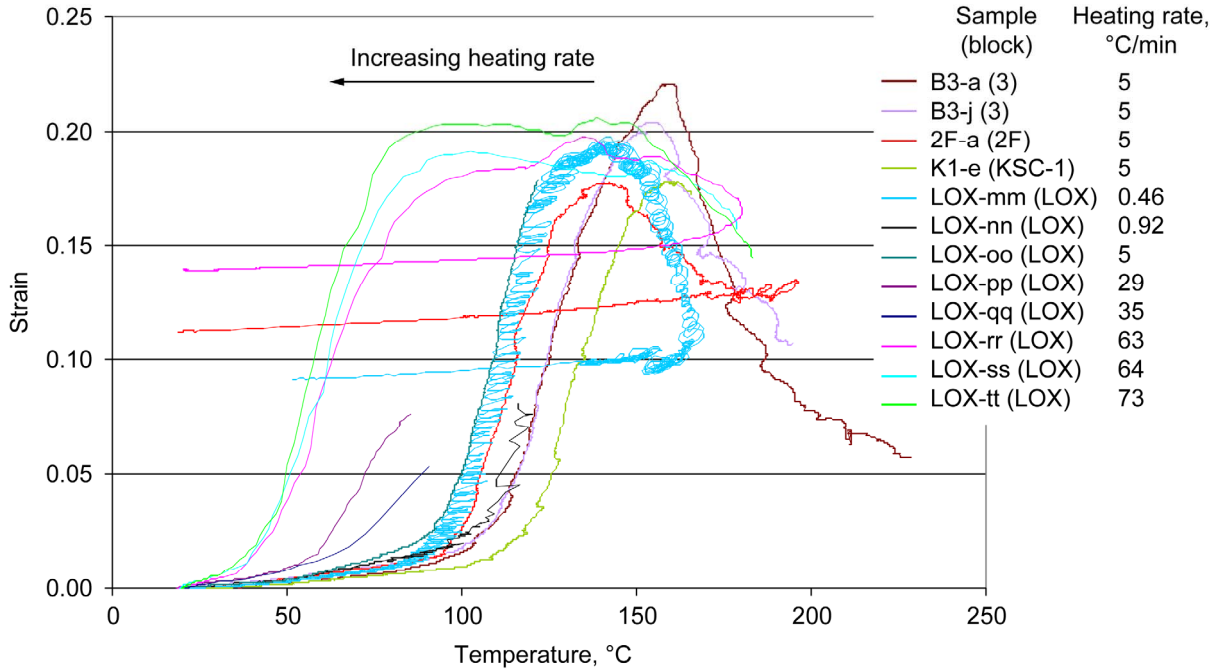

Figure 46.—Thermal expansion of BX–265 foam samples, in perpendicular-to-rise direction, at different heating rates.

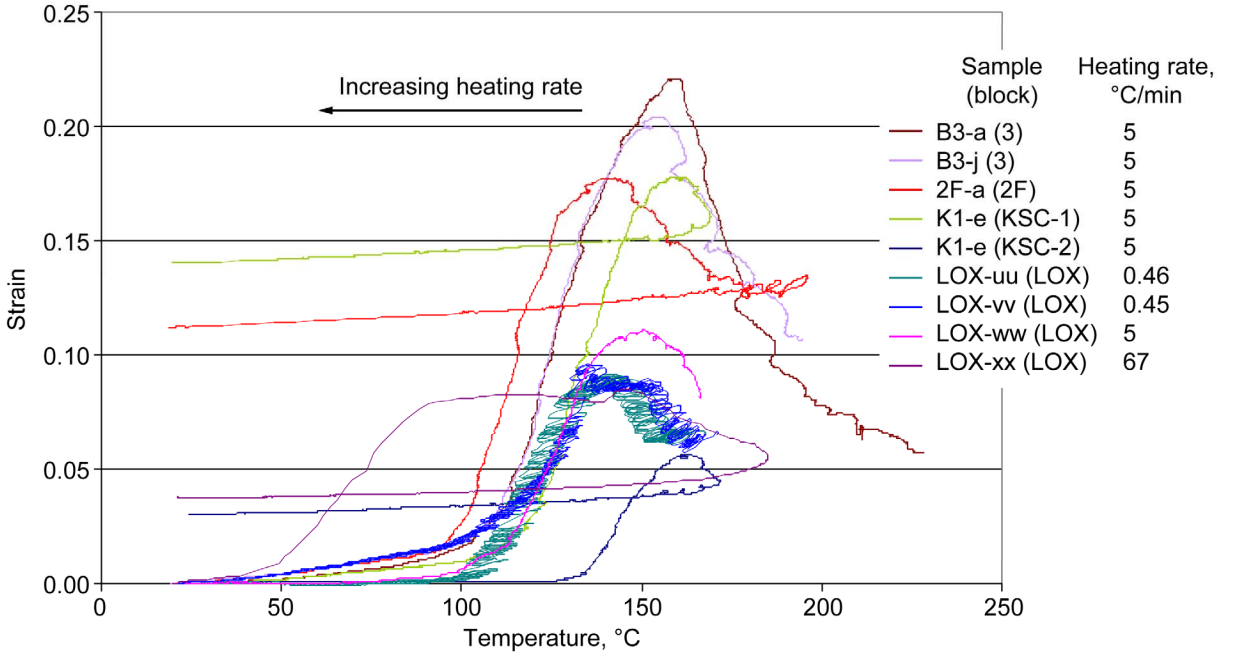

Figure 47.—Thermal expansion of BX–265 foam samples, in rise direction, at different heating rates.

Glass Transition Temperature, T_g

The glass transition temperature (T_g) of the BX–265 was investigated using a modulated differential scanning calorimeter (MDSC) technique. We preferred this method since it would gives us a direct measurement of the T_g of the polymer. Other techniques, such as CTE and torsional damping involve the foam block, and the results could be confounded by mechanisms associated with both the cell structure and the internal pore pressure. All tests were conducted on the ball-milled powder taken from six blocks of foam. Heating was conducted in a flowing nitrogen environment using a heating rate of 5 °C/min (9 °F/min), which matches the heating rate for most of the CTE tests. Three samples per block were measured. These tests were originally conducted in October 2007 and then repeated in November 2007. Additionally, samples were measured on foam that had been dried for 7 days (168 h) at 20 °C (68 °F). This would result in approximately 80 percent of the equilibrium moisture level as shown in figure 31.

The T_g was taken to be the inflection point of the reversible heat flow-temperature curve as shown in figure 48. The onset of T_g was also recorded, since this point would represent the temperature at which the polymer chains begin to move. This point is crucial to explaining the mechanical properties.

Figure 49 shows the MDSC trace for three samples taken out of block 1. The inflection T_g is shown with the arrows and is approximately 135 °C (275 °F). A summary of the inflection T_g is given in figure 50 for all of the foam blocks. The samples measured in October had a slightly lower T_g than those measured in November. With the exception of the data from the KSC–3 batch, which had higher T_g values, the data from the other foams were similar, showing minimal scatter. The dried foam exhibited T_g values that were similar to the measurements taken in November. Since moisture is a known T_g suppressor (refs. 12 and 13), it is suspected that the foams contained more moisture during the October measurements. This is likely consistent with the ambient room humidities in Cleveland during that time of the year. It is unclear why the KSC–3 foam batch had a slightly higher T_g than the other batches.

The onset T_g is presented in figure 51. These values exhibit much more scatter than the inflection T_g, probably due to the interpretation of where the data curves deviated from the straight line (see the schematic in fig. 48). The average T_g values along with the standard deviations are listed in table IX. Due to the higher scatter, all three conditions can be pooled for the onset T_g to yield an average of 86.6 °C with a 7.8 °C standard deviation (188±14 °F).

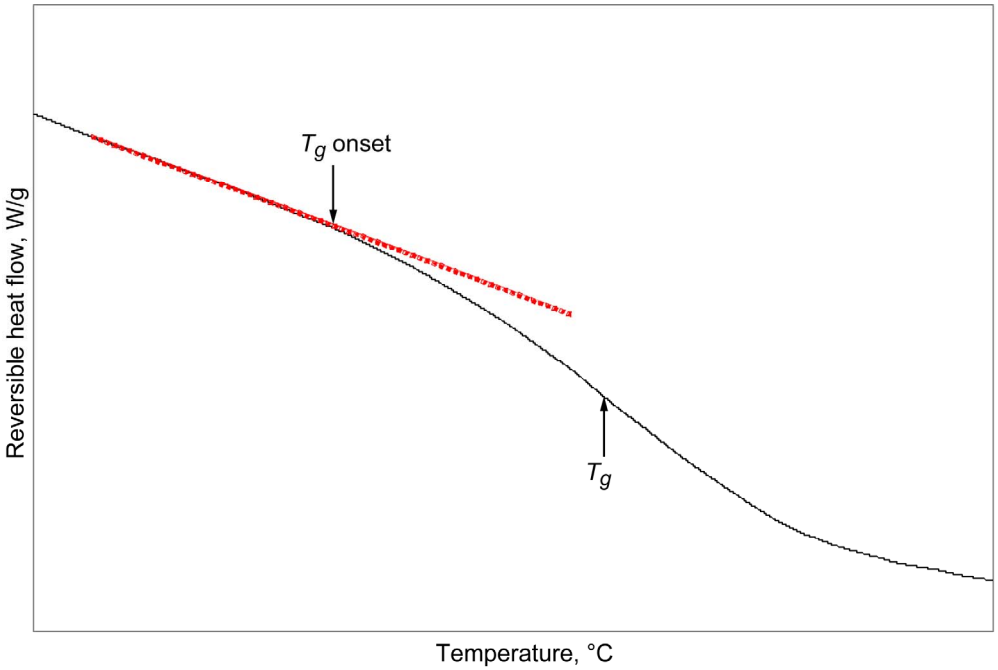

Figure 48.—Location of glass transition temperature (T_g) and its onset.

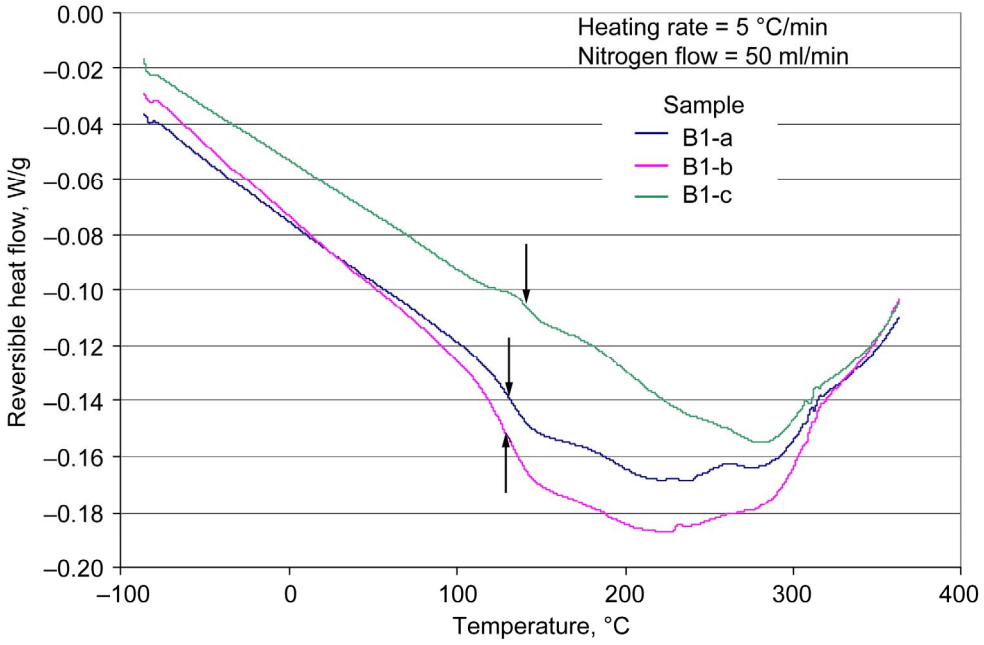

Figure 49.—Differential scanning calorimetry traces for BX–265 block B1 powder samples in 50-ml/min flowing nitrogen heated at 5 °C/min; arrows denote glass transition temperatures.

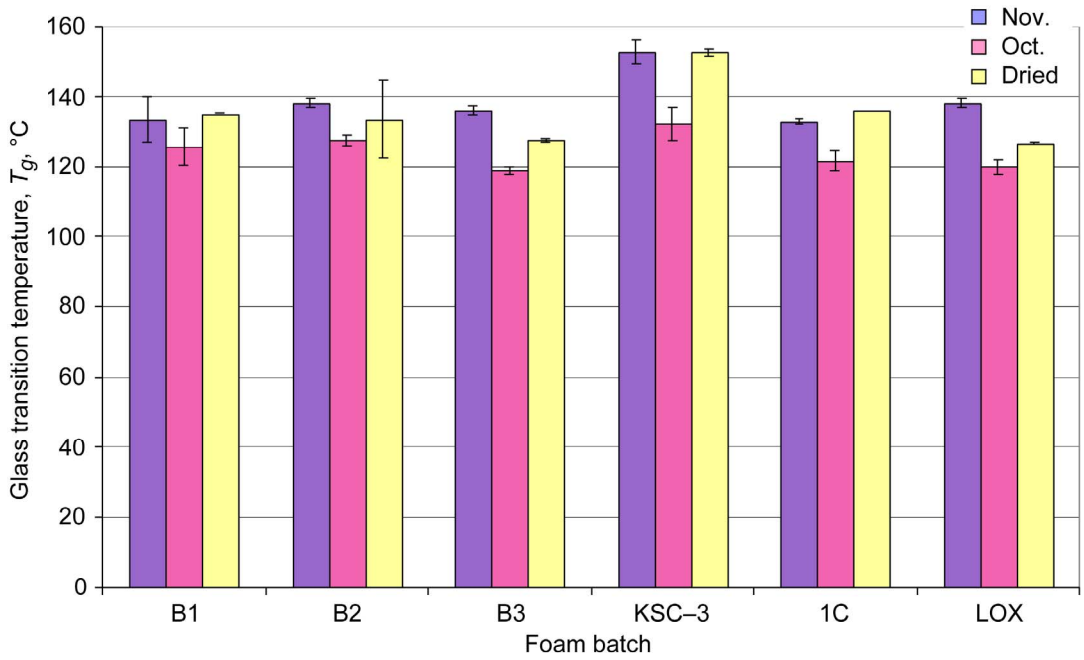

Figure 50.—Glass transition temperatures (T_g) for BX–265 foam batches; results for dried samples and samples tested in October and in November. Error bar equals one standard deviation.

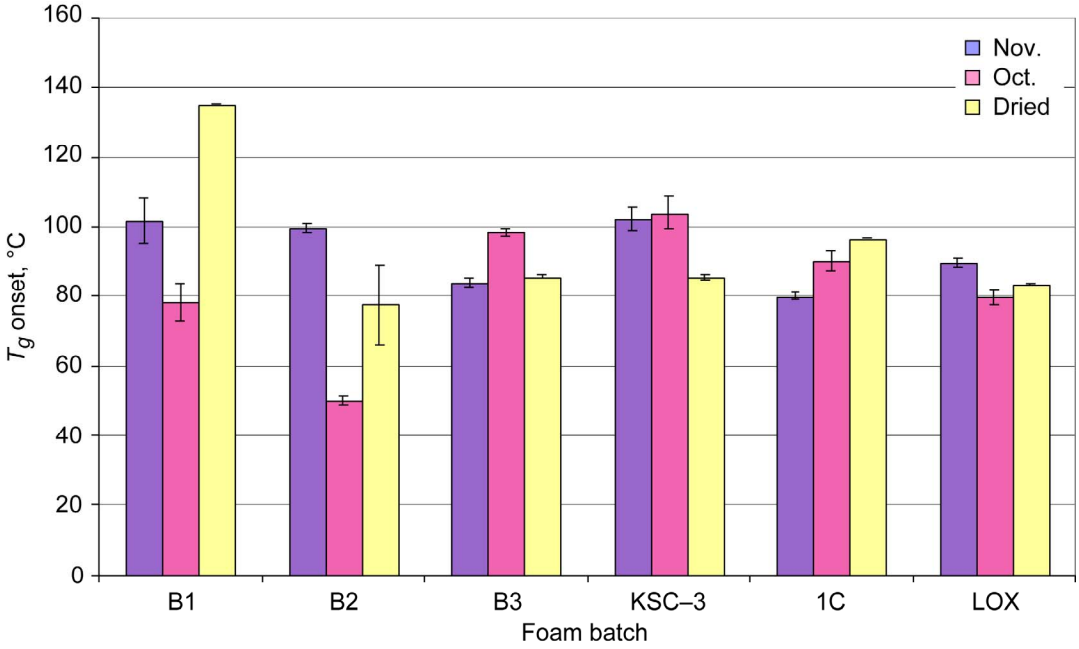

Figure 51.—Onset of glass transition temperatures (T_g) for various BX–265 foam batches; results for dried samples and samples tested in October and in November. Error bars equal one standard deviation.

TABLE IX.—BX–265 FOAM GLASS TRANSITION TEMPERATURES FOR THREE MEASUREMENT CONDITIONS

Conditions	Glass transition temperature,[a] *Tg*, °C	
	Inflection	Onset
As-received		
October[b]	123 (3.5)	83 (9.1)
November[c]	136 (5.0)	93 (12.7)
Dried[d]	131 (10.1)	82 (36.5)

[a]Numbers in parentheses are corresponding standard deviations.
[b]Tested in October.
[c]Tested in November.
[d]Dried for 168 h at 20 °C.

Time-Dependent Mechanical Behavior

To help support some of the more advanced modeling efforts, a few tests were conducted on the LOX foam. These tests were designed to give preliminary data on time-dependent properties of the foam. Three tensile tests were conducted at 20 °C (68 °F) with the load applied perpendicular to the rise direction of the foam. All tests were run in load control. The first specimen was loaded to 262 kPa (38 psi) and then unloaded to zero load at a rate of 3.03 kPa/s (0.44 psi/s). The sample was held at zero load for 2 h to recover. The second sample was loaded at a rate of 3.03 kPa/s to 262 kPa, held for 1 h, unloaded to zero load, and held for 2 h. The third sample was treated identically, with the exception that the loading and unloading rates were an order of magnitude slower, 0.303 kPa/s (0.044 psi/s). The stress-strain curves are all given in figure 52. There are a few noteworthy points gained from this graph. First, all loading paths result in hysteresis in the stress-strain curves, indicating that the behavior of the foam is not nonlinear elastic. Second, the loading moduli of all three samples are identical, showing no load rate effects. In fact, both the loading moduli and the yield points are consistent with results from a series of tensile tests on the LOX foam reported in reference 1. However, the unloading modulus is larger than the loading modulus for each sample, indicating that stiffening has occurred. The sample exhibiting the most creep strain exhibits the highest unloading modulus. Third, there is a substantial amount of creep at the maximum load. Finally, all samples show partial strain recovery when fully unloaded.

Figure 53 gives the creep behavior for the foam samples at a stress of 262 kPa. Sample LOX-zz, which was run at the faster rate, crept more than sample LOX-aaa. The amount of creep for both samples was large and unexpected at room temperature. Sample LOX-zz crept nearly 4 percent in a 1-h period.

The amount of recovery at zero load is shown in figure 54. All three samples exhibit partial strain recovery, amounting to approximately 2 percent strain for sample LOX-zz. The sample with no hold at load (LOX-yy) recovered the least amount. The other two samples have nearly reached equilibrium after 2 h. Note that none of the samples recovered more than half of the unloaded strain.

Zero-Load Creep

In order to further define the behavior of the foam and assist in model development, the temperature dependence of the creep at zero load was investigated. Time-dependent strains in the foam will be shown to be the result of a complex process involving several mechanisms. However for simplicity time dependency in this section will be referred to as creep, where the driving force is the pressure buildup inside of the cells. All samples were taken from the LOX foam block, had dimensions of 13 by 13 by 51 mm (0.5 by 0.5 by 2.0 in.), and were taken perpendicular to the rise direction. They were heated in the optical thermal expansion rig at a heating rate of approximately 4 °C/min (7 °F/min) to various

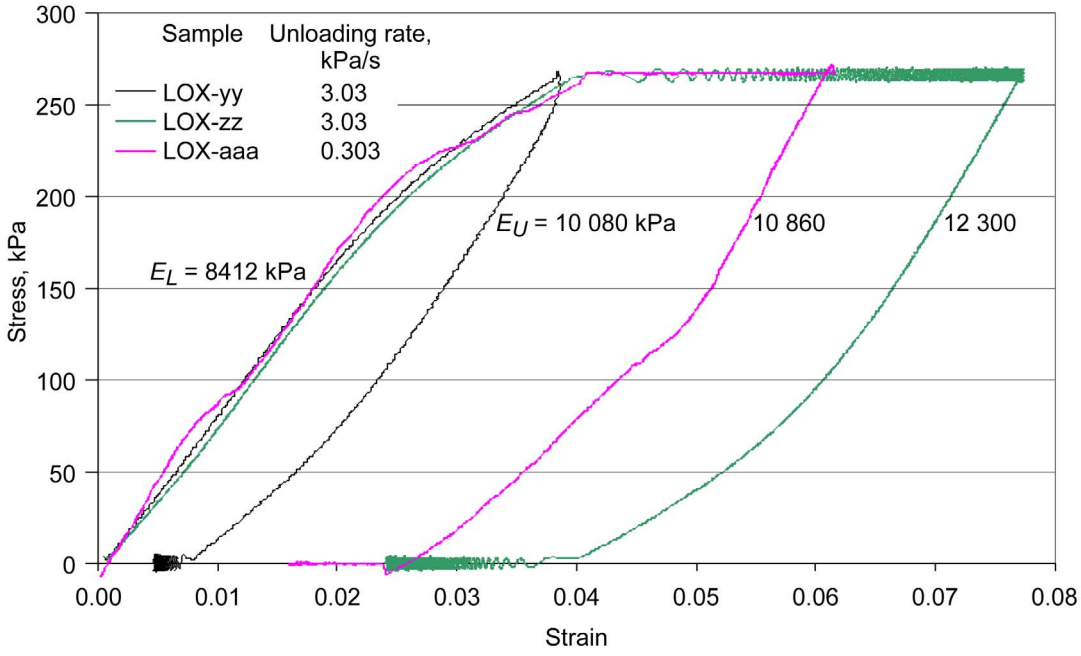

Figure 52.—Stress-strain curves for time-dependent studies of BX–265 LOX block foam, where E_L is loading modulus and E_U is unloading modulus. Sample LOX-yy: loaded to 262 kPa at 3.03 kPa/s, unloaded to zero load at 3.03 kPa/s, and held for 2 h. Sample LOX-zz: loaded to 262 kPa at 3.03 kPa/s, held for 1 h, unloaded to zero load at 3.03 kPa/s, and held for 2 h. Sample LOX-aaa: loaded to 262 kPa at 0.303 kPa/s, held for 1 h, unloaded to zero load at 0.303 kPa/s, and held for 2 h.

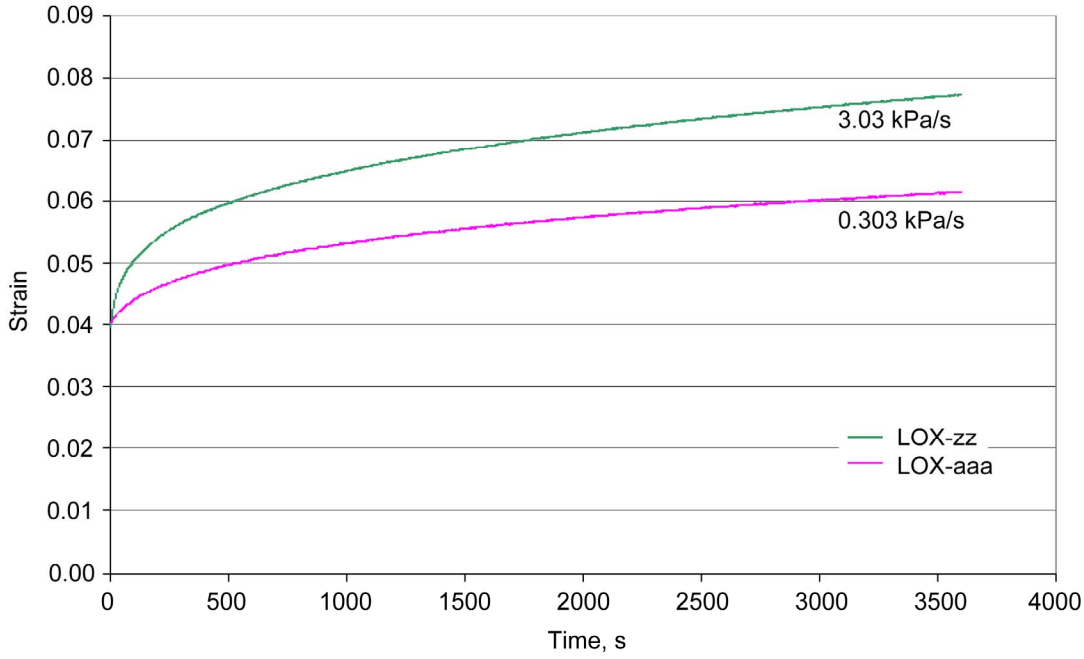

Figure 53.—Creep for BX–265 LOX block foam samples at 262 kPa in perpendicular-to-rise direction; loading rates are given in figure 52.

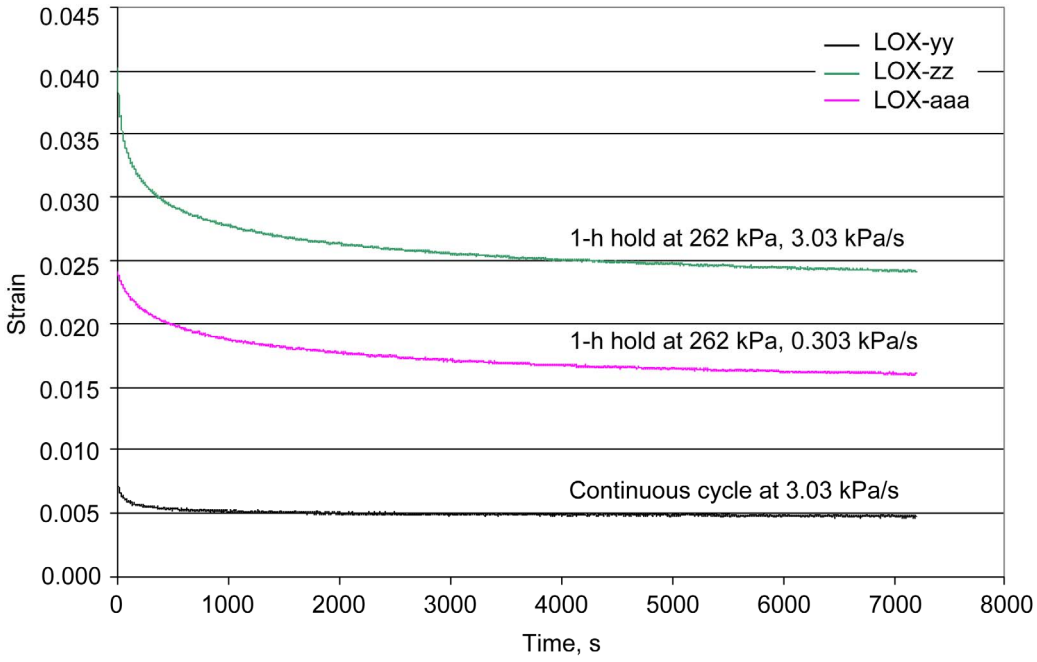

Figure 54.—Strain recovery of BX–265 LOX block foam samples for 2-h holds at zero load; loading conditions are given in figure 52.

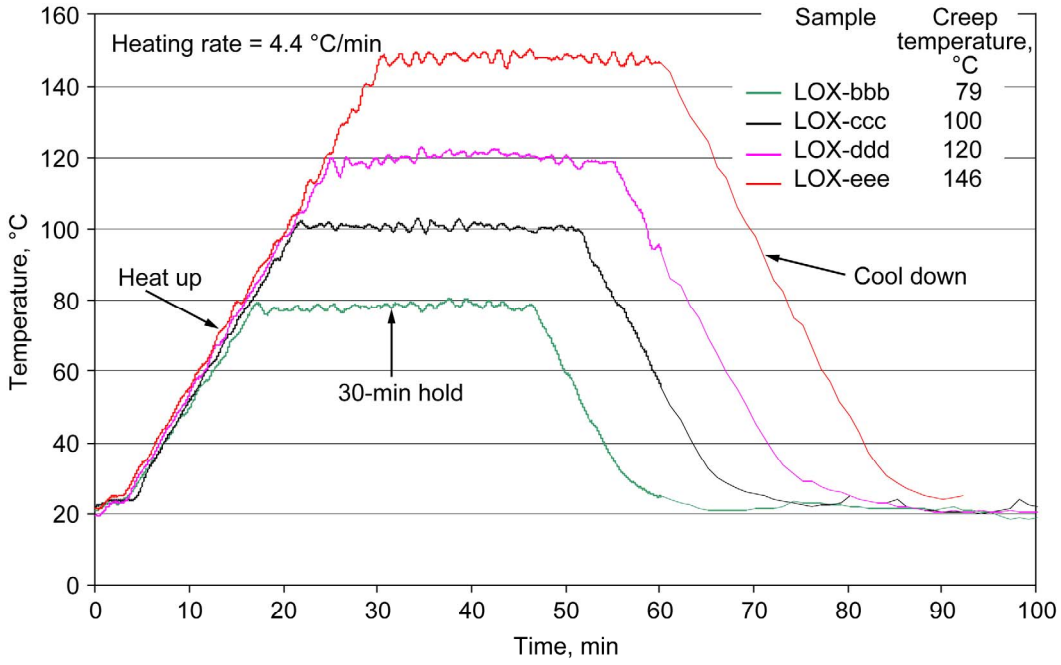

Figure 55.—Temperature profiles for zero-load creep tests of BX–265 LOX block samples, perpendicular-to-rise direction. Samples are heated at 4.4 °C/min and held at their respective temperatures for 30 min.

temperatures and then held at that temperature for 30 min. Expansion was measured continuously throughout the test. Examples of the temperature profile are shown in figure 55. A summary of the samples is given in table X and includes the sample density, number of knit lines, temperature of the 30-min hold, initial and final strain during the hold, and the total creep strain, with a final column

TABLE X.—PROPERTIES FOR LOX BLOCK CREEP SAMPLES

Sample number	Density, g/cm^3	Knit lines	Creep temperature, °C	Initial strain,[a] percent	Final strain,[b] percent	Total creep strain,[c] percent	Timing[d]
LOX-bbb	0.0351	2.0	79	0.92	0.90	–0.02	Late
LOX-fff	0.0362	2.0	90	1.99	2.74	0.76	Early
LOX-ggg	0.0345	1.8	92	0.90	1.03	0.13	Late
LOX-hhh	0.0350	2.0	95	1.50	2.76	1.26	Late
LOX-iii	0.0354	2.0	95	1.90	3.85	1.96	Early
LOX-jjj	0.0358	1.3	100	5.80	11.32	5.52	Earliest
LOX-kkk	0.0348	1.5	101	1.46	3.10	1.64	Late
LOX-lll	0.0345	2.0	111	6.30	10.16	3.86	Late
LOX-mmm	0.0367	2.1	114	9.45	15.65	6.20	Medium
LOX-nnn	0.0335	1.0	116	7.01	12.22	5.21	Late
LOX-ooo	0.0345	2.0	120	7.20	12.17	4.97	Late
LOX-oo	0.0367	2.0	124	18.35	21.40	3.05	Early
LOX-ppp	0.0355	2.0	135	21.09	21.88	0.79	Early
LOX-qqq	0.0340	1.5	146	12.83	16.12	3.29	Latest
LOX-rrr	0.0346	2.0	Step	0.81	0.81	0.00	Late
LOX-sss	0.0347	1.9	Step	2.00	2.63	0.63	Early

[a]Strain upon reaching desired temperature.
[b]Strain after holding at temperature 30 min.
[c]Difference between initial and final strains.
[d]Occurrence of rapid expansion point in figure 56.

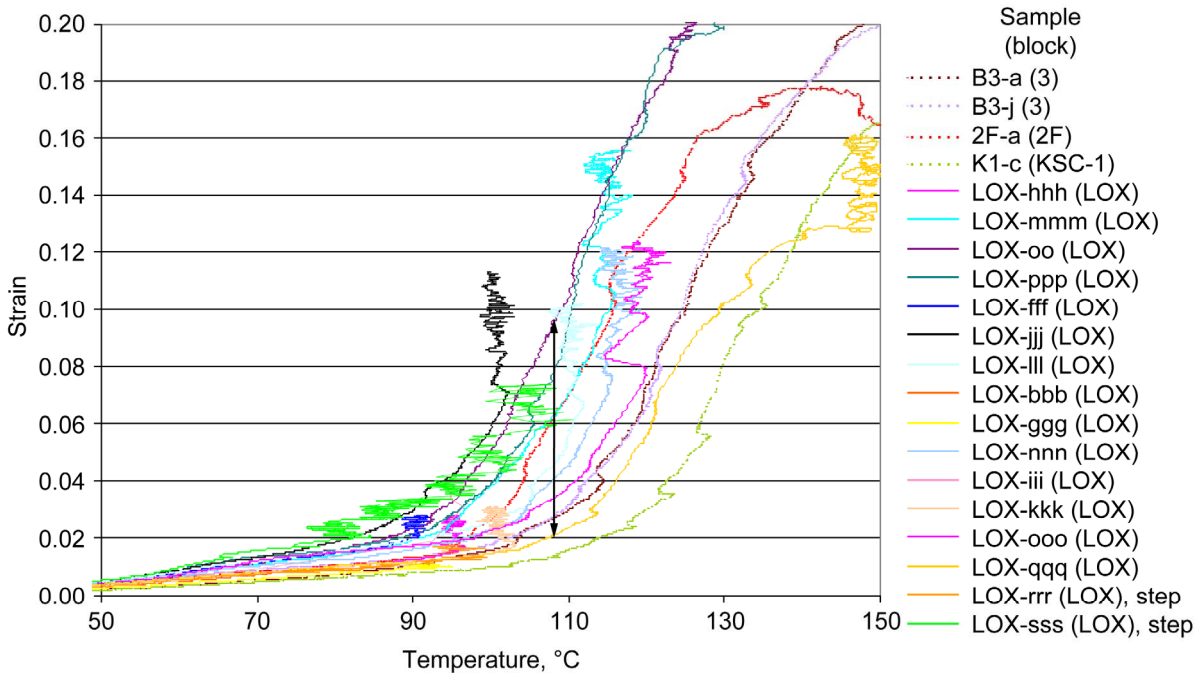

Figure 56.—Thermal expansion curves for creep tests (solid lines) and reference curves for continuously heated samples (dotted lines) for BX–265 foam samples. Last two samples were tested in step creep mode.

describing the thermal expansion curve. The majority of the samples contained approximately 2 knit lines and had a density near 0.036 g/cm^3. However, as will be pointed out later, small differences in the density had significant effects on the thermal strains. An enlarged version of the thermal expansion curves is shown in figure 56. The creep response can be identified by the vertical line at the end of each test. Also shown in this figure for comparison are a few select curves (dashed lines) from continuously heated samples cut from other blocks of foam. The heating up of the creep samples shows normal thermal

TABLE XI.—PROPERTIES FOR LOX BLOCK STEP CREEP SAMPLES

	Sample number					
	LOX-rrr			LOX-sss		
Density, g/cm^3	0.0346			0.0347		
Knit lines	2.0			1.9		
Creep temperature, °C	Initial strain,[a] percent	Final strain,[b] percent	Total creep strain,[c] percent	Initial strain,[a] percent	Final strain,[b] percent	Total creep strain,[c] percent
76	0.81	0.82	0.00	-----	----	-----
80	0.90	0.88	–0.03	2.03	2.63	0.60
86	0.97	1.00	0.03	2.66	3.09	0.44
90	1.12	1.19	0.06	3.07	3.35	0.28
95	1.28	1.73	0.05	3.54	4.15	0.61
100	----	----	-----	4.32	5.66	1.35
106	----	----	-----	5.86	7.36	1.51

[a]Strain upon reaching desired temperature (fig. 59).
[b]Strain after holding at temperature 30 min (fig. 59).
[c]Difference between initial and final strains.

expansion behavior that falls within the values from the continuously heated foam samples. As indicated in earlier sections, there is a lot of scatter in the thermal expansion curves. The location of the expansion curve is slightly correlated with the sample density. This creates a problem in comparing the data from these curves since the rapid expansion begins at lower temperatures for some specimens than for others. For example, if one views the double arrowed line in figure 56 the expansion strain for sample LOX-oo (124 °C, or 255 °F) at 108 °C (226 °F) is already at about 10 percent. For sample LOX-qqq (146 °C, or 295 °F) the expansion strain at 108 °C lags behind and is only at 2 percent. Thus in table X the final column is an attempt at qualifying the position of the curve. If the rapid expansion occurs at lower temperatures, then the curve lies to the left and is defined as “early.” If the expansion occurs at higher temperatures, then the curve falls to the right and is termed “late.” This must be considered when examining the creep data since at any given creep temperature the initial creep strain could vary greatly. An example of this can be observed in table X. Consider samples LOX-ooo and LOX-oo, both of which contain 2.0 knit lines and have nearly identical creep temperatures (120 vs. 124 °C, or 248 vs. 255 °F, respectively). These samples have drastically different densities. Sample LOX-ooo has a density of 0.0345 g/cm^3 (2.154 lb/ft^3) whereas the density of sample LOX-oo is 0.03669 g/cm^3 (2.291 lb/ft^3). Based on previous discussions, this should delay the expansion of sample LOX-ooo compared with sample LOX-oo. This can in fact be observed by examining the initial strain at the beginning of the creep regime. The strain for the low-density sample (LOX-ooo) is 7.20 percent and the strain for the high-density sample (LOX-oo) is 18.35 percent. These data also indicate that the density of the foam is affected by something other than just knit lines.

The creep behavior of the foam taken from LOX is shown in figure 57. This figure shows the expansion strain versus time from the beginning of the heating. Starting at approximately 20 min into the test, the samples begin to expand at a rapid rate. At a heating rate of 4 °C/min, 20 min represents a temperature of 100 °C (212 °F), which coincides with the rapid expansion shown in figure 56. At the lowest hold temperatures, there is little if any creep observed during the tests. The specimen LOX-bbb, held at a temperature of 79 °C (174 °F), not only did not show creep, but the sample actually contracted during the test as noted in table X. This is probably due to off-gassing of the sample and contraction of the polymer. As the creep temperature is increased to 92 °C (198 °F), the sample LOX-ggg exhibits some minimal creep. Table X shows a difference of 0.13 percent strain occurring between the beginning and end of the hold time. Coupled with other samples tested in this temperature range, this behavior suggests that creep becomes active at a temperature between approximately 80 and 90 °C (176 and 194 °F).

Figure 58 is a repeat of select curves from figure 57. The arrows in figure 58 indicate the beginning of the hold times (creep regime) for each test. Using the arrows, the reader can get a better view of how much creep is actually occurring during each test. The end of the hold time occurs when there is a sudden

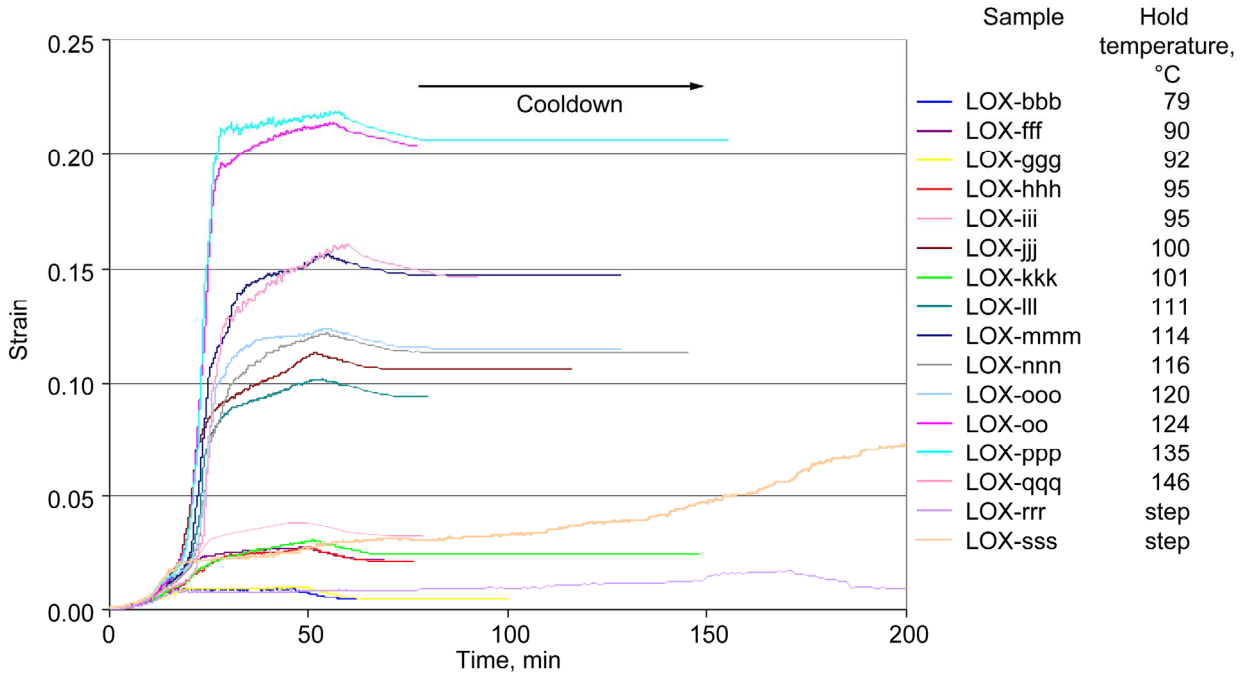

Figure 57.—Creep curves for BX–265 LOX block foam samples. Last two samples were tested in step creep mode. Start of "Cooldown" denotes end of hold time.

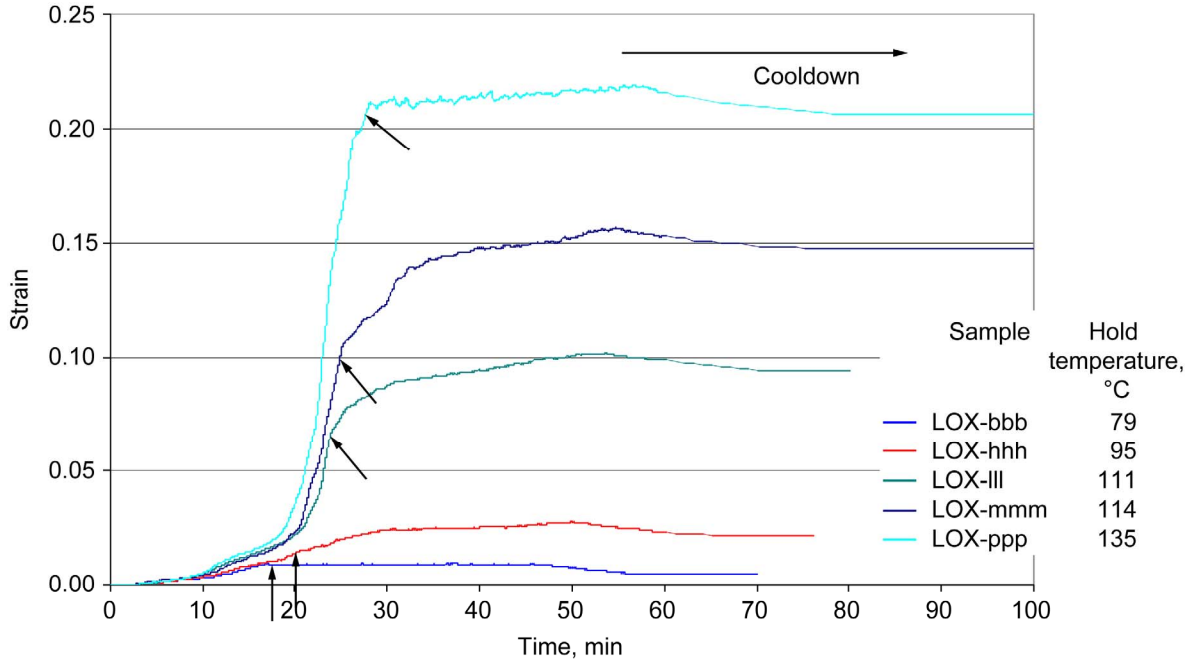

Figure 58.—Selected creep curves of BX–265 LOX block foam samples from figure 57. Arrows depict beginning of hold time. Start of "Cooldown" denotes end of hold time.

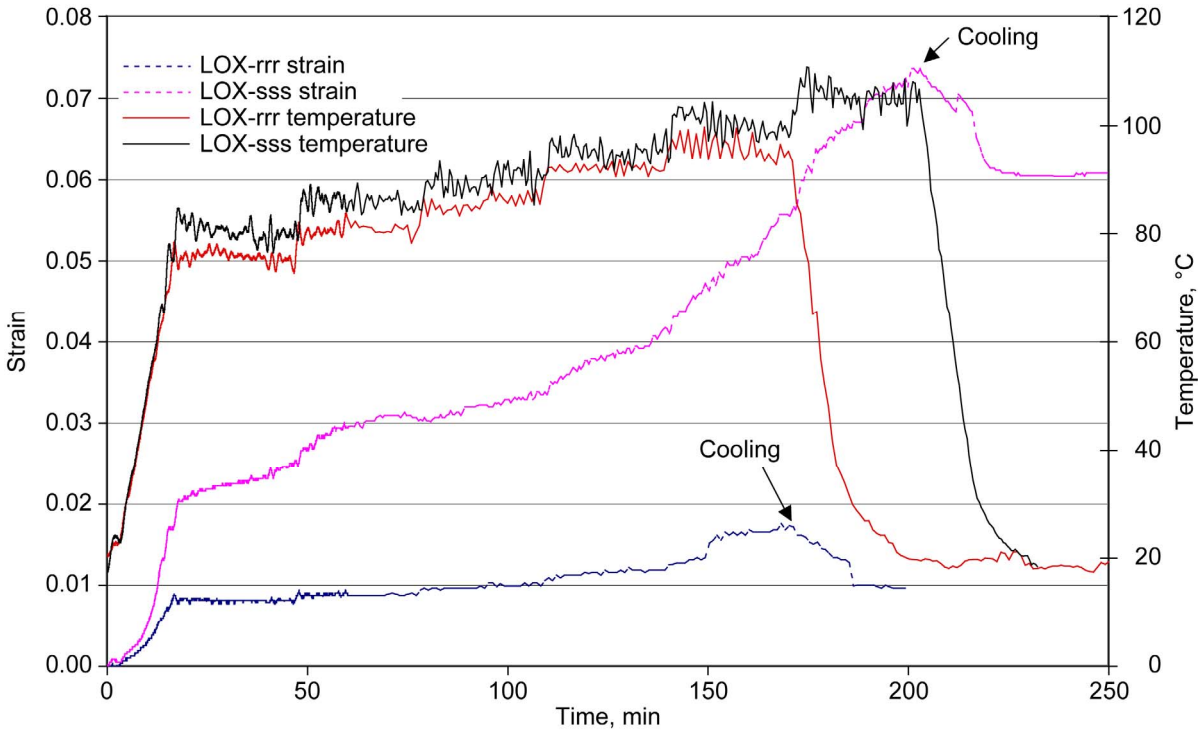

Figure 59.—Step creep tests of BX–265 LOX block foam samples.

contraction of the sample. This occurs at approximately 60 min and is depicted by the arrow marked as "cooldown." The data in figure 58 were chosen as having the most consistent creep behavior (knit lines and density considered).

Above 90 °C creep begins to play a larger role in the expansion process (fig. 57). Between 90 and 100 °C there are creep strains accumulated during the 30-min hold of between 0.75 and 1.95 percent. At still higher temperatures 100 through 120 °C, the accumulated creep strains range between 3.9 and 6.2 percent. This range of strains is maintained for still higher temperatures until approximately 135 °C (275 °F) and above at which point the accumulated strains appear to decrease. Note again that the initial creep strain, and to some extent the accumulated creep strain, is dependent upon the density and how early the rapid expansion occurs on the individual thermal expansion curves.

Two additional samples were tested in step creep mode. During these tests, the temperature was held for 30 min, and then the temperature was raised by approximately 5 °C (9 °F) and held for another 30 min. This process was repeated several times. The purpose of this test was to help better define the temperature at which creep begins. The strain and temperature history for both of these samples is shown in figure 59. The first hold temperature for sample LOX-rrr was 76 °C (169 °F) and for sample LOX-sss was 80 °C (176 °F). The creep strains are tabulated in table XI. Note that both samples have the same density and number of knit lines. However, sample LOX-sss expanded at lower temperatures, as shown in figure 56. Thus this sample registered higher strains at any given temperature. Note that the temperature for the activation of creep is 86 °C (187 °F) for sample LOX-rrr and 80 °C (or less) for LOX-sss. These temperatures are where positive strain increases occur. This is the same range over which creep was observed in the single creep temperature tests given earlier.

One hypothesis for the foam expansion is that increasing the temperature raises the cell gas pressure. During a hold at constant temperature, it is also suspected that additional gases may be generated and released into the cells, causing the pressure to rise. To investigate this point, specimens of both blocks of foam and ball-milled powder were heated at 10 °C/min (18 °F/min) to 80, 90, and 100 °C and held for a period of time. Weight loss was measured continuously. Infrared spectroscopy of the effluents was also

performed during the hold time. Figure 60 shows weight loss data as a function of time at the three different temperatures. In all cases the samples continue to lose weight during the hold times, and do not reach saturation even after 120 min. For the holds at all temperatures, the powder samples lose more weight than the blocks (table XII), as would be expected since there is more surface area exposed in the powder samples. It can also be observed in table XII that as the hold temperature increases, the amount of weight loss increases for the powder samples. For the bulk samples, the percentage decrease in weight is the same at 80 and 90 °C, but is greater at 100 °C. The infrared spectroscopy showed most of the weight loss to be water with very small amounts of CO_2.

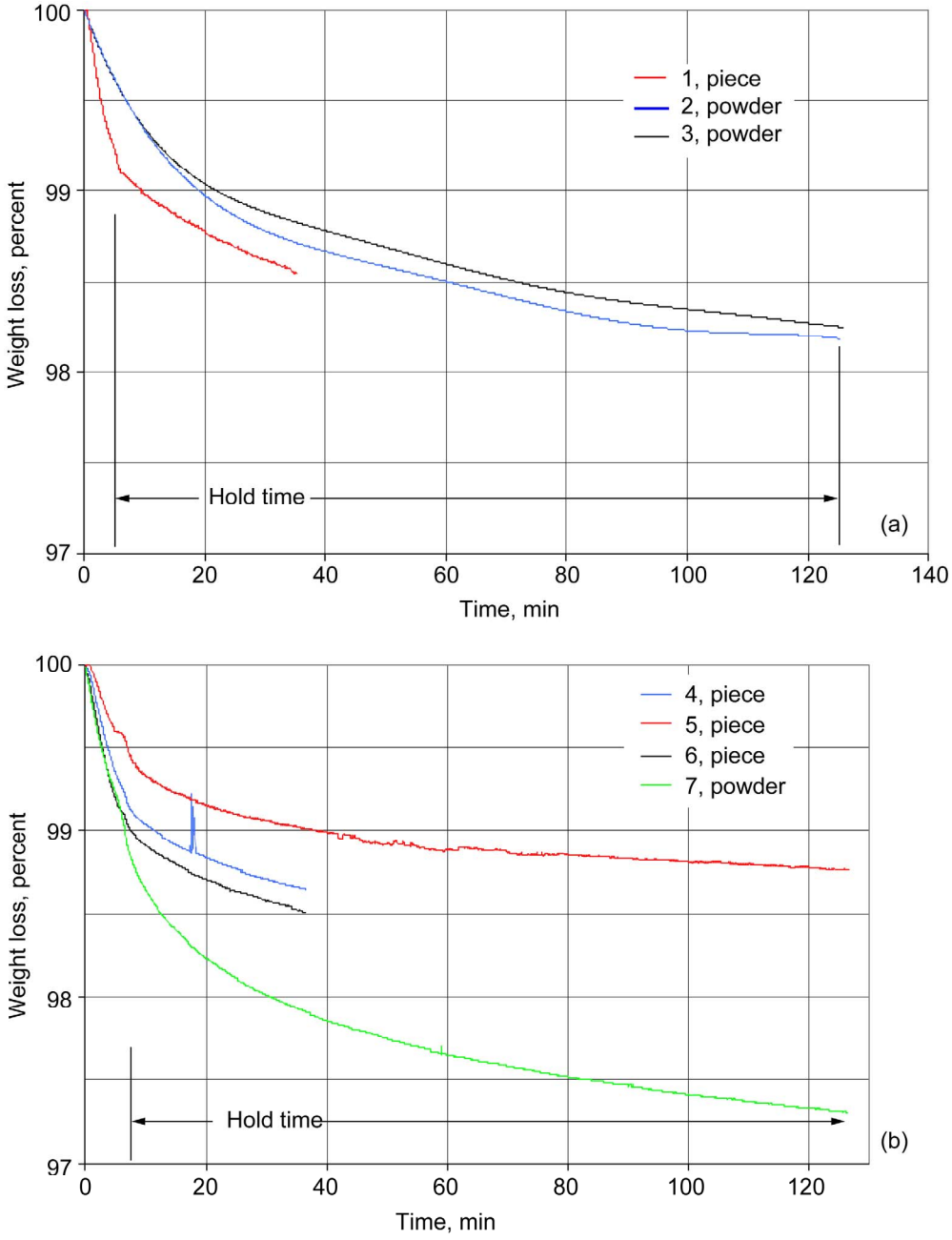

Figure 60.—Weight loss due to outgassing of BX–265 LOX block foam samples upon heating at 10 °C/min and holding in air at different temperatures. (a) 80 °C. (b) 90 °C. (c) 100 °C.

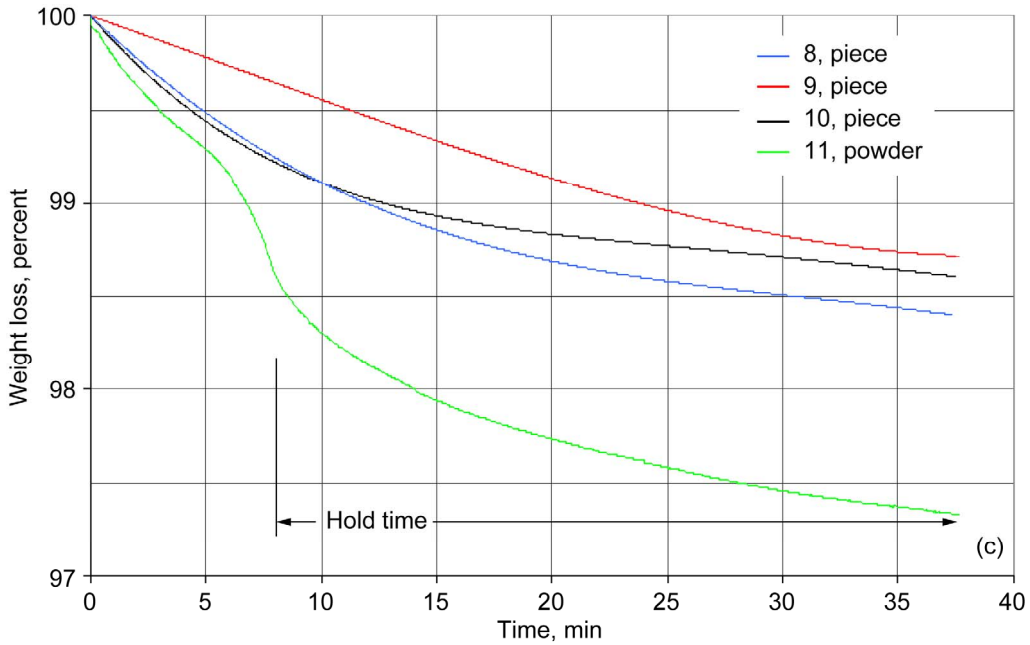

Figure 60.—Concluded. (c) 100 °C.

TABLE XII.—WEIGHT LOSS OF LOX BLOCK FOAM FOR 30- AND 120-MIN HOLDS AT TEMPERATURE

Hold temperature, °C	Sample, form	Weight loss after 30-min hold, percent	Weight loss after 120-min hold, percent
80	1, piece	0.58	----
	2, powder	.83	1.31
	3, powder	.73	1.27
90	4, piece	0.49	----
	5, piece	.41	0.66
	6, piece	.49	----
	7, powder	.95	1.55
100	8, piece	1.03	----
	9, piece	.91	----
	10, piece	.68	----
	11, powder	1.20	----

Discussion

This study has shown that the foam is a complex material and its properties can be influenced by myriad items. The foam itself can be thought of as a structure consisting of a polymer skeleton with gas-filled cells. Therefore, the foam properties become a mixture of both those of the polymer, and those of the cell structure. As an example, thermal expansion was shown to be affected by density, the number of knit lines, and the amount of water vapor. Many properties are dependent upon the size of the foam cells, and shape of the cell can also impart anisotropic properties (ref. 14). In order to make sense out of the data, it is imperative that a pedigree be collected for each specimen. It is recommended that the following information be collected for each foam sample, regardless of test type: Density, number of knit lines, specimen dimensions, knit line separation, and cell size. In addition, for the model developed from these studies (ref. 1), the values of L and θ should also be provided for that particular foam spray: L is the length of a side of a hexagonal face in the foam cell; and θ is the half angle between two sides of a

hexagonal face of a cell. These parameters are described in more detail in reference 14. All of this information is required to properly correlate the results and implement the model.

Thermal expansion is known to be an important property in the use of the foam on the ET. The mismatch in thermal expansion between various foams, and the foam and the metallic tank can lead to significant strains, foam fracture, and possible foam shedding. Because of its importance, a great deal of effort was spent on thermal expansion in this study. Figures 2, 4, 5, and 9 show the thermal expansion behavior in the perpendicular-to-rise direction for various foam spray lots. The behavior is typified by a limited expansion from –250 °C (–418 °F) to approximately 100 °C (212 °F); the coefficient of thermal expansion (CTE) in this range varies from 3.5×10^{-5}/°C to about 2.0×10^{-4}/°C (1.9×10^{-5} to 1.11×10^{-4}/°F), respectively. At temperatures of approximately 100 °C the foam begins to expand rapidly with further increase in temperature, reaching peak strains between 20 and 25 percent. Thereafter, the foam begins to contract, continuing until the foam dimensions are smaller than the original size. This would occur at temperatures 300 to 350 °C (572 to 662 °F), slightly higher than those estimated to exist in the ET application. If the foam is cooled from some elevated temperature, there is a slight contraction during cooling (fig. 2). The CTE during this contraction is approximately 1×10^{-4}/°C (5×10^{-5}/°F) and is consistent regardless of the temperature from which cooldown occurs. This suggests that this is pure elastic contraction. Since the contraction during cooldown is slight, this results in a residual strain in the foam upon reaching room temperature. This residual strain can be very large and on the order of 20 percent if the foam was cooled from near the peak strain temperature. If the foam is cooled from very high temperatures, it is conceivable that the residual strain could be smaller than the original foam dimensions. Permanent dimensional changes have been observed by others on polymeric foams (refs. 15 to 18). While this residual strain may not be of large importance to the ET application, it is of great importance in molding of rigid foams. In these applications residual strains can cause residual stresses, component warping, and large errors in dimensional tolerance (refs. 16 and 17). One of the more significant outcomes of the measured thermal expansion strains is that the majority of the total strain is inelastic (creep strain). This is important in assessing the amount of tensile stress induced into the cold material by thermal gradients.

The thermal expansion behavior of this foam is complicated and involves a number of events during heating. First is simply the increase in pore gas pressure due to increasing temperature. Based on the universal gas law, an increase in temperature will cause an increase in the pressure of pore gases if the volume of the cells remains the same. Added to this pressure increase is the addition of additional gases to the pores due to effluents caused by reactions within the polymer skeleton. Increasing the cell volume will result in a corresponding decrease in the pore pressure. The TGA work shown in figure 25 indicates that the polymer begins to outgas as the temperature rises above room temperature. Various effluents are produced during this decomposition, with water vapor being a key component at temperatures below 100 °C. At the peak strain temperature of 150 °C (302 °F), a weight loss of 4 percent is already observed (fig. 26), and this could contribute significantly to additional pore pressure increases. Pore pressure increases have been suggested as an important thermal expansion mechanism by several researchers (refs. 10, 16, 17, and 19).

As with most materials, an increase in temperature reduces the strength of the polymer. The polymer becomes viscoplastic in behavior and can readily deform with time under load at temperature. In fact, figures 52 and 53 show that the foam can exhibit substantial time dependency even at room temperature. Additionally, zero-load creep tests on the foam have shown that at a temperature between 80 and 90 °C (176 and 194 °F), time-dependent deformation due only to the internal gas pressure can occur (figs. 57 and 58). In this temperature range, the onset T_g was also observed. The average onset T_g for all samples (fig. 51) is 86.6 °C (188 °F). This change in polymer properties allows the increased pore pressure to inflate the foam cells causing a large increase in expansion strain. The change in cell size has been observed in this study by examining the cells in the hot stage of an SEM. During this test the foam was heated incrementally and individual foam cells were observed. The movement of the cell walls due to expansion and contraction was measured and thermal strains were calculated. The expansion was shown to be large and consistent with the expansion strains measured on the bulk foam. Although a change in

foam cell size has been previously documented (ref. 16), it was only shown via measurements taken before and after heating. To the authors' knowledge, the current study is the first to show the changes in the cell size in situ and also to calculate the response strains at the various temperatures for individual cells.

As temperature continues to rise, the pore pressure continues to increase and the foam continues to expand. At some point as shown in figure 2 and at approximately 150 °C, a peak is reached in the expansion strain. We know that the rise in strain is caused by cell pressurization and not a result of the CTE of the polymer because the measured CTE for the polymer (figs. 22 and 23) is negative. At still higher temperatures the foam begins to shrink. A few factors can contribute to the turnaround in behavior. Shortly before attainment of the peak strains, the faces of the foam cells develop cracks. At temperatures slightly above 150 °C many large, multicell cracks were observed (figs. 17 and 18). These cracks can allow the gas to escape, thus relieving the pressure within the foam cells. Along with this mechanism the polymer itself has been shrinking since the temperature began to rise. At about 140 °C (284 °F), the polymer skeleton undergoes a more rapid contraction as shown in figure 23. The shrinkage of the polymer is consistent with its weight loss observed by the TGA experiments. Continued polymer decomposition results in suspected thinning and finally perforation of the cell faces (fig. 19) as evidenced near 200 °C (392 °F), where rapid weight loss is observed during TGA experiments (fig. 26). Both the shrinkage of the polymer and the large-scale cracking in the foam are sufficient to cause dimensional contraction in the foam blocks. These events show that the BX–265 is unstable above room temperature and that this instability can result in significant dimensional changes and an increase in the foam stresses if the foam boundaries are constrained. Moreover, cracking (a few millimeters in length) was observed in the foam entirely due to thermal changes. Restriction of the foam on the ET from adhesion to various components of the tank may result in even more strain and larger tearing of the foam.

It was observed in the expansion tests interrupted at various temperatures (fig. 16) that cracking begins in the cell faces, such as those shown in figures 20 and 21. In order to define the temperature (or degree of stress) at which cracking begins would require much more effort than was warranted for this study. Based on the SEM observations, we speculate that the cracking begins in the temperature regime of 130 to 150 °C (266 to 302 °F). A predecessor to the cracking is probably face wrinkling as a result of stresses in the cell (refs. 10 and 12). While not extensively studied here as a thermal expansion mechanism, we have used face wrinkling to define the damage zone in front of a crack tip of a fracture toughness sample (B. Lerch, J. Thesken, R. Sullivan, and D. Fedor, 2007, NASA Glenn Research Center, in Fracture Behavior of Polystyrene Foam in Support of ET Foam Modeling, presented to ET Project Office, NASA Marshall Space Flight Center). This allowed us to calculate minimal, required sample dimensions based on the size of the fracture process zone for the application of linear elastic fracture mechanics.

Face cracks appear to initiate at low stresses, and their propagation is usually stopped by the thicker edges (fig. 21). The edges have a deltoid (triangular) cross section, and measurements yielded an edge length for this of 17 μm (6.7×10^{-4} in.) (ref. 1). This is much greater than the face thickness, bounded by SEM measurements to be between 0.1 and 1.0 μm (3.9×10^{-6} and 3.9×10^{-5} in.) (ref. 1). Other researchers have documented the face membrane thickness for other polyurethane foams to be ~2 μm (7.9×10^{-5} in.) (ref. 20) and ~1 μm (3.9×10^{-5} in.) (ref. 21). Thus the cell edges should be the last element to break in the cell. This suggests that an appropriate strength model would be a cell consisting of only edges having the appropriate length and cross section, and this was indeed done in reference 1.

The thermal expansion data plotted in figure 2 fall into two groups, designated as A and B. Group B expands almost 10 °C (45 °F) earlier and reaches a higher peak strain than does group A. The characteristic difference between these two groups appears to be density, with foam samples having densities less than 0.035 g/cm^3 (2.19 lb/ft^3) falling into group A. Part of the density difference can be accounted for by the number of knit lines in the sample (fig. 3). What causes the rest of the density difference is unknown. One thought was that the higher density might be caused by additional moisture. More moisture would increase the weight (density), and could create more pore gas pressure. This

explanation is plausible since the expansion of the foam between ambient and 80 °C is higher for group B than for A. Likewise, the higher density group B samples experienced the onset of rapid expansion at a lower temperature, consistent with a reduction in T_g of the polymer due to higher moisture contents (refs. 12 and 13). The thermal expansion in group B also attained about 5 percent higher peak strains, as one would expect for more pore gas. However, attempts to increase the moisture content of the foam by conditioning did not show similar changes in its thermal expansion response (figs. 42 and 43). Although it would be convenient to explain the thermal expansion difference based on the number of knit lines, the correlation is not 100 percent; see for example specimen B3-f in figure 2, which contains two knit lines yet falls into the low-density group A.

The BX–265 is a sprayed-on foam that rises during curing. Hence the cells become elongated in the rise direction, leading to anisotropy in many properties of the foam. Thermal expansion is one of these properties. Figure 10 shows the difference in thermal expansion between the perpendicular-to-rise and rise directions. Two obvious differences can be observed. The maximum expansion in the rise direction is much less (~4 times) than in a direction perpendicular to the rise. Also, the temperature at which the rapid expansion occurs is much higher (by 50 °C, or 90 °F) in the rise direction. There is again a knit line (density) effect on expansion. The number of knit lines affects the onset of rapid expansion and the peak expansion strain. It is speculated that the specimens with more knit lines have a higher moisture content and hence a slightly lower T_g. This would lead to softening of the polymer at a lower temperature and cause a rapid expansion also at lower temperatures. While this explanation is suitable for the perpendicular-to-rise direction (figs. 2, 4, and 5), the opposite appears to be true for the rise direction. In this direction (fig. 10) the specimens with multiple knit lines actually soften at a higher temperature. There is not a consistent explanation for the effect of knit lines on thermal expansion.

Anisotropy in expansion was also observed in individual cells during the in situ measurements (figs. 13 to 15). Even the cell in figure 13 shows that there is a much smaller change in the height of the cell than there is in the width. This is consistent with the fact that the cell sides parallel to the height are more compliant, and the cell tends to modify its shape to that of a sphere. The elongated structure of the cell is such that under hydrostatic stress the cell will expand in the perpendicular-to-rise direction more than the rise direction.

The expansion in the rise direction at lower temperatures is less than in the perpendicular-to-rise direction, and in some cases a slight contraction occurs. An enlargement of this expansion is given in figure 11. A contraction was also observed in this temperature regime by studies at Ames (Tina Panontin, NASA Ames Research Center, Return to Flight External Tank TPS Verification Microstructural Characterization and Fracture Process Assessment, March 30, 2005), and the peak contraction strain is similar (–0.4 percent) in both studies.

Conditioning was performed on the foam to investigate the effects of drying and moisturizing, since moisture has been mentioned in foam shedding problems. Loss of weight as a result of drying was shown to be a function of temperature (fig. 31). When dried at room temperature the foam loses approximately 2.5 percent of its weight at saturation. At 40 °C (104 °F) the weight loss was observed to be as high as 8 percent (fig. 33). This is expected since the higher temperature releases more moisture and other volatile substances from the polymer. What is not clear is why the equilibrium moisture content appears to be a function of the specimen thickness. Both figures 31 and 33 show an influence of sample thickness on weight loss, and this is better defined in figure 34. There is a linear relationship between 1/thickness and percentage weight loss, with thicker samples having less of a percentage weight loss. It was expected that the equilibrium moisture content would be the same and the sample thickness would only affect how quickly equilibrium was attained. Van Krevelen and Hoftyzer (ref. 22) state that for polymeric textiles an inverse relationship is observed between thickness and weight loss. However, it is not mentioned if this refers to the equilibrium moisture content or the absorption rate. We postulate that moisture absorption is restricted to a surface layer on the order of 2.5 mm (0.1 in.) deep. Therefore on a percentage weight loss basis, the thicker samples would indicate less weight loss.

Drying the foam seems to flatten the expansion curve at the lower temperatures (fig. 35). Up to a temperature of about 45 °C (113 °F), the expansion is the same as the as-sprayed foam. However,

between temperatures of 50 and 80 °C (122 and 176 °F) the foam begins to contract (fig. 36). This could be due to the lack of water vapor left in the pore gases, preventing additional expansion of the cells. After the onset of rapid expansion, the dried foams do not expand as much as the as-sprayed foams. This could also be due to the lack of water vapor and other volatiles in the foam cell gases. Note that none of the four dried samples had reached their equilibrium moisture content. Hence each has a different moisture content and presumably a different T_g. This may explain why the samples with the largest weight loss (i.e., least amount of water) did not rapidly expand until higher temperatures.

The weight loss due to drying is partially-to-completely reversible. Figure 37 shows that half of the weight was gained back just from removing the samples from the drying oven. All of the weight loss may have been reversed had either more time passed, or the RH in the room been higher than 25 percent. Rodriguez-Perez et al. (ref. 16) have also shown a weight gain in polyolefin foams due to the material picking up moisture from the room humidity. Figure 38 shows partial-to-full recovery in weight loss for the 16 samples previously dried. It is suspected that saturation had not yet occurred in the thicker samples and consequently they only had partial weight reversal. The ambient RH was higher (66 percent) when these samples were exposed, so they gained more weight than the previous set of samples. When conditioned in an oven at 95 percent RH, the samples had over a 2.5-percent weight gain (fig. 41) and this is a complete weight reversal from the dried condition (see fig. 31 for an equivalent dried weight loss). Hence there is a several percentage weight change that can occur in the foam due to the uptake or removal of water vapor, and given sufficient time at temperature and humidity, the change can be completely reversible. Eventually however, the foam will reach a equilibrium water content, with the amount depending on the temperature and local humidity conditions.

These results are in contrast to those conducted at Marshall (Butkus, L. and Wolfe, J., Wright-Patterson Air Force Base, Water Absorption by ET Foam, presented to Columbia Accident Investigation Board). In this report four ET foams were exposed to 52 °C (126 °F) at 95 percent RH for 7 days (168 h) to check for weight gain. None of the foams gained more than 0.83 percent weight, and the BX–250 gained only 0.16 percent weight. BX–265 was not tested. The conclusion of this report was that the ET foam cannot absorb significant amounts of moisture. The data conducted on BX–265 in the current study showed (fig. 39) the as-sprayed BX–265 foam to have a percentage weight gain between 0.7 and 1.4 for 4 days at 40 °C in 95 percent RH. The lower percentage weight loss for the BX–250 foam may have been due to a number of factors. The obvious is that it is a slightly different foam chemistry, although all of the foams tested at Marshall showed lower percentage weight gains. Second, the test temperature of 52 °C was higher than that used on the BX–265 in this study. At 52 °C the BX–265 is estimated to have lost approximately 2 percent of its weight as shown in the TGA tests in figure 26. Hence there is a competition between weight gain from moisture uptake and weight loss from outgassing. Also, if the samples tested at Marshall were thicker (perhaps equal to or greater than 51 mm, or 2 in.), they may also show less of a percentage weight gain than the BX–265 samples tested in this study. Note that the foams could gain more percentage weight if they were first dried. Drying does not necessarily mean exposure in a drying oven. Drying can occur simply by resting in an ambient environment with a low humidity. Hence, if the foams had been sitting in a high-humidity environment for a long time, they will tend to gain less weight when saturated in a humidity chamber. Finally, the Marshall samples were reported to have sealed surfaces, and this could have reduced their moisture absorption.

Since weight gain and loss involve diffusion and diffusion is time dependent, it is reasonable to assume that thermal expansion could also be time dependent. In fact, the data shown in figures 46 and 47 for various heating rates indicate that the expansion is indeed a function of heating rate. We postulate that expansion is a competitive process between gas expansion and gas pressure relief via diffusion through the cell walls. Menges et al. (ref. 17) showed that heating at slower rates allows more time for the cell gas to diffuse out of the cell. Given a slow enough heating rate, the foam may actually shrink during heating because of the contraction of the polymer and the absence of sufficient pore pressure because of this diffusion. If the heating rate is high enough to not allow diffusion through the cell walls, then the gas expansion would fully be applied to expansion of the foam cells. The foam could then expand at lower temperatures, and this was shown to be the case for expansion in both directions at high heating rates

(figs. 46 and 47). At the fastest heating rates the expansion strain can maintain its maximum value over approximately a 70 °C (126 °F) range, although it is unclear why this occurs. It is also possible that the T_g is lowered for faster heating rates since moisture has not had much time to escape; this could also lead to the rapid expansion at lower temperatures. This rate effect has implication to the ET: At heating rates observed in ascent, the expansion strains could reach 5 percent after only a temperature rise to 50 °C, and at this temperature the foam may still have sufficient strength to develop significant stresses and perhaps cause cracking or foam spallation.

The few preliminary tests to probe the time-dependent behavior of the foam have shown that there is extensive creep even at room temperature. When loaded in the perpendicular-to-rise direction, the post-yield creep stress 262 kPa (38 psi) used in these tests represented 73 percent of the ultimate tensile strength of the foam. The accumulated creep strain in just 1 h was between 2 and 4 percent, depending on the loading rate. This is a considerable amount of strain, particularly since the foam at this temperature is below the onset T_g by 67 °C (121 °F). However, this is consistent with results from Traeger and Hermansen (ref. 15) who have shown that creep becomes rapid when urethane foams are stressed to just 40 percent of the ultimate strength of the foam. It would be interesting to know how much creep could still be observed at such loads for subzero temperatures.

The time-dependent results in figure 52 show that there was no change in either the modulus or the yield stress when the loading rate was altered by an order of magnitude. It was expected that the test using the lower loading rate would have exhibited both a lower modulus and yield strength. Creep modeling (ref. 2) on this foam has necessitated the use of an “aging” component to correlate available mechanical results. Thus there may be competition between aging and rate-dependent effects. These two mechanisms may have cancelled each other producing the outcome in figure 52. In this case, “aging” means stiffening of the polymer structure. Additional evidence of this stiffening can be observed in the unloading modulus, where the sample that crept the most had the highest unloading modulus. It is also interesting to observe that the unloading modulus for all three samples was significantly higher than their respective loading modulus. Clearly understanding the time-dependent behavior of the foam is in its infancy and would require much more work to develop effective models.

Being consistent with time-dependent behavior, the foam can creep at elevated temperatures. Zero-load creep tests (figs. 55 to 59) indicate that at temperatures above 80 °C, the foam exhibits time-dependent behavior. The behavior is complex and involves the attainment of the onset T_g, continued outgassing of the foam (figs. 60(a) to (c)), increase in the pore pressure, and diffusion of the gas out of the cell pores. If the temperature is not high enough, and consequently the pore pressure does not increase enough, the foam will actually shrink at temperature because of thermal contraction of the polymer. This can be seen by the negative creep observed in figure 58 for sample LOX-bbb tested at 79 °C (174 °F). Although the creep of the foam may have limited application to the ET, as with residual strain it can be important to the molding of rigid foams (refs. 16 and 17).

This investigation has provided critical test data for a better understanding of the behavior of BX–265, and for assistance in the development of structural models for the foam. One suggestion for a modeling approach is the creation of a unit foam cell that consists of edges having the same dimensions as those observed in the actual foam. Since the edges appear to be the overwhelming carrier of stress in this material, this approach is certainly a reasonable first attempt. Such a model has been created and applied successfully to the ET foams (ref. 1). However, this model does not address many of the salient features that occur above room temperature. A fully functioning model would have to include the rise in gas pressure with temperature, added pore gas, and subsequent increases in pore pressure due to polymeric decomposition, crack development in the foam, as well as time-dependent effects of both the polymer skeleton and the foam structure. Two additional models were initially investigated to address these points. One was a soils model, capable of dealing with the increase in pore pressure (R.M. Sullivan, NASA Glenn Research Center, Station #1593 Ice Frost Ramp Structural Analysis Results, Sept. 15, 2006, presentation to ET program office). The second (ref. 2) was a micromechanics model, which should handle the time-dependent properties of the foam. Both of these models were given a cursory look, and work was terminated in order to focus on the structural model.

Summary and Conclusions

A set of detailed investigations was conducted on the space shuttle external tank's (ET's) BX–265 foam. The studies were aimed at better defining the behavior of the foam. Additionally, experimental data were provided for guidance in model development. The foam behavior is complex and is influenced by the cell geometry, the cell gas pressure, polymer softening, thermal decomposition of the polymer, and moisture content. The following studies were performed:

1. Thermal expansion

a. Thermal expansion is dependent on the orientation of the foam cells. Expansion is greater in the perpendicular to the rise direction.

b. Foam expansion is slow between cryogenic temperatures and approximately 100 °C (212 °F), above which the foam rapidly expands to very large strains. At still higher temperatures the foam begins to contract.

c. Thermal cycling leads to residual dimensional changes in the foam.

d. The onset of the rapid thermal expansion is dependent on heating rate. As the heating rate increases, the rapid expansion occurs at lower temperatures.

e. Expansion of the foam is due to the increase in gas pressure inside the foam cells. Individual cell expansion was documented during heating and was consistent with bulk expansion measurements.

f. Foam cracking due to heating to 160 °C (320 °F) was observed. The cracks became even larger at higher temperatures.

g. Above room temperature the polymer skeleton material was found to shrink when heated via observation of polymer cell fragment expansion.

2. Thermogravimetric analysis

a. Weight loss was documented when the foam was heated above room temperature. Approximately 5 percent weight loss was achieved by 200 °C (392 °F). Above this temperature the weight loss rapidly increased, until the foam was nearly consumed at 700 °C (1292 °F).

b. In general, a higher heating rate delayed the weight loss.

c. The foam lost the most weight in a vacuum environment, and the least amount in a nitrogen environment. Heating in air resulted in an intermediate weight loss.

d. There is an approximate 40 percent weight loss in vacuum at 315 °C (599 °F), the maximum shuttle ET service temperature.

3. Moisture effects

a. The foam can lose up to 2.5 percent of its weight at 20 °C (68 °F), and 8 percent of its weight at 40 °C (104 °F) with prior drying in a vacuum oven. Weight loss saturation times are typically 1000 h.

b. Weight loss is proportional to 1/thickness of the foam sample.

c. In an environment of 40 °C and 95 percent relative humidity weight gain due to moisture uptake can be as high as 1.5 percent.

d. The foam can gain even more percentage weight if it was previously dried.

e. The foam weight gain or loss is reversible and depends on the humidity difference as well as the time and temperature in a particular environment.

4. Glass transition temperature (T_g)

a. The inflection T_g for six batches of foam was averaged to be approximately 130 °C (266 °F) and was affected by the moisture content of the foam.

b. The onset T_g for the six batches, representing the first movement of the polymer chains, was 87 °C (189 °F).

5. Time-dependent properties

a. When held for 1 h at 262 kPa (38 psi) tension, the samples crept 2 to 4 percent.

b. When unloaded to zero stress and held for 2 h, the samples recovered approximately half of their unloaded strain. Further recovery does not take place, indicating that the deformation is only partially reversible.

c. Creep can occur at elevated temperatures, caused only by the increase of the internal cell gas pressure. The critical temperature at which this begins is between 80 and 90 °C (176 and 194 °F).

d. The maximum creep strain for a 30-min period was 6.2 percent, and this occurred at 114 °C (237 °F). Both higher and lower temperatures resulted in less creep.

e. At temperatures of 80 °C and above, the foam continually loses weight because of outgassing and thermal decomposition. This can increase the cell gas pressure and continue to drive creep mechanisms.

References

1. Sullivan, R.M.; L.J. Ghosn; and Lerch, B.A.: Elongated Tetrakaidecahedron Micromechanics Model for Space Shuttle External Tank Foams. NASA/TP—2009-215137, 2009. http://gltrs.grc.nasa.gov
2. Bednarcyk, Brett A., et al.: Analysis of Space Shuttle External Tank Spray-On Foam Insulation With Internal Pore Pressure. J. Eng. Mater. Technol., vol. 130, 2008.
3. Sullivan, Roy M.; Ghosn, Louis J.; and Lerch, Bradley A.: An Elongated Tetrakaidecahedron Model for Open-Celled Foams. NASA/TM—2007-214931, 2007. http://gltrs.grc.nasa.gov
4. Sullivan, Roy M.; Ghosn, Louis J.; and Lerch, Bradley A.: A General Tetrakaidecahedron Model for Open-Celled Foams. Int. J. Solids Struct., vol. 45, issue 6, 2008, pp. 1754–1765.
5. Sullivan, Roy M.; Ghosn, Louis J.; and Lerch, Bradley A.: Application of an Elongated Kelvin Model for Space Shuttle Foams. AIAA 2008–1786, 2008.
6. Yakushin, V.A.; Stirna, U.K.; and Zhmud, N.P.: Effect of the Chemical Structure of the Polymer Matrix on the Properties of Foam Polyurethanes at Low Temperatures. Mech. Compos. Mater. (translated from Mekh. Kompozitnykh Mater.), vol. 35, no. 4, 1999, pp. 351–356.
7. Leite, N.F.; and Miranda, L.C.M.: Photoacoustic Characterization of the Effects of Air Inclusion on the Thermal Properties of Foamed Polyurethane. J. Mater. Sci., vol. 27, no. 20, 1992, pp. 5449–5452.
8. Morimoto, Kiyotake; Suzuki, Toshio; and Yosomiya, Ryutoku: Thermal Conductivity and Thermal Expansion Behavior of Glass Fiber-Reinforced Rigid Polyurethane Foam. Polym. Eng. Sci., vol. 24, issue 12, 1984, pp. 943–949.
9. Xian, Zhu, et al.: Linear Expansion of Polyurethane Foam at Low Temperature. China Report: Science and Technology, JPRS–CST–85–039, 1985, pp. 44–62.
10. Almanza, O., et al.: Thermal Expansion Coefficient and Bulk Modulus of Polyethylene Closed-Cell Foams. J. Polym. Sci. Part B, vol. 42, no. 20, 2004, pp. 3741–3749.
11. Weiser, Erik S.; Nemeth, Michael P.; and St. Clair, Terry L.: Assessment of Technologies for the Space Shuttle External Tank Thermal Protection System and Recommendations for Technology Improvement. NASA/TM—2004-213238, 2004.
12. Materials Solutions, Polymer Composites: Glass Transition Temperature. http://vircon-composites.com/4_2_2.asp Accessed Sept. 4, 2008.
13. DSM Engineering Plastics: Effects of Moisture. http://www.dsm.com/en_US/html/dep/stanyl_effects_of_moisture.htm Accessed Sept. 4, 2008.
14. Gibson, Lorna J.; and Ashby, Michael F.: Cellular Solids: Structure and Properties. Cambridge University Press, New York, NY, 1997.
15. Traeger, R.K.; and Hermansen, R.D.: Properties of Structural Foams. J. Cell. Plast., vol. 7, no. 4, 1971, pp. 189–194.

16. Rodriguez-Perez, M.A.; Almanza, O.; and De Saja, J.A.: Anomalous Thickness Increase in Crosslinked Closed Cell Polyolefin Foams During Heat Treatments. J. Appl. Polym. Sci., vol. 73, no. 14, 1999, pp. 2825–2835.
17. Menges, G.; Hiemenz, C.; and Targiel, G.: Waermeausdehnungsverhalten von Polyurethanschaumstoff. Gummi Asbest Kunstst., vol. 30, no. 9, 1977, p. 626.
18. Fritsch, Peter, et al.: Zum Temperaturverhalten von Polyurethan-Strukturschaumstoff. Plaste Kautsch., vol. 22, no. 6, 1975, pp. 489–495.
19. Rodriguez-Perez, M.A., et al.: Thermal Expansion of Crosslinked Closed-Cell Polyethylene Foams. J. Polym. Sci. Part B, vol. 36, no. 14, 1998, pp. 2587–2596.
20. Schwartz, N.V.; and Bomberg, M.T.: Image Analysis and the Characterization of Cellular Plastics. J. Therm. Insul., vol. 15, 1991, pp. 153–171.
21. Akabori, Kanji; and Fujimoto, Kazuo: A Method for Measuring Cell Membrane Thickness of Polyurethane Foam. Int. Prog. Urethanes, vol. 2, 1980, pp. 41–60.
22. Van Krevelen, D.W.; and Hoftyzer, P.J.: Product Properties (II) Environmental Behaviour and Failure. Properties of Polymers—Their Estimation and Correlation With Chemical Structure, ch. 26, Elsevier, New York, NY, 1976, p. 523.

REPORT DOCUMENTATION PAGE		Form Approved OMB No. 0704-0188

1. REPORT DATE *(DD-MM-YYYY)*	2. REPORT TYPE	3. DATES COVERED *(From - To)*
01-04-2009	Technical Memorandum	

4. TITLE AND SUBTITLE
Experimental Investigations of Space Shuttle BX-265 Foam

5a. CONTRACT NUMBER

5b. GRANT NUMBER

5c. PROGRAM ELEMENT NUMBER

6. AUTHOR(S)
Lerch, B., A.; Sullivan, R., M.

5d. PROJECT NUMBER

5e. TASK NUMBER

5f. WORK UNIT NUMBER
WBS 524238.08.02.03.04

7. PERFORMING ORGANIZATION NAME(S) AND ADDRESS(ES)
National Aeronautics and Space Administration
John H. Glenn Research Center at Lewis Field
Cleveland, Ohio 44135-3191

8. PERFORMING ORGANIZATION REPORT NUMBER
E-16572

9. SPONSORING/MONITORING AGENCY NAME(S) AND ADDRESS(ES)
National Aeronautics and Space Administration
Washington, DC 20546-0001

10. SPONSORING/MONITORS ACRONYM(S)
NASA

11. SPONSORING/MONITORING REPORT NUMBER
NASA/TM-2009-215292

12. DISTRIBUTION/AVAILABILITY STATEMENT
Unclassified-Unlimited
Subject Category: 27
Available electronically at http://gltrs.grc.nasa.gov
This publication is available from the NASA Center for AeroSpace Information, 301-621-0390

13. SUPPLEMENTARY NOTES

14. ABSTRACT
This report presents a variety of experimental studies on the polyurethane foam, BX-265. This foam is used as a close-out foam insulation on the space shuttle external tank. The purpose of this work is to provide a better understanding of the foam's behavior and to support advanced modeling efforts. The following experiments were performed: Thermal expansion was measured for various heating rates. The in situ expansion of foam cells was documented by heating the foam in a scanning electron microscope. Expansion mechanisms are described. Thermogravimetric analysis was performed at various heating rates and for various environments. The glass transition temperature was also measured. The effects of moisture on the foam were studied. Time-dependent effects were measured to give preliminary data on viscoelastoplastic properties.

15. SUBJECT TERMS
Polyurethane foam; External tank; Thermal expansion; Viscoelastic; Microstructure; Damage; Glass transition temperature

16. SECURITY CLASSIFICATION OF:			17. LIMITATION OF ABSTRACT	18. NUMBER OF PAGES	19a. NAME OF RESPONSIBLE PERSON
a. REPORT	b. ABSTRACT	c. THIS PAGE			STI Help Desk (email:help@sti.nasa.gov)
U	U	U	UU	62	19b. TELEPHONE NUMBER *(include area code)* 301-621-0390